ALMA MATER STUDIORUM – UNIVERSITÀ DI BOLOGNA

SCHOOL OF ENGINEERING AND ARCHITECTURE

DEPARTMENT OF ELECTRICAL, ELECTRONIC AND INFORMATION ENGINEERING "GUGLIELMO MARCONI"

MASTER DEGREE IN ELECTRICAL ENERGY ENGINEERING

MASTER THESIS

in

Applied Measurements for Power Systems

DESIGN AND CHARACTERIZATION OF A SYSTEM FOR LOSS FACTOR MEASUREMENT IN MV UNDERGROUND CABLE JOINTS UNDER TEMPERATURE VARIATION CONDITIONS

AUTHOR
Filippo Lama

SUPERVISOR:
Prof. Lorenzo Peretto

CO-SUPERVISORS:
PhD. Abbas Ghaderi
Prof. Roberto Tinarelli

Academic Year 2017/18

Session II

Per aspera
ad astra

Contents

Abstract

Cable joints are considered to be the weakest components of the MV cable network, being the ones with the highest failure rate. Furthermore, from statistical analysis of different cable network failure data, a noticeably increase in cable joint breakdowns has been showed during summer months. The request for Distribution System Operators to avoid line outages as much as possible indicates a significant need for non-invasive diagnostic technologies able to monitor the health condition of MV cable junctions. Moreover, a better knowledge is required on the main causes of the detected increase in cable joint failure rate, in which temperature seems to play an important role. The present master thesis consists in the design and complete characterization of a simple and cheap laboratory setup for loss factor measurements on cable joints. Using the developed circuit, tan delta measurements are performed on four thermally cycled cable joint samples and the trend in relation to temperature variations has been investigated and widely discussed. In particular, it has been found that the loss factor of cable joint samples decreases considerably when temperature rises and vice-versa. From result analysis, some hypotheses have been made trying to explain this particular behavior of the loss factor versus temperature. In particular, temperature variations seem to cause expansions and contractions of the different dielectric layers present in cable joint, giving rise to pressure fluctuations at the interface between them. Consequently, variations in the breakdown strength of the joint insulation system and in the amount of conduction losses are expected to happen. These conclusions must be demonstrated by future studies and tests on cable junctions. It is worth saying that a conference proceeding has been published from the present work, and, currently, a journal paper is submitted, waiting to be approved.

Abstract

Sommario

I giunti sono considerati i componenti della rete di media tensione in cavo aventi il più alto tasso di guasto. Per le utilities di distribuzione è di primaria importanza ridurre il più possibile il numero di interruzioni delle linee in cavo. Sono dunque necessari maggiori studi diagnostici riguardanti il monitoraggio delle condizioni operative dei giunti di media tensione. Oltre a ciò, è richiesta anche una maggiore analisi delle cause che portano, nei mesi estivi, ad un considerevole aumento di guasti nei giunti stessi. In particolare, sembra che le variazioni di temperatura abbiano un ruolo di primaria importanza in tale fenomeno. La presente tesi magistrale consiste nel design, nella caratterizzazione e nella taratura di un semplice ed economico setup di laboratorio per la misura del fattore di perdita nei sistemi di isolamento di giunti di media tensione. Utilizzando il circuito sviluppato, il fattore di dissipazione viene misurato in quattro giunti sottoposti a cicli termici. Viene dunque analizzato l'andamento del fattore di dissipazione in relazione alle variazioni di temperatura: ad un aumento di questa, il valore del fattore di perdita tende a diminuire e viceversa. Dall'analisi dei risultati, sono state effettuate ipotesi al fine di determinare le cause di tale andamento. In particolare, sembra che le variazioni di temperatura provochino espansioni e contrazioni dei diversi strati di isolante presenti nei giunti, causando dunque variazioni di pressione nell'interfaccia fra gli strati stessi. Da tali oscillazioni di pressione si ritiene che ne conseguano modificazioni nella rigidità dielettrica del sistema di isolamento della giunzione e nella corrente di conduzione che lo attraversa. Le precedenti ipotesi dovranno essere dimostrate e saranno oggetto di studio per futuri test. Dal presente lavoro, è seguita la pubblicazione di un contributo in atti di convegno e, attualmente, un articolo di ricerca è in attesa di essere pubblicato.

Sommario

1 Introduction

1.1 Background

Underground cable joints are considered to be one of the MV cable network apparatuses with the highest failure rate [14; 15; 17]. In fact, cable joints are hand-made systems installed on field usually under non controlled environmental conditions. Hence, the entrance of contaminants in joint insulation during the installation and the relatively high possibility to make mistakes in the mounting are just a few of the factors that could lead to premature joint faults. The high criticality of these cable accessories can be also understood by highlighting that the sudden failure of only one cable joint leads to the outage of the entire cable line to which it is connected. A cable line outage due to a cable joint breakdown leads always to costly and time consuming maintenance actions since the whole component has to be replaced with hand working by specialized workmen. That fact causes also discomforts on the final users, experiencing long electric power interruptions. The request to avoid as much as possible such line failures indicates a significant need of non-invasive diagnostic methods and technologies to assess the condition not only of the whole cable system but also, particularly, of cable joint accessories. In fact, nowadays, several diagnostic techniques are actually used for the analysis of the whole cable line condition, considered as a system of cable segments, joints and terminations. However, a lack of investigations about simple and cheap techniques focusing directly on cable joints has been detected. Condition assessment of these apparatuses trough the monitoring of health parameters is of primary importance in order to apply predictive maintenance on them and consequently reduce the high number of failures caused by their breakdown. In particular, this work focuses on the application of the loss factor diagnostic tool on cable joints considering its advantage to provide a good estimation of the whole insulation health condition of the tested apparatus using a relatively simple and cheap laboratory setup.

1.2 Problem statement

The statistical analysis of different MV cable networks failure data show that cable joint failure rate increases noticeably during the summer months of the year [24; 25; 26]. From the same studies, it has been demonstrated that these peaks in cable joint breakdowns seem to be not correlated with their working conditions due to their low load conditions during all the monitoring years. Hence, it has been argued that environmental temperature could play an important role on the failure rate of cable joints. A possible explanation could be found in the continuous day-night temperature variation coupled with the mean high temperature of the summer period that may cause instabilities inside the joint structure. However, due to a lack of literature about this phenomenon, many investigation about the effect of temperature on the health state of complex insulation systems as cable joints have to be further performed. The effect of a better knowledge of this phenomenon is expected to lead to a better understanding on how it is possible to monitor cable joint health state on-site, considering always the final purpose to decrease of cable line outages events.

1.3 Objective and approach

The present master thesis has an approach mainly experimental and deals with underground medium voltage straight cable joints with different design and constructed in laboratory or on site. In view of the problems introduced in the latter, this work has the objective to design and completely characterize a simple and cheap laboratory setup to measure the loss factor of cable joint with a sinusoidal applied voltage having magnitude of $1kV_{rms}$ and 50 Hz of frequency. Then, once the system has been designed and constructed, loss factor measurements have been performed on cable joint samples subjected to hot-cold daily thermal cycles. The purpose is to investigate and discuss the response of the loss factor during variations of joint temperature. In particular, the target is to correlate loss factor variation to joint thermal condition in order to infer the effect of environmental temperature variation on the health condition of the joint. This work

has intended to be only the starting point for a deeper investigation on why so many cable joint fail during summer period. Hence, during the discussion of the results found, some suppositions, supported by literature data, have been made: these must be demonstrated by future works on this subject. It must be always remembered that the general aim is to find a method to perform in a reliable and cheap way diagnostic measurements on the most critical component of the cable network. In this way, it is expected to reduce of the high number of cable outages since preventive maintenance on cable joints could be effectively performed.

1.4 Thesis organization

The first chapter of this thesis is intended to be a brief introduction of the subject treated, highlighting also the aim and the objectives of the whole work. Chapter 2 is a theoretical overview about the literature present in the field of cable joints and loss factor measurements, explaining everything could be useful to the understanding of the measurement setup design and to the discussion of the loss factor results. In the third chapter is explained in detail the design and the characterization of the loss factor measurement circuit and LabVIEW program. Chapter 4 presents firstly how measurement data have been statistically analyzed, focusing on the measurement errors, and then loss factor results of cable joint samples are presented, focusing on the linking with the temperature condition of the joint themselves. In chapter 5, measurement results are widely discussed, making also some supposition, based on literature analysis, on the causes that lead to the found loss factor trend versus temperature. The conclusions and the future and works, required to demonstrate the suppositions made in the latter stage, are the objects of chapter 6. As last, chapter 7 and 8 contain respectively the acknowledgments for this master thesis and all the references, useful to support the theoretical part and the hypotheses made.

This page intentionally left blank

2 Theory

2.1 MV Cable Joints

Distribution power cables for medium voltage underground lines are usually manufactured with standard lengths of some hundreds of meters and they are delivered to the customers wound on drums. A typical drum containing, for example, 500 meters of XLPE insulated three core cable with conductor sections of 240 mm^2 can weight up to 7500 kg [1]. Then, because of handling issues for the cable factories, it is clear that there are manufacturing limits in terms of maximum length of the cable segments. Furthermore, very heavy drums with very long wounded cable segments would cause issues not only during the manufacturing processes but also during transportation and installation at site. Therefore, from what just said, in order to create long distance cable lines the only way is to connect together many cable segments using accessories called cable joints. Cable joints are then an integral part of a power cable distribution system and they must perform the same basic functions as the cable lines on which they are installed. In other words, they must behave totally as a perfect continuation of the cable line. Furthermore, in addition to providing conductor connections for the full current rating of the cable and an adequate insulation, cable joints must also ensure an electrical stress control at the cable screen ends and they must also protect the cable connection against water, dust or pollution ingress [2].

It must be underlined that, in the present study, only straight single core joints are analyzed, namely joints connecting two pieces of single core cables both insulated with polymeric materials, being the most common ones. Thus, different cable joint designs as three core cable joints, T or Y branch joints or transition joints for the connection of cables having different insulation materials (for example polymeric and paper insulated cables) are not treated in the present thesis. Now, the cable joint structure highly depends not only on the cable segments connected but also on the line voltage and operating environment: in this study medium voltage cable joints with voltage class of

36 kV are considered. In this case, the cable joint structure is similar to the one of the cables that it is connecting and, besides of connector and electric stress control, it includes joint insulation, joint insulation semiconductor, joint shield and outer sheath, as it will seen in the following [3]. However, also by only considering medium voltage straight joints, it is not possible to define a common general joint structure. In fact, the joint structure may vary depending on manufacturing choices about the field grading type and about the type of installation technology of the insulating materials. Thus, the subsequent treatment is organized in order to explain step by step the best practice for the installation of a medium voltage cable joint, focusing on the different possible solutions that could be used when two pieces of cables have to be connected together. However, to make lighter this part, it is better to explain firstly the most common methods used to perform electric field stress control and grading.

2.1.1 Field grading systems

Regarding medium voltage cable joints, electrical stress field control is required both at the outer semiconductor screen termination of the cable segment and at the cable connector position. In fact, as it will be explained in the 2.1.2 subsection, the cable joint installation requires the removal of both the cable shield and the outer semiconductive layer, external to the main cable insulation. Because of this, the electric field generated by the conductor is not confined anymore inside the insulation and critical electric field strengths occur at the cut edge of the outer cable seminconductive layer due to the densification of equipotential lines. Consequently, partial discharges or surface corona may occur in that region, reducing the lifetime of the entire system and enhancing the risk of breakdown [4]. In other words, the termination of the dielectric semiconductive screen produces an increase in the potential gradient between the dielectric and the surrounding space [2], as it can be seen in figure 2.1.

Considering the cable joint purpose, namely to electrically connect two cable segments, the removal of the cable shield and of the outer seminconductive layer is unavoidable since the inner conductor has to be made available for the connection.

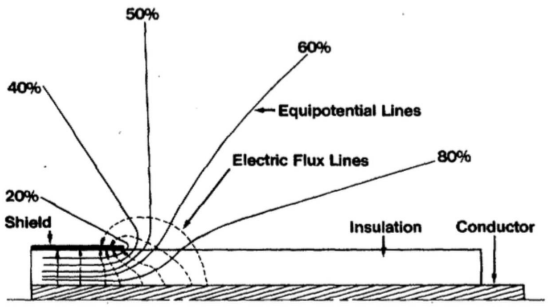

Fig 2.1: *Ungraded electric field equipotential lines at the dielectric semiconductive screen termination* [5].

Consequently, solutions to reduce the intensity of the electric field stress at the semiconductive screen end must be found. In particular, the two most common types of stress control used in cable joints to achieve a more distributed electric field are the geometrical stress control and the refractive stress control [3]. Other stress control technologies however exist, as impedance stress control or non linear stress control, but they are not analyzed in the present study.

2.1.1.1 Geometrical stress control

The main idea about geometrical stress control is to spread the equipotential lines more evenly by using a conductive cone shaped electrode (called also deflector) placed on the top of the cable, at the cut edge of the semiconductive screen. The equipotential lines follow the curved shape of the stress cone, especially designed for this purpose, resulting in a more uniform distribution of them, eliminating the high stress area highlighted in figure 2.1 with dashed lines. Thus, when the outer semiconductive layer is removed from a cable, the screen cut area is covered with a predesigned conductive cone, as rendered in figure 2.2, leading to a reduction of the potential gradient at the cable dielectric surface to a level in which discharges will not occur [2; 4].

The geometrical stress control is used in several MV and HV cable accessories and, in the case of cable joints, the conic electrode is nowadays directly extruded on the internal part of the main insulating body. In this way, the shape of the deflectors can be very carefully designed in order to spread the electric field present in the critical point

as much as possible. Sometimes, to achieve the latter objective, are used complex simulations and mathematical models, as it can be seen in studies [38; 39].

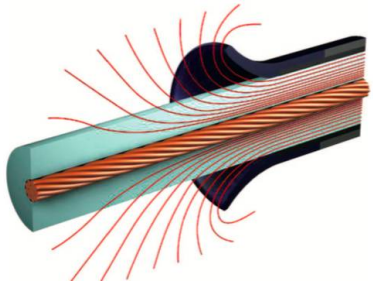

Fig. 2.2: *Field distribution in a cable end with geometric stress control* [4].

As it will be seen, this grading technology is used in general only in premolded cold shrink joints. In fact, variations of the designed cone shapes due to bad applications must be minimized: the installation and operative condition of stress cones are very important since stress control does not work properly if the ideal curve of the deflectors is deformed [6]. In other words, stress cones are used only in cold shrink cable joints since, during the installation of hot shrinkable insulating tubes, a not even application of the heat by the jointer might cause deformation of deflectors.

2.1.1.2 Refractive stress control

The main idea about refractive stress control is to use a layer of nonconductive material with high permittivity wrapped around the area where the electrical stress have to be lowered. As well explained in [4], this stress control method is based on the fact that the permittivity of the refractive material (ε_{r2}) is always much higher than the one of the cable insulation (ε_{r1}) and of the surrounding environment (ε_{r3}). Thus it holds :

$$\epsilon_{r2} > \epsilon_{r1} \geq \epsilon_{r3} \tag{1}$$

By figure 2.4 it can be seen that there is a change in the electrical field distribution where the insulation and refractive material are in touch. The magnitude of this

refraction is determined by the incident angle of the flux lines, passing from one dielectric to another, and by the ratio of the dielectric constant of these materials. Thus, as expressed by equation (2), the higher is the dielectric constant ratio, the farther the electric field will be refracted towards the cable end [5].

$$\frac{\tan(\alpha_2)}{\tan(\alpha_1)} = \frac{\epsilon_{r2}}{\epsilon_{r1}} \tag{2}$$

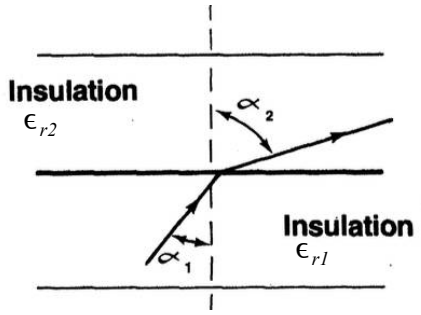

Fig. 2.3: *Electric flux refraction at dielectric interface* [5].

Hence, thanks to the latter equation, wrapping the cable end with material characterized by a very high permittivity, the equipotential lines are spread further apart determining an electric field coming from the cable insulation more gradually spread. The major limitation of this technique is the enhancement dielectric losses in the refractive material and, consequently, cable accessories in which this technique is applied must be designed with adequate heat transfer in order to avoid local overheating [4]. Furthermore, during the design of these kind of stress control system, it must be considered the fact that charge carriers may accumulate at boundaries between materials and affect the local field distribution [4]. Despite this, the use of high dielectric constant grading systems offers the advantage that, in order to achieve a more distributed electric field over the cable termination surface, only a simple extruded tube is used instead of a complex rubber molded stress cone: the device can be then more compact, while the same effect is reached [5]. Therefore, the use of these materials is extremely common for stress control purposes in polymeric cable accessories characterized by both hot shrink or cold shrink technologies. Furthermore, these materials can be provided in the joint kits as

separated tubes to be shrunk before the installation of the main joint insulation or, even better, they can be directly extruded on the internal part of the joint main insulation tube leading to a reduction of bad installation risks.

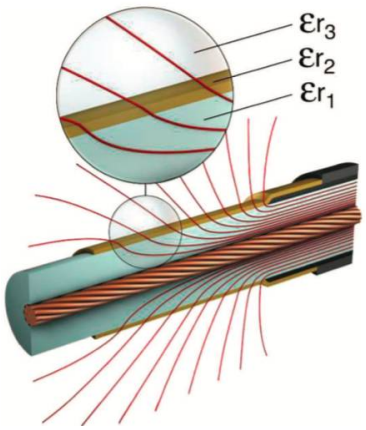

Fig. 2.4: *Field distribution of a cable end with refractive stress control material* [4].

2.1.2 Construction procedure

After the discussion about the needs of having a stress control on cable ends when the outer cable shield and semiconductor layer are peeled off, in the following the detailed joint construction procedure is going to be explained step by step. In this way, it is easy to present the main different types of medium voltage cable joint components that are used in practical applications.

2.1.2.1 Installation site

The first main aspect about joints that must be underlined is that, differently than power cables, which are extruded in factories in a controlled clean environment, the cable junctions are completely assembled and installed on field, where two cable lines have been already settled. Indeed, cable joint components are generally produced by manufacturers and sold to distribution utilities in kits that have to be mounted by expert workers at the installation site. Now, even if the environment in which cable segments

and joints are constructed is so different, it is required that they must have the same long term reliability. It follows that the joint installation is a crucial stage for the health of the entire cable line: the risk of contaminations or human errors during the joint mounting is very high. Thus, besides the obvious need of experienced jointers, also the characteristic of the installation site are very important. Best practice recommendations for a well planned joint site are [7]:

- a safe working environment;
- as dry as possible with no standing water in the working area;
- sheltered from rain and wind;
- free from contaminations as dust.

2.1.2.2 Cable preparation

The preparation of cable ends that have to be connected is the first stage of joint installation and it is required for all types of joints. It must be remembered that, in the present work, only procedures referred to polymeric cables are considered. The cable preparation is performed considering the purpose to provide a proper electrical and mechanical integrity when the joint connection will be installed. In particular, the preparation procedure basically consist in the accurate peeling of all the cable insulating and semiconductive layers, one by one, using special tools. The metallic shield is them stripped back or the cut: the different procedure depends basically on the type of conductive screen present in the cable segment, namely a shield with copper wires or with aluminum foil [44]. Starting from the end of a cable segment, the objective of the jointer is to organize it as in figure 2.5, obtaining as final result all the different cable layers separated with enough distance to make connections properly.

It has to be highlighted that, during cable preparation, the worker must use specific removal tools depending on the cable insulation material and manufacturer in order to not perform a bad cable peeling. In particular, much care must be taken in not making cuts on the insulation surface or making an irregular conductive screen edge. These errors must be absolutely avoided since they can determine, for example, the creation of

air voids in the interface between the cable insulation and the main joint insulation. These voids are the perfect environment for partial discharges that could possibly lead to early-life failures, as it will be more clear later. Hence, cable joint installers must be aware about these possibilities and pay great attention on the cable preparation stage.

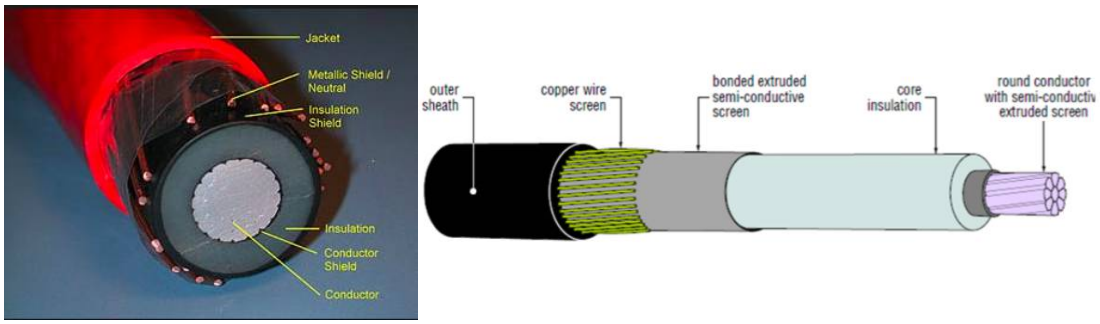

Fig 2.5: *Single-core MV cable with strippable insulation screen and copper wire earth screen before and after the preparation* [11; 7].

In the end, before installing the components of the joint kit, the prepared cables should be cleaned to remove any dirt and some insulating oil or grease should be spread over the cable insulation, using proper gloves [7; 44]. The reason of these actions will be more clear after the explanations about surface discharges, treated in section 2.3.

2.1.2.3 Connectors

Once the ends of both cable segments have been peeled off, the two bared conductors have to be tightly connected together, ensuring a good electrical connection. While the original method of making the connection between the two cable conductors was by soldering them, now this practice has been fully replaced by the use of metallic connectors which provide a reliable contact between the cables without the request of very skilled workers, as the soldering does [7]. In particular, the correct length of insulation have to be removed during the cable preparation to allow the full insertion of the bared wires into a metallic connector body. There are mainly two different connector types: compression connectors and mechanical (or bolted) connectors.

The compression connectors are constituted by a smooth aluminum or copper tube inside which the two conductor ends of the cable are inserted. Then, an hydraulic or

hand-operated press equipped with specially designed dies (indent, hexagonal or circumferential) is utilized to deform the metallic tube and produce a low resistance electrical contact with good mechanical grip between the two conductor ends [2].

Fig. 2.6: *Hexagonal compression die and copper compression connector* [7].

The mechanical or bolted connectors consist in metallic cylinders provided by screws which are tightened in order to make a strict contact with the internally placed conductors ends. In MV applications, most of those have shear-head screws where the head part of the screw breaks away when the correct tightening torque is reached [7]. After the screws break, the connector surface must be smoothened to obtain a cylindrical shape and so prevent electric field peaks: projecting points are removed with abrasive tools and semiconducting tape or mastic is usually added inside the holes left by the breaking of the screws [3].

Fig 2.7: *Bolted connector installation* [7].

Like compression connectors, also the mechanical ones provide a good connection also if they are installed by operators with lower skills comparing to the ones required for soldering. Furthermore, mechanical connectors have the advantage of not requiring

particular installation tools, as the compression ones. In contrast, they are more expensive due to the major manufacturing processes needed.

2.1.2.4 Main insulation application: heat shrink and cold shrink joints

After the installation of the connector, the joint main insulation has to be mounted. Its purpose is to protect the active parts from ground, as in a conventional cable line. Furthermore, since the removal of the shield over the cable insulation layer changed the radial symmetric distribution of the electric field and consequently high stress areas are created at semiconductor shield end, also the field grading system has to be installed. Its purpose, as previously explained, is to better spread the equipotential lines and eliminate the mentioned high stress regions. Now, cable joints can be categorized in different groups depending on the main insulation installation technology. In all the cases, the aim is to insulate the inner connector from ground using a tube made of dielectric elastomeric material that has to be shrunk as tight as possible around the connector itself. It is exactly this shrinking technology that differentiate the type of cable joint. In particular, the heat shrink joint type indicates that the insulating material tube and the cable jacket are tightened by heating; the cold shrink joint type indicates that the insulating tubes are stretched onto a plastic spiral and placed on the cable as they contract when the spiral is removed [8]. In the following, these two main insulating technologies are discussed more in detail considering also the most common field grading system used for every joint type.

The heat shrinkable property is created firstly by extruding or molding the polymeric material into the required cylindrical shape and then by crosslinking them. The components are subsequently warmed, expanded and cooled in this expanded state: when heat will be applied to the material, the memory given by the crosslinking causes the fact that the material tends to return to the shape in which it was crosslinked [2]. On medium voltage joint kits that are based on this technology some different heat-shrinkable tubes are usually present. They have different purposes, namely refractive

stress control, insulation, screening and environmental protection jacket. These tubes have to be concentrically heat shrunk one after the other. However, more modern joint kits include on one single heat-shrinkable body more tubes extruded together, as the stress control tube and main insulation, in order to ensure an easier and faster installation, making less probable human errors in shrinking the materials. The installation process of heat shrinkable tubes consists in the positioning and in the heating of them with propane or butane gas torches (figure 2.8) until the tube uniformly shrinks around the cable connector or around the underlaying tube [7]. It must be underlined that, before the tube shrinking, usually some void filler adhesive tapes are wrapped around the cable seminconductive screen ends and sometimes around the cable connector. Independently by the type of semiconductive screen or metallic shield removal method, this practice reduces the probability of air void formations in these high stress areas, after the installation of the tubes; it is an important practice, since, these voids are the region in which partial discharges, driven by the high electric field, are usually located, causing eventually the breakdown of the cable joint [9].

Fig 2.8: *Shrinking of joint insulation tubes* [7].

The heat shrink technology is widely used for junction applications due to its capability of covering wide ranges of cable types and sizes. However, its clear disadvantage is the need of heating means on site (usually a gas flame) and, mostly, the requirement of expert and skilled jointers able to shrink the various tubes in an uniform way, without creating dangerous air voids on the internal part of the insulating tube [10]. Cold shrink technology offers an application range in terms of cable sizes similar to that

of heat shrink one but without the requirement of heat application. Cold shrink technology is based on elastomeric flexible materials as silicon rubber (SiR) or EPDM. The insulating tube is pre-stretched by the manufacturer onto a plastic support tube or spring. When the spring is extracted by the jointer, the insulating pre-stretched tube collapses around the cable connector and tightly shrinks around itself, as it can be seen in figure 2.9. Cold shrink kits usually have fewer components than the heat shrink ones. In fact an important advantage of this technology is the possibility to combine independent functional layers over the same support: the stress grading tube, the main insulation and the semiconductive main insulation screen are usually molded in an all-in-one tube, making installation much faster and easier and minimizing the human error as much as possible [3; 10]. Furthermore, being elastomeric, a cold shrink tube continues to grip the cable after the installation, unlike an heat shrink one which freezes its state, becoming very hard after the application: cold shrink tubes are then capable to follow in a better way subsequent movements of the internal core, such as thermal expansions or contractions [2; 3].

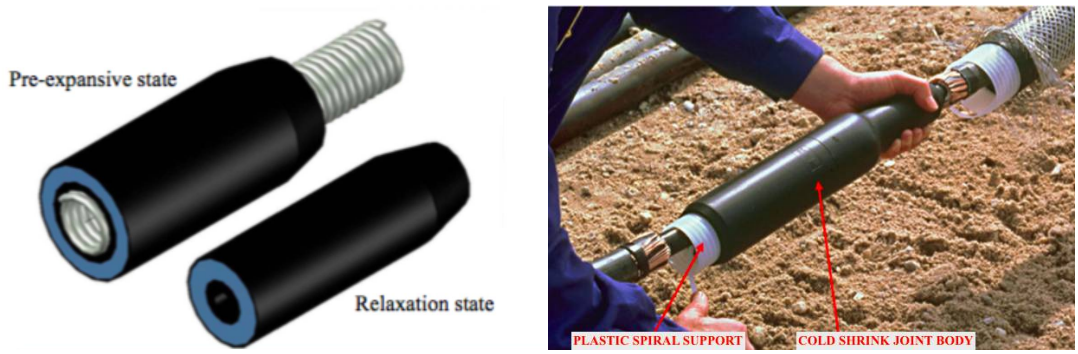

Fig 2.9: *At left, structures of the cold shrink cable joint under pre-expansive state and relaxation state* [15] *while, at right, installation of a cold shrink joint body with spiral tape holdout* [10].

For what concerns the field grading system present in this type of joints, both refractive stress control tubes or geometric grading deflectors can be used. Usually, in cold shrink tubes, the field grading system is premolded directly on the internal part of the main insulation body, regardless of the type of grading used. The use of one grading system instead than another one depends mainly by manufacturer choices.

2.1.2.5 Metallic shield and outer protective sheath

After the installation of the main insulation tube, in both cases of cold or heat shrink type, the cable joint looks as composed by an internal layer of field grading material, an intermediate layer of dielectric insulating material and an outer layer composed by semiconductive material. This external layer works exactly as the continuation of the outer semiconductive shield of the cable segment and has the same purpose, namely to provide a smooth and void-less transition between the insulating material and the external metallic grounded shield. In fact, after the installation of the shrinkable tube, an external metallic shield has to be wrapped around the joint ensuring the screen electrical connection, across the joint area, between the two jointed cable segments. The metallic mesh wrapped over the joint insulation has then the same purpose of the cable grounded metallic shield, namely to obtain a symmetrical radial electric stress within the dielectric by eliminating any longitudinal stress on insulation surface and to deflect any leakage current to ground.

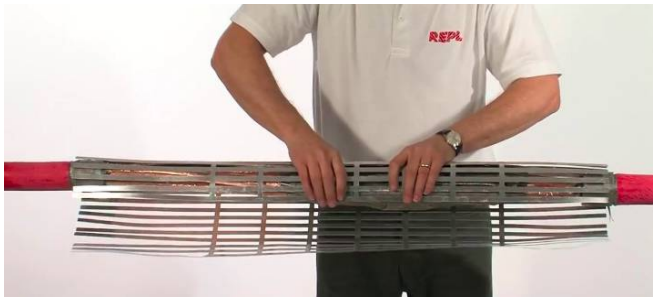

Fig 2.10: *Installation of the external metallic mesh on a three core MV cable joint* [12].

After the installation of the metallic shield, a final shrinkable layer must be installed: the outer sheath sealing tube. Its purpose is the same of the cable jacket, namely to protect the overall joint from moisture and water ingress and also to increase the mechanical and chemical resistance of the overall system. The outer sheath can be both heat or cold shrunk around the metallic mesh of the joint, usually depending on the tightening technology used for the inner insulating tube. However, the elastomeric materials used for the cold shrink joints cannot be used on every situation since, due to

their particular softness, they are not as strong against environmental stresses as materials used for heat shrink joints. Hence, in some cases, hybrid typologies of joints could be used, characterized by and internal main insulation body (together with stress grading and seminconductive shield) that is cold shrunk and by an outer protective sheath made of an heat shrinkable tube [3; 8]. In this way, the cold shrink benefit of an all-in-one insulation body are kept but the external mechanical strength is increased.

2.1.3 Cable joint overall view

After the description of the procedures needed for the jointing of two medium voltage cable segments, it is useful to give an overall view of two completed medium voltage straight single core joints, one characterized by the heat shrink technology and the other by the cold shrink one. It must be remembered that, in reality, the design of cable joints, even if they are characterized by the same stress grading and shrinking technologies, could vary between different manufacturers.

In figure 2.11, coming from a Tyco Electronics power cable accessories catalogue [9], the exploded view of an heat shrink cable joint with refractive tube as field grading system can be seen. Besides the bolted grey cable connector and the XLPE light blue cable insulation, it can be noticed also the semiconducting void filler yellow tape wrapped around the semicondutive cable shield end. As said, the tape purpose is to provide a smoother and void-less surface transition between the peeled cable semiconductor and the cable dielectric material. Furthermore, it can be recognized:

1. the electrical stress control tube that providing a smoothing action on the electric field over the connector and cable screen ends through refracting grading principles;
2. the EPDM/EPR insulation joint body and the black outer insulation screen composed of heat shrinkable conductive polymers;
3. the metallic joint shield that ensures the correct cable screen connection across the joint and makes possible the electrical contact with the outer joint screen;
4. the outer protective joint sheath.

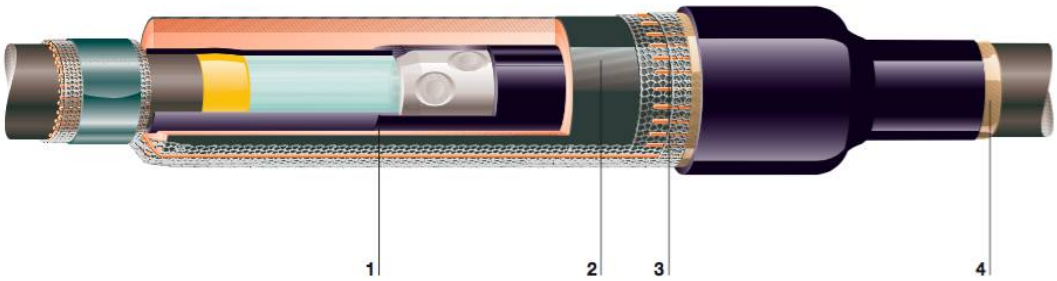

Fig 2.11: *Heat shrink medium voltage cable joint* [9].

In figure 2.12, taken from an REPL cable accessories product catalogue [13], the exploded view of a cold shrink joint with geometrical grading cones premolded inside the cold shrink joint body is represented. It can be recognized:

1. the bolted cable connector;
2. the XLPE cable insulation;
3. the semiconductive cable screen;
4. the stress control deflectors placed over the cable screen cut;
5. the seminconductive inner layer, placed around the connector to make the inner high voltage electrode more cylindrical shaped leading to a more radial electric field in the middle of the joint insulation;
6. the silicon rubber joint insulation body;
7. the semiconducitive joint insulation outer screen;
8. the metallic mesh connecting the shields of the two jointed cable segments;
9. outer protective joint sheath.

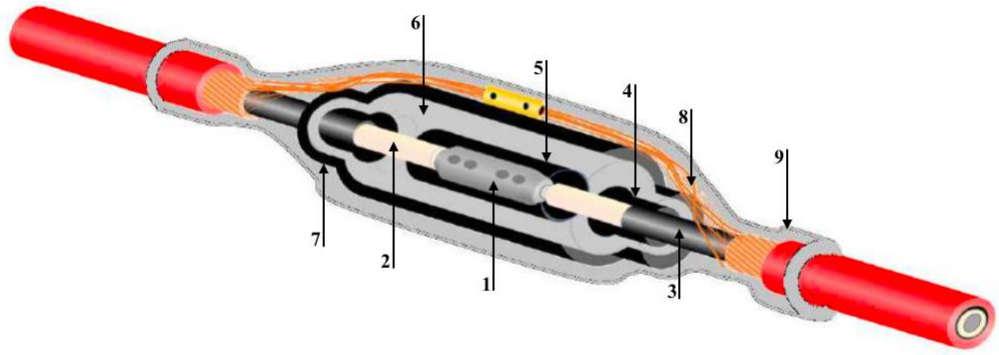

Fig 2.12: *Cold shrink medium voltage cable joint* [13].

2.2 Analysis of cable joint failure rate

It has just been analyzed the joint structure and constructing procedure. The main consideration that stands out is that a cable joint system shows a visibly more complex structure than cable one. Furthermore, as previously said, cable joints are assembled on-site by hand working while cables are completely made on factory mainly using automatized extrusion processes. This fact leads necessarily that, on cable joints, the risk of installation based defects due to poor workmanship is higher than in any other component of the cable line. In particular, by considering that a typical medium voltage line can be several kilometers long with about fifty cable joints made by different workers with different abilities and in various site conditions and by considering that a single cable joint fault leads to the outage of the whole cable line where it is installed, it can be understood how critical these components are.

In a wide and precise study about statistical life data analysis on MV cable joints [14], the following conclusions have been obtained analyzing the record of failures happened on a particular Dutch region: more that 80% of power-delivery outage related failures in 10 kV medium voltage networks were caused by failures in cable systems and approximatively 65% of cable line breakdowns were caused by internal component related defects while the remaining 35% of failures were caused by external defects (such as excavator digging); considering the 65% of internal component related defects, the majority of failures (44%) occured in cable joints. Other statistical data referred to the Chinese cable network show that, considering cable faults, in the recent 10 years even the 63% of them is caused by cable joints breakdown [15]. Also failure statistics presented in [17] about the Norwegian grid show that joint failures are one of the major causes of cable line outages (figure 2.13). From what said, it can be concluded that cable joints are, in most of the cases, the weakest link of the whole cable system and that they are the component that mostly affects the reliability of cable lines. The fact that joints are subjected to an higher number of failures than cable segments is intuitive since, as mentioned above, premature faults in joints could derive not only from

manufacturing defects in the factory or in-service issues (as strong overvoltages) but there is also an high probability that they could be caused by errors during the hand-made installation on site. In fact, as stressed many times, the quality of these accessories is strongly sensitive to worker experience and care. Furthermore, as highlighted in [14], joints are subjected to higher electrical, mechanical and thermal stresses comparing to cable segments, they are mounted in field, very often under non-ideal circumstances, and expensive reliability testing procedures are not usually performed.

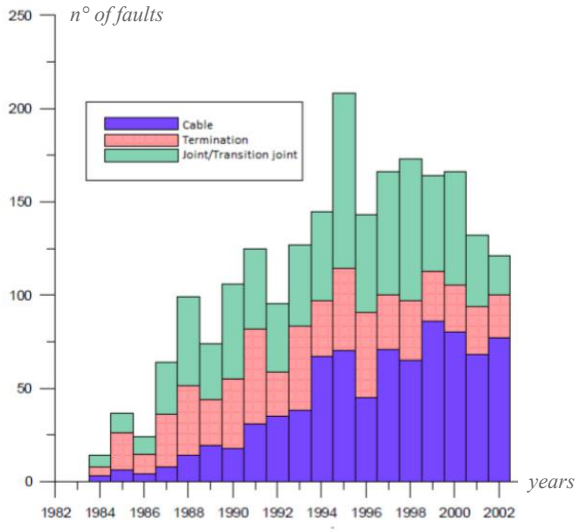

Fig 2.13: *Failure statistics for Norwegian grid owners. XLPE cables and accessories* [17].

The most common causes of joint faults, induced by either operational, environmental or human induced stresses (or a combination of these), can be identified in the following list of defects [3; 14; 16; 17] :

- sharp edges on connectors that locally increase the electric field;
- moisture, water and dust ingress;
- irregularities in the surface of the cable insulation causing voids;
- air voids between different heat shrink tubes;
- faulty positioning of the cold shrink body;
- bad peeling of the cable semiconductor layer;
- cable insulation incisions.

Basically, the presence of large voids due to irregularities in the inner surfaces determines the initiation of internal or surface partial discharges while the ingress of water and moisture determines the initiation of the water treeing phenomenon. In these cases, the joint breakdown might be only a matter of time: the life of the cable accessory is expected to be definitely decreased in comparison to the design one.

The study already mentioned presenting cable fault statistics in China [15] not only shows that the 63% of cable line outages is originated by cable joints faults but also underlines that the 73% these faults are caused by interfacial discharges. In [19] even higher percentages are presented. Now, a cable joint, as it has been said in the latter section, could be constituted by several kinds of dielectric interfaces (due to the presence of many concentrical layers of different materials): the most critical one affecting the electrical performance of the system is the interface between the cable insulation and the internal part of the joint insulation body, as shown with red dotted lines in figure 2.14.

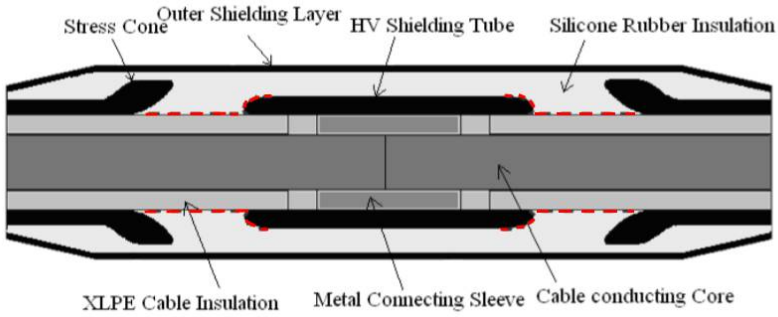

Fig 2.14: *Schematic diagram of a prefabricated cold shrink joint body with the critical interface highlighted* [15].

This interface is considered to be the weakest part of the cable system because phenomena as mechanical relaxation, variations in interfacial pressure or reduction of interface fit could cause the decrease of the dielectric strength in the interface region, leading to stronger surface discharges and, eventually, to tracking failure [18]. It must be underlined that “tracking failure” is the name given to the breakdown phenomenon

characterized by the total bridging between the HV electrode and the grounded cable semiconductive shield through a discharge on the concerned interface. This discharge occurs after the formation of a conductive path linking the electrodes that is originated thanks to small partial discharges happening in microscopic imperfections (as cavities, protrusions or contaminants) located at the interface. Moreover, as it will be wider explained in section 2.3, on these joint regions is present an AC electric field characterized by high magnitude of tangential component. This fact tend to further increase the strength of partial discharges in the microscopical air voids located at the interface and to orient them on a direction parallel to the interface itself.

Many studies analyzed in general the breakdown characteristic at the interface between two dielectrics [22; 27; 29; 30; 31; 33]; other studies analyzed also the interfacial breakdown properties under different pressures [18; 21; 23; 28; 32] or with different surface roughnesses [19; 20; 28] and also the effect of joint body deformations after the installation on the electric field distribution at the interface [15]. In all these investigations it is always strongly affirmed that the interface between the cable insulation and the joint insulation is unavoidably the weakest point in cable joints due to the always high risk of interfacial tracking failures. Hence, since interfaces are considered the most critical point of cable joints and since cable joints are considered the most critical part of the cable system, it is convenient to go deeper in this subject, as done in section 2.3.

At last, it must be put emphasis on the fact that the fault of only one cable joint leads necessarily to the outage of the whole cable line in which it is installed. This results in costly and time consuming maintenance since the whole component has to be replaced by hand working. Furthermore, these failures in distribution cable lines cause discomforts on the final users that experience long electric power interruptions. It is then important to avoid as much as possible such line failures by performing predictive maintenance, line analysis, measurement of health parameters and condition assessment particularly on cable joints.

2.2.1 Influence of ambient temperature on cable joint failure rate

It has just been explained that joints are considered the most vulnerable component of the underground cable network, being characterized by the highest failure rate. Now, cable joint failures seem to don't have a constant distribution in time. Considering one calendar year, some on-site studies show that failures of medium voltage underground cables, and especially their joints, are concentrated during the summer period, when environmental temperatures are higher [24; 25; 26]. This behavior has been recorded in Italy by the Italian electrical energy distribution utility ENEL Distribuzione through data analysis of medium voltage underground cable failures occurred in the territory of Lazio, Abruzzo and Molise [26] but also on the territory of the city of Palermo [24]. In particular, during the period 2010-2013, on the territory of Lazio, Abruzzo and Molise has been occurred 2660 failures on medium voltage cable lines, two third of which involving cable joints: about the 60% of these joint failures occurred in the summer period, as it can be seen by figure 2.15. The same failure pattern in relation to year months has been found by a study collecting cable joint failure data in Netherlands, where also the temperature of the soil on the cable joint surrounding area has been monitored [25]. In figure 2.16 are represented the results of this study where in the left plot are represented the average failure per month occurred in the period 2002-2006 and on the right one are represented the joint failure data per month occurred only in the year 2006. It must be underlined that, in all the three mentioned studies, the cable joints where buried under one meter of soil, hence not directly affected by temperature changes. Furthermore, in all the three cases, the monitored cables were very low loaded. In particular in [25], in order to determine if the current had some contribution in the failures, it was analyzed if a current increase could be found in the cables under observation before one failure occurrence. However, no significant changes could be seen which could be related to joint failures. Also in [26] is evidenced how the underground temperatures, also in the proximity of cable line, were independent from the transmitted current, due to the very low electrical load.

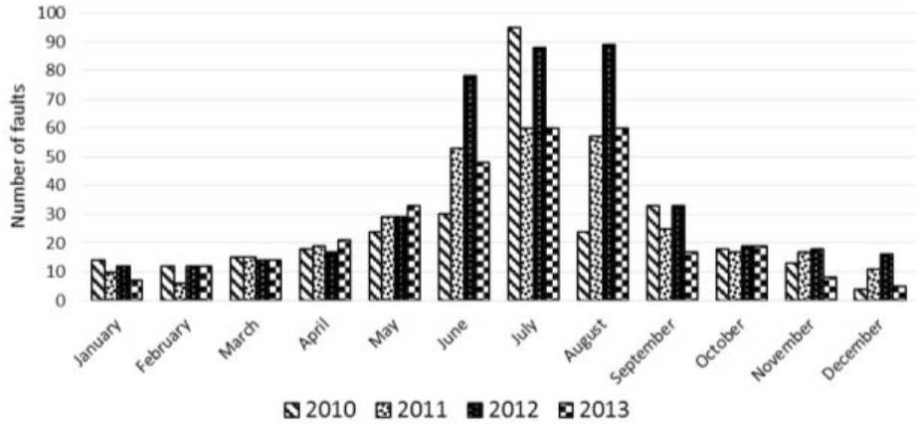

Fig 2.15: *Monthly distribution of failures of joints of MV underground cables recorded on years 2010-2013 in the territory of Lazio, Abruzzo, Molise* [26].

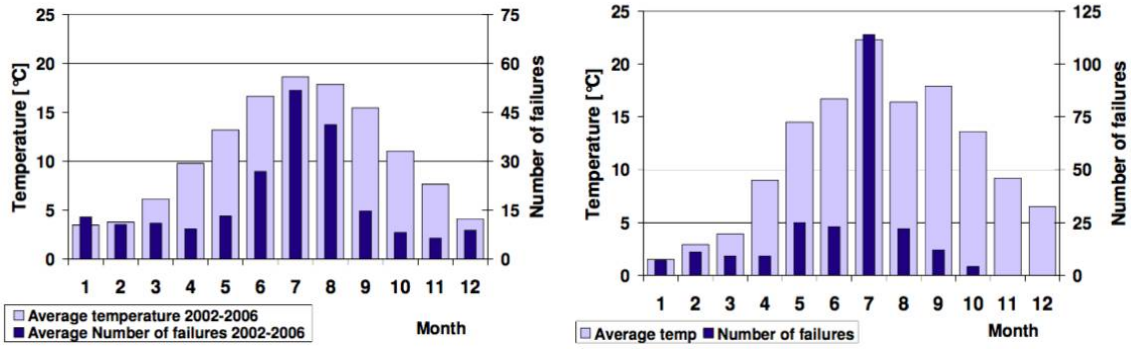

Fig 2.16: *at left average ambient temperature per month and average number of cable joint failures recorded in the period 2002-2006 and at right the data of only year 2006* [25].

In [25] it has been recorded that the peaks in the average daily ambient temperature are often followed by an increasing number of failures. In [24], the day-night temperature cycles at joint site has been recorded, together with external pressure and relative humidity, which have not shown particular changes over time.

From these studies, the high correlation between number of joint failures and ambient temperature indicate that possibly there could be a relation between these two phenomena. An explanation of this fact, proposed in [26], might be obtained considering the Arrhenius's Law which, briefly, states that an increment in temperature is always followed by a reductions of the life of any insulating material. This is due to an enhancement of insulation degradation processes linked with temperature rise: premature failures of cable and joints are then expected to increase as well.

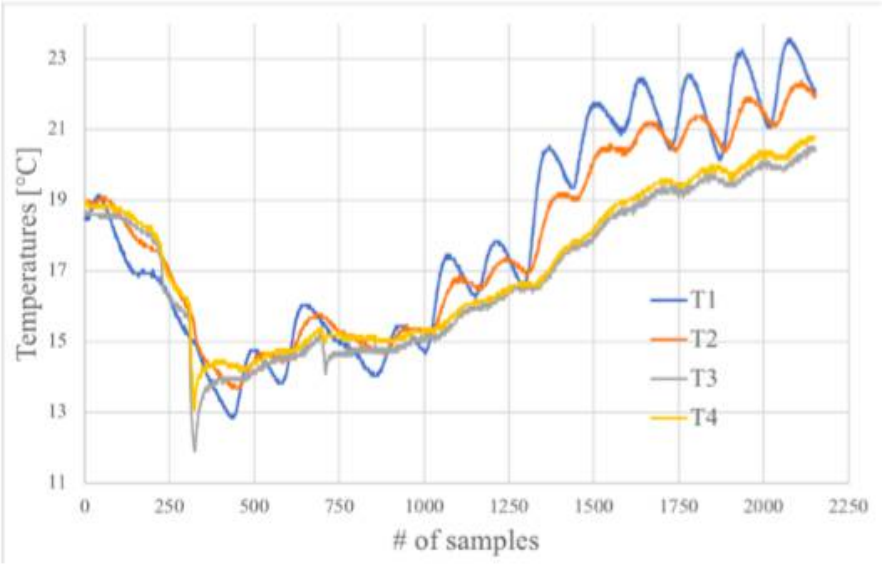

Fig 2.17: *Nine days temperature acquisition: temperature T1 above the asphalt, T2 in the middle between surface and joint, T3 and T4 and the end and in the middle of the joint buried at one meter depth* [24].

However, the great increase in joint failure rate registered in the mentioned studies could be not only related to the accelerated aging of joint insulating materials due to higher summer temperatures, as stated by the Arrhenius' Law. In fact, the recorded temperatures were always inside the capability limits of cable segments and joints. In particular, it must not be forgotten that cable joints are hand-made systems with a lot of weak points, as highlighted in the previous sections. Then, also as suggested in [24] and [26], the continuous day-night temperature variations coupled with the higher mean temperature during summer period may cause instabilities inside the joint structure leading to the formation of microscopic voids where partial discharges may occur, becoming the starting point of premature joint faults. Furthermore, thanks to polymeric material relaxation phenomena driven by temperature variations, cavities at dielectric interface could increase in number and dimension, increasing the risk of surface tracking. However, further investigations have to be done on that topic.

As suggested in [24], it is advisable to perform better studies on parameters and indices related with insulating heath of joint systems, as loss factor and partial discharge measurements. It may be also useful to measure the rate of variation of health indices in

relation to temperature cycles on cable joints applications trying to infer the causes that lead to a such high increase of joint failures during the summer period. The objective of these researches is also to find a convenient and effective method to perform monitoring of cable joints health condition on-site. This might lead to a decrease of cable line outages and disservices, being then able to schedule predictive maintenance actions. In particular, in the present thesis response of the loss factor, measured in some cable joint samples, is analyzed in relation to hot-cold temperature cycles.

2.3 Theory of interfacial discharges

By analyzing the literature about breakdowns on surfaces between two solid dielectrics, the aim of this section is to present the mechanisms of the interfacial breakdown phenomenon and the parameters that mostly affect it. In fact, a better understanding of the tracking failures is required since, as affirmed in section 2.2, according to statistics they are one of the major causes of cable joint failures. As a consequence, the interface created between the cable dielectric and the shrunk joint insulation has necessarily the bad reputation to be one of the most critical region of the cable joint system, namely of the entire power cable network.

Generally, all electrical insulation systems consist unavoidably of a combination of different insulating, conductive and semiconductive materials. As it can be inferred by figures 2.11 and 2.12 but mostly by figure 2.14, in the case of cable joints a solid-solid interface exists between the cable dielectric material (generally XLPE) and the shrunk insulating material of the joint (generally SiR or EPDM/EPR). Now, obviously the cable joint has to be designed to withstand the service electrical stress of the cable system in which it operates. The overall breakdown strength of a complex insulation system, as it is the one of a cable joint, is not defined as the breakdown strength of the main joint insulating material but it strongly depends by the lowest breakdown strength of the system, namely the one of the interface between the different insulations, as it is going to be explained. In fact, as presented in different studies [20; 21; 27; 28], the

combination of two solid dielectrics causes the formation of voids at the interface due to microscopic imperfections, such as protrusions or contaminants; then the real area of contact between the two solids is smaller than the apparent one. The polymeric interfaces in cable joints are usually made of a soft and an hard material (for example XLPE-EPDM or XLPE-SiR) in order to reduce as much as possible this phenomenon. In any case, the formation of microscopic cavities is unavoidable during the contact between two solid surfaces also because the assembly of system like joints is not done with an automated process under clean room conditions [20; 28].

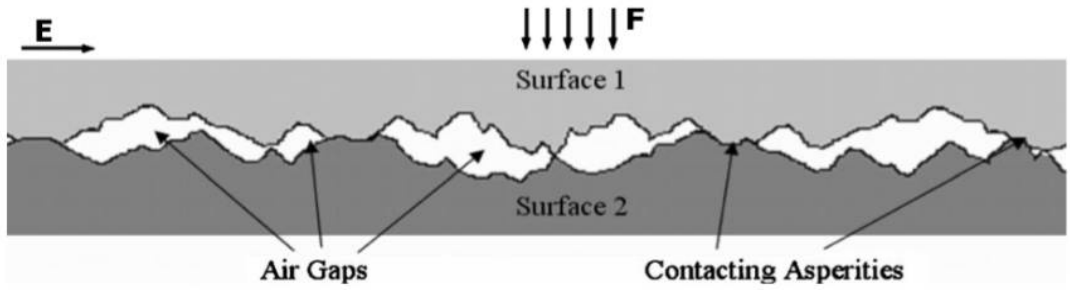

Fig 2.18: *Schematic illustration of a solid-solid interface. The total contact area consists of voids and contact spots* [27].

2.3.1 Mechanism of interfacial breakdown

When the interface is assembled under dry conditions, the cavities are filled with air and, being the dielectric strength of air is much lower than that of the polymeric insulation, the breakdown strength of the voids is necessarily lower comparing to the surrounding bulk insulation one [28]. By using insulating liquid or gel, as mineral oil or silicon grease, before assembling the two dielectrics, the breakdown strength inside the voids could be increased but, in any case, it results to be considerably lower than the bulk insulations one [27]. Therefore, when an electrical field crosses the interface, there is an high risk of partial discharge initiation inside the cavities. In particular, the worst situation arises when an high electrical stress is applied in parallel to the interface, namely when the electric field that crosses the interface is characterized by an high tangential component, considering the interface direction. In fact, looking at figure 2.18,

the interface can be considered as a string of voids having lower dielectric strength comparing to the contact spots that keep the voids apart. In [21] a model of the interface consisting of a series of connection of spherically shaped voids and contact region is presented, as shown in figure 2.19.

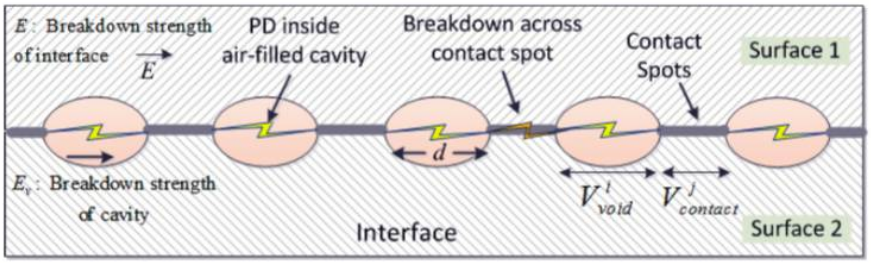

Fig 2.19: *An electrical model of interfacial breakdown* [21].

The initiation of partial discharges inside the cavities, on a direction parallel to the interface, is driven by the the tangential electric field. This phenomenon is assumed to be the main mechanism that might lead to the total interfacial breakdown. Indeed, during the partial discharge activity, the breakdown of the gas inside the void causes the slow but gradual degradation and carbonization of the polymeric material of the contact spot, eroding it and releasing conductive materials in the internal boundary of the contact spot. That eroding action determines, in the time, the breakdown across some contact spots. The spot breakdown is also due to a localized electric field enhancement caused by the short circuiting of the voids during the partial discharge action [21; 27]. Hence, a conductive paths starts to bridge the voids along the interface and a complete longitudinal breakdown of the interface is only a matter of time.

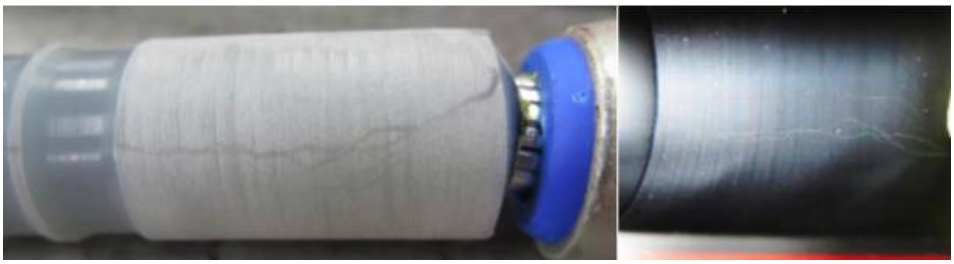

Fig 2.20: *Electrical tree formed on the interface between the cable insulation (at left) and the internal part of the joint tube (at right)* [3].

It must be underlined that, unluckily, the interface region of cable joints is the point in which the tangential component of the electric field distribution culminates. In fact, even if field grading strategies are adopted ensuring that the electric field crosses the interface as gradually as possible, tangential components of the electric field will be always present, due to the unavoidable particular geometry of the joint. This phenomenon can be appreciated in figure 2.21 where the equipotential lines of a cable joint with geometrical field grading are plotted together with the interfacial electric field stress, split in normal and tangential component. Cable joints with refractive stress control have a similar electric field distribution too [9; 34]. Hence, the problem of interfacial discharges is absolutely a topic that have to be considered in the design and in the installation of cable joints. In particular, it is important to analyze the parameters that affect the interfacial breakdown strength in order to understand how practically manage the harmful phenomenon of interfacial discharges and then recognize the situations in which it is most probable that surface tracking could happen.

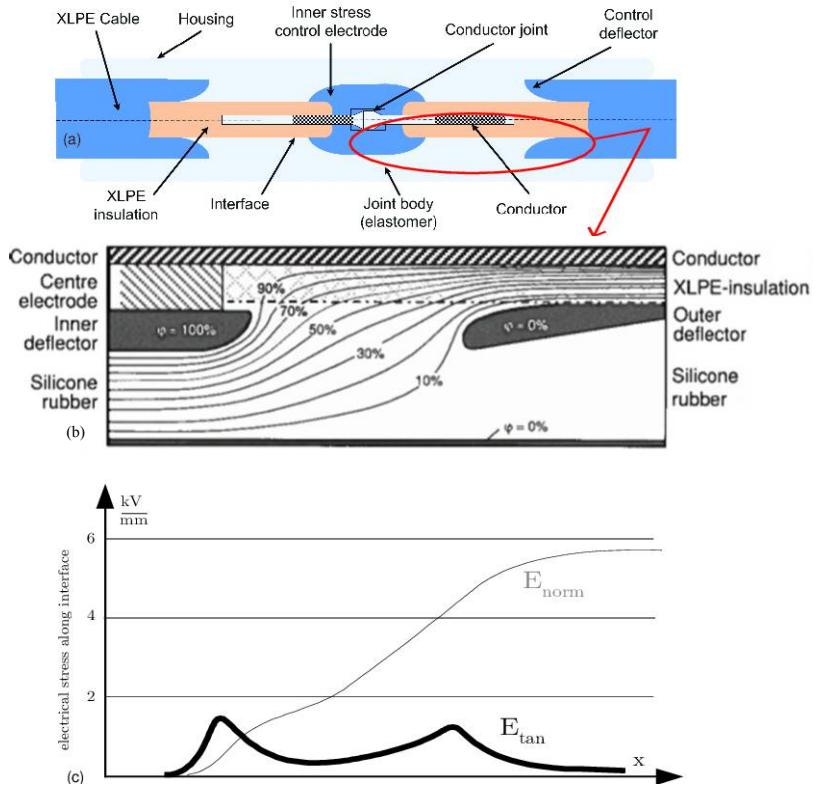

Fig 2.21: (a) *Section of a prefabricated silicone joint.* (b) *Equipotential lines distribution.* (c) *Normal and tangential electrical stress plot* [20; 27].

2.3.2 Parameters affecting the breakdown strength at dielectric interfaces

The latter treatment presented the reason why air-filled cavities are considered to be the preferable starting points for the tangential breakdown paths that propagate along the contact area of two dielectrics. It has also been said that these voids are unavoidably present in hand-made assembled dielectric systems as cable joints are. In order to avoid the arise of partial discharges on the interfacial voids, as mentioned before, the use of insulating liquid or greases while assembling the two dielectrics could increase the breakdown strength inside the cavities, increasing then the ignition voltage of partial discharges. However, two other aspects have to be taken into the account. In particular, to avoid partial discharges, the cavity size has to be kept at the minimum possible, namely the real contact area between the dielectrics should be as large as possible: the real area of contact (and consequently the dimension of the voids) strongly depends on surface roughness and contact pressure at the interface [21; 22]. Hence, also these two parameters affect the breakdown strength of the interfacial voids.

2.3.2.1 Effect of insulating liquid or grease

In practical applications it is common to apply insulating oil or grease over the cable dielectric before the application of the main insulation tube of the joint. This dielectric grease has basically three functions: lubrication, anti-seizing and, mainly, void filling. In fact, in case of rough interfaces, greasing is found to play an important role in eliminating air cavities: filling the voids with liquid insulating material, which has an higher breakdown strength comparing to the air one, improves the dielectric performance of the interface quite a bit. Results from the experimental work [22] show that, in case of sanded surfaces (thus highly rough with many big air voids), greasing has the effect to increase of the 40% the tangential breakdown strength of the interface. Another similar experimental work [32] reported that, by filling the cavities with the application of silicone grease on both the surfaces to be put in contact, the interfaces tends to work as a perfect blend of two bulk dielectric. In fact, the interfacial dielectric

strength is in this case ~2.7 times higher than the one of an interface without silicone grease and, furthermore, it seems to obey to the same law as the one which rules the dielectric strength of bulk EPDM (differently than in case of a dry interface without the grease). In [31], experiments show that the application of silicone grease to the interface leads to retardation of surface discharges and to an increasing in the surface partial discharges inception voltage. Now, it must be considered that greasing may not eliminate all air cavities and that, with aging, the grease tends to dry as a small quantity of oil migrates out of it: small air cavities might arise at the rough interface causing reductions of the interfacial dielectric strength [22]. Also experimental results in [29] show that the grease properties noticeably degrades with aging.

2.3.2.2 Effect of surface roughness

The experimental work [22] investigates the effect of surface roughness on the breakdown voltage of EPDM-XLPE and EPDM-EPDM interfaces considering a tangential AC electric field component applied. The results show that the dielectric strength of smoother interfaces are consistently higher that the one of rougher interfaces due to the presence, in the latter, of more and bigger interfacial voids in which more powerful and harmful dischargers will initiate. Furthermore, it has been reported that the dielectric strength of a smooth EPDM-XLPE interface is higher that that of a smooth EPDM-EPDM interface and, furthermore, it has been argued that possibly this fact is due to the better charge trapping at the XLPE surface [22]. Also in other experimental works [20; 28] the breakdown test performed on dielectric interfaces showed that an increased interfacial roughness results in a reduced interfacial breakdown strength due to the higher peaks and deeper valleys formed in the surface profile leading to the presence of larger cavities at the interface. Even in [19], thanks to the tests performed, it has been concluded that, increasing the interfacial smoothness, the occurrence of oxidation reactions and the formation of carbonization paths at the interface become more difficult and, therefore, the initial discharge voltage, the tracking failure voltage and the time to tracking failure show an increase in comparison to a rougher interface.

Concluding, through the results of the latter studies it is possible to affirm that, in order to improve the performance of the interface created between two polymeric dielectrics, two materials having surfaces as smooth as possible must be used. Consequently, the sanding of the cable dielectric surface in cable accessories should be absolutely avoided.

2.3.2.3 Effect of contact pressure

The effect of the interfacial pressure on partial discharge inception voltage has been investigated experimentally in [18]. In this study, it results that the initial discharge voltage in an XLPE-SiR interface shows an increasing value when the interfacial pressure rises. Furthermore, in this case, the tracking failure needs a longer time to occur. The same phenomenon is observed in [21] where the increase of longitudinal breakdown strength with rising contact pressure is explained to be due to the fact that the diameter of interfacial cavities is expected to significantly decrease by applying higher pressures. In particular, as explained in [27], considering figure 2.18, the effect of an increment of the normal force F is to increase the number of contacts between surface asperities leading to a large contact area for supporting the increasing mechanical force. Consequently, this phenomenon also causes the reduction of interfacial voids dimension: the real area of contact between the two dielectrics is consequently higher. It must be remembered that a decreasing diameter of the cavities restrains the initiation of partial discharges since the inception voltage consequently increases. Hence, the propagation of the consequent carbonization of the contact spots is more difficult with smaller cavities. So, the full breakdown of the interface is expected to be much less likely if higher contact pressure is present.

Also other studies have been made on this field, as [30; 31; 32], always finding that an higher interfacial pressure leads to an higher dielectric strength of the interface. In particular, in [30] EPDM/EPDM and EPDM/XLPE interfaces were tested considering also aging processes; it has been obtained that EPDM/EPDM interfaces seem to maintain dielectric strength with aging much better than the EPDM/XLPE ones. Also in [29] aging tests on EPDM/EPDM and EPDM/XLPE interfaces are performed finding

that the dielectric strength of unaged interfaces is visibly higher than aged ones and arguing that this result could be due to degradation of the interfacial pressure of the interfaces themselves. At last, in [33] XLPE-SiR interfaces are analyzed, emphasizing the fact that the majority of premolded joints are made by silicon rubber: their mechanical performance degrades after operation for several years resulting in the decrease of interfacial pressure and then, as shown in the study, to a decrease of breakdown voltage. Concluding this speech, it must be paid much attention during the installation of cable joints, especially the heat shrink ones, in order to avoid the loss of interfacial pressure. The more care is taken in the joint insulation installation, the more is lengthened the life-span of cable joints, avoiding premature interfacial breakdowns.

2.3.3 Considerations about cable joint installation

Summarizing what it has been just presented, the breakdown strength of a dielectric interface increases if:

- the applied pressure increases;
- smoother dielectric surfaces are used;
- the voids at the interface are filled with insulating liquid or grease.

Hence, also as concluded in [31], tightly fitted, smoothed and dry interfaces equipped with a layer of silicon grease have the best performance, as it can be seen also from figure 2.22. In particular, this diagram refers to an XLPE-XLPE interface but, in any case, the graph trend is expected to be the same also for XLPE-SiR or XLPE-EPDM interfaces thanks to the results found in the different studies explained before. The graph shows that, in case of absence of insulating grease, the breakdown strength of the interface is always higher that that of air but not as strong as the bulk material strength, even under very high contact pressure and surfaces smoothness. However, as also underlined in [20], interfaces could perform similarly as the bulk materials when an insulating grease is present, the applied pressure is high and the the contact surface is as smooth as possible. Thus, concluding, during the installation of power cable joints much

care must be taken in smoothing interfaces as much as possible, in applying an uniform grease layer and in performing a good tightening of the shrinkable joint tubes. The attention on the respect of these actions by the jointers is then fundamental: from the care taken in the installation of the interface depends the strength of the cable joint from harmful interfacial partial discharges.

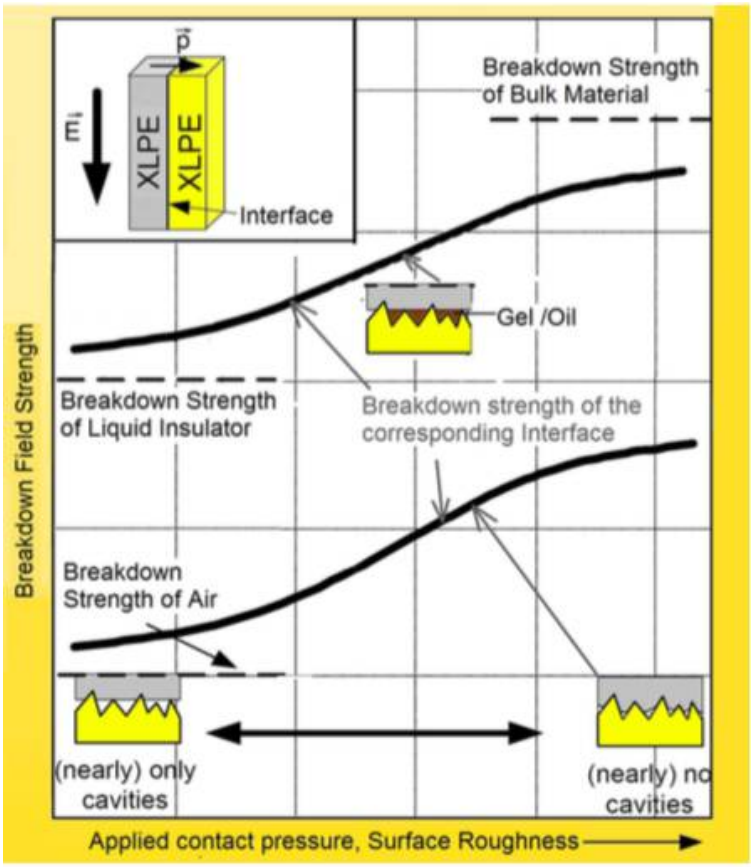

Fig 2.22: *Tangential breakdown strength of interfaces versus applied contact pressure and surface roughness* [27].

Obviously, jointers must be also careful in avoiding the ingress of contaminants as water or dust that could possibly fall on the interface during the installation. In fact the existence of water droplets or conductive particles at the interface cause a strong reduction in the breakdown strength of the insulation system being extremely easier, in this case, the formation of a conductive path that bridges the high voltage electrode and the ground electrode of the joint.

2.4 Theory of loss factor

As mentioned before, the present study focuses on loss factor measurements in cable joints and in their possible correlation with temperature variations of the cable accessory. On this section, it is briefly explained what practically the loss factor is and why it can be used as diagnostic tool for electric insulating systems.

Ideally, a dielectric material should behave as a perfect capacitance when inserted between two parallel conductive armatures. In this case, if a sinusoidal voltage V is applied to the material, the sinusoidal current flowing through the dielectric is expected be a pure capacitive current, shifted then by 90 degrees compared to the applied voltage. In this ideal case, the active power dissipated in the insulating material should be equal to zero. Now, in the real world, dielectric materials show inherent losses since they are characterized necessarily by finite value of resistance. Furthermore, there could be impurities in the insulation and defects in the installation or in the production of the material itself that could further reduce its resistivity. So, in this case, a dielectric material inserted between two parallel conductive armatures cannot be represented anymore by a simple capacitance: a resistor in parallel to the capacitor should be added in order to account the losses generated in the material when a sinusoidal voltage is applied. In reality, the resistor that models the conduction losses could be placed either in parallel or in series with the ideal and lossless capacitance, depending on the electric system that has to be modeled [55]. Taking into the account shielded medium voltage cables and referring to the IEEE Guide for Field Testing and Evaluation of the Insulation of Shielded Power Cable Systems [45], in this case the insulation system is modeled as a capacitance C, representing the capacitance between the conductor and the external shield, in parallel to a resistance R, that stands for the real power losses on the insulating material itself. In the present study, being the overall geometry of a medium voltage straight cable joint similar to the one of a shielded cable, in order to give the definition of the loss factor, the parallel model is used.

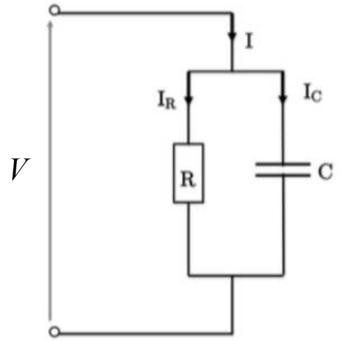

Fig 2.23: *Equivalent parallel circuit for a real insulating material* [36].

Because of what previously explained, considering a sinusoidal voltage V applied to a dielectric material, the current I flowing through it is no longer shifted by 90 degrees from V but it expected to be shifted by a lower angle. In fact the total current I is now constituted by two components: the current I_C , which has 90 degrees of phase shift to the applied voltage, and the current I_R , in phase with the applied voltage. The phasor diagram relative to the circuit in figure 2.23 is represented in figure 2.24:

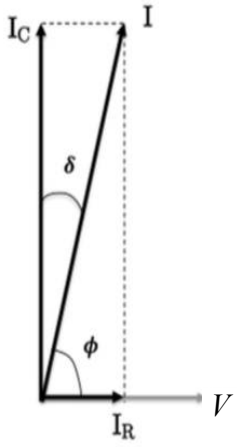

Fig. 2.24: *Phasor diagram for the parallel equivalent circuit* [36].

In general, the resistive current component I_R is much smaller than I_C . In fact, it is true that the insulating material has a finite value of resistance but, despite that, its

resistance is usually characterized by an enormous value and, so, the resistive current magnitude results to be much lower in comparison to the capacitive one. In other words, the capacitive impedance is usually expected to be much lower than the resistive one. As presented in [36], using the geometric relations of figure 2.24, the value of the tangent of δ, namely the angle between the total current and the capacitive current component phasors, can be simply expressed as the ratio of the magnitude of the resistive and capacitive current components:

$$\tan \delta = \frac{I_R}{I_C} \tag{3}$$

Therefore, tan δ, also indicated as loss factor, dissipation factor or tangent delta, can be defined as a relative measure of the amount of the real power dissipation in a dielectric material, being directly proportional to the resistive current component magnitude. The tan delta measurement on an electric insulation apparatus can be then used as a diagnostic test that permits the assessment of the state of aging or damage of the cable insulation [35; 37]. In fact, the more resistive current flows through the insulation, namely the more the dissipation factor is high, the more the insulating material is losing its dielectric properties since higher resistive losses are occurring over it. This fact could be due to aging or other causes as, for example, the introduction of contaminants inside the dielectric. Hence, as indicated in [45], the loss factor measurement can be used as diagnostic technique also on cables, estimating the general condition and the quality of their insulation system, considering a same system under the same voltage level and frequency.

It is important to notice that the tan delta method is able to assess only the overall condition of the insulation under test. Indeed, using this index it is not usually possible to differentiate specific defects, as for example it can be done with the analysis of partial discharge patterns. Furthermore, the loss factor method is effective only as a trend measurement since, from a single measurement of tan delta, only a rough degree of insulation system degradation can be obtained, mainly based on the experience of the reader [35]. Indeed, the value of the loss factor is strongly dependent on the insulation

material type and on the geometry of the system: two equipments that have the same function but made with different materials or with different designs may show contrasting values of tan delta. However this does not mean that one system is more degraded that the other. Hence, by the knowledge of only one tan delta value taken completely out of contest in which it has been measured, it is not possible to state if an insulating material shows good or bad dielectric properties.

As explained in [37], in order to establish the dielectric condition of the tested system, a comparison between the measured value of the loss factor and a known reference is performed. In particular the reference usually is:

- loss factor value on systems with same design, materials and location;
- values measured when the system was new;
- trend of loss factor values over time.

Then, for example, if an increase in the dissipation factor value over time is detected on a same equipment, it can be concluded that the condition of its insulating system is degrading: proper maintenance actions should be taken when the tan delta value exceeds an historically established threshold for the particular insulation type and design under test [45]. Obviously, in order to recognize a trend in the loss factor values of a particular dielectric system, records of dissipation factor measurements must be maintained over a certain period of time. Thus, in other words, a progressive increase in the tan delta value over time on a same equipment under test is a wake-up call warning that the average condition of the dielectric is worsening more and more with time. This fact could be caused by many factors that may not be directly recognized through dissipation factor tests: as said before, the loss factor is an indicator of the average health of an insulation system, based to past measurements. As an example, in the case of complex insulating systems like cable joints, an increase of the measured tangent delta could be caused by many factors besides the normal insulation aging as the ingress of water drops in the dielectric interface, the loss of interfacial pressure of the shrunk joint tube or maybe a raise in the severity of partial discharges on a small knife cut in the cable insulation.

Now, even though with dissipation factor measurements the precise cause of dielectric worsening cannot be recognized , loss factor analysis could be anyway a very interesting method to monitor the health condition of critical systems as cable joint accessories. Indeed, loss factor measurements need a relatively simpler setup comparing to other non-invasive diagnostic methods as, for example, partial discharge analysis. Moreover, through them, it is possible to easily track the whole history of the equipment under test, having an idea of what could be its reliability by only looking at few data. Furthermore, by correlating the loss factor recorded values to other environmental quantities (as pressure or temperature) it could be inferred how the whole cable joint system responds to these stresses, namely if the overall insulating condition worsens or not with some changes in surrounding environmental conditions. In the end, it must not be lost the sight of the principle aim of the distribution system operators, namely to reduce the high number of cable outages due to cable joint breakdowns by performing maintenance before their occurrence. Dissipation factor tests on cable joint can give enough information to the user in order to achieve that goal.

In the present master thesis, variations of tan delta in relation to temperature oscillations are investigated since, as seen in 2.2.1, the temperature cycles to which cable joints are subjected on site over the days and over the years are supposed to play an important role in their accelerated aging and premature breakdown. Then, understanding how a diagnostic indicator as the loss factor depends by the temperature in the complex joint insulation system is surely an important aspect that has to be better investigated. In fact, by correlating the dissipation factor of cable joint samples to the temperature in which it has been measured, the effect of thermal changes on the complex insulating joint systems could be studied and discussed. Furthermore, through this analysis, some supposition could be made about the reason why such increase in joint failure rate happens during summer period, after peaks of daily temperature.

3 Method

3.1 Test objects

The samples used for loss factor measurements are four medium voltage straight cable joints. Two of them were constructed in laboratory by the company REPL while the other two were made by ENEL workers on site, in a MV cable line located in the territory of Bologna. The possibility of testing both laboratory and on-field made joints is interesting since it is possible to investigate the tan delta behavior under temperature variations in samples constructed in very different working conditions.

3.1.1 REPL joints

The two samples made in laboratory by REPL are cold shrink joints. Both joints connect two pieces of 130 mm^2 aluminum cables insulated with XLPE having a length of about 0.5 m and shielded with aluminum foils. The insulating material used for the joint main insulation body is the silicone rubber (SiR). On these joints the geometrical stress control technique is used: a conic electrode is placed where the semiconductive shield of the cable is peeled off. The two samples chosen for the tests have two different glass transition temperature (T_G) values: 100 °C and 150 °C. However, from the geometrical point of view, they are perfectly equal.

It is important to underline that the REPL samples are not cable joints that have been fully completed yet. In fact the outer layer and the shielding metallic mesh are absent, respectively (1) and (2) on figure 3.1. Only the joint cold shrunk main insulation body and, obviously, the bolted cable connector are present, respectively (3) and (4) on figure 3.1. However, in order to perform dissipation factor measurements, the outer metallic mesh is fundamental since it must be used as ground electrode for loss factor measurements. This sample arrangement is showed in some other studies regarding tan delta measurements in cable joints [46, 47] or, similarly, on loss factor measurement setups for MV cables, where the cable shield is used as ground electrode [40, 41].

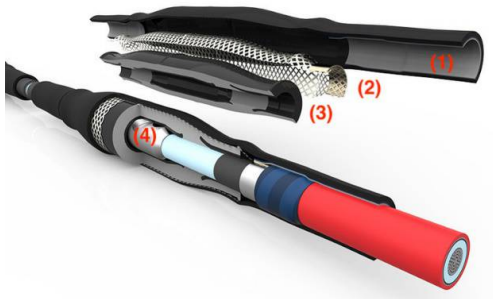

Fig. 3.1: *REPL cable joint cross section* [42].

Therefore, some aluminum foil layers has been wrapped and tighten with rubber bands around the joint insulating body to recreate the ground electrode. Furthermore, a cable has been tightly connected to the aluminum shield in order to make quickly available the ground connection for the measurement circuit. The purpose of this action will be more clear after section 3.4.

Fig. 3.2: *REPL cable joint before and after sample preparation.*

3.1.2 In-field made joints

The other two samples has been constructed by ENEL jointers after a fault occurrence on an actually working medium voltage line. The workers were not previously informed that the joints they were making would be removed after the installation. This was done to guarantee actual in-field working conditions. In the following, it is referred to these two samples as In-field Cable Joints samples 1 and 2.

Both samples connect two pieces of 130 mm^2 aluminum cables, one of which insulated with XLPE and shielded by an aluminum foil while the other one insulated

with EPR and shielded with copper wires. The two cables pieces, connected by the joint, have a length of about 0.3 m, differently than REPL joint, due to a different cut done by ENEL workers. This difference in length between the two sample typologies has a non negligible impact on the value of the sample capacitance and, consequently, on the value of tan delta. That fact makes comparisons of tan delta values between REPL and In-field joint samples difficult to be interpreted. In any case, this should not be a problem since it is not completely correct to compare the value of the loss factor between samples having different geometries and made with different materials. In fact, as explained on section 2.4, tan delta is a good health indicator for an insulating system only if it is associated with previously values measured on the same equipment: the loss factor is a diagnostic tool based on trend measurements [43]. In particular, one the purposes of this work is to make a comparison between loss factor measurements on cable joints constructed in very different working conditions taking into the account not their values but their behaviors in relation to temperature variations. In other words, between different samples, it is compared not the value of the loss factor but only if the loss factor responds in the same way to joint temperature changes.

Fig. 3.3: *In-field Cable Joint sample made on field by ENEL workers.*

Returning back to the sample description, the two in-field made cable joints are of the cold shrink type, like REPL ones. Furthermore, thanks to assembly instructions kindly provided in paper form by ENEL [44], also the joint constructing procedures are known. Hence, according to [44], instead of using field deflectors, in these samples high permittivity stress control tubes are present for field grading purposes, extruded together with the main insulation body. Furthermore, differently than REPL samples, the in-field

joints have been fully completed by ENEL workers: it is not present only the main insulation body. So, the shielding cage that connects the armatures of the two cable segments has been already mounted. Thanks to this, the preparation of these two samples were easier than the REPL one: it was enough to tightly connect a small cable on one of the two cable shields in order to make the ground connection available, as it can be seen in figure 3.3.

3.2 Tan delta measurement circuit

One of the main purposes of this thesis is to design and characterize a laboratory measurement circuit able to calculate the loss factor of a joint sample in an easy and cheap way, without using *ad hoc* tan delta measurement devices.

3.2.1 Working principles

As seen in section 2.4, an ideal insulating system is represented by a pure capacitor while, in the real situation, every dielectric system is characterized by a certain value of conductivity. Hence, a certain amount of resistive current always flows through it. According to the *IEEE Guide for Field Testing and Evaluation of the Insulation of Shielded Power Cable Systems* [45], shielded cables can be represented through an equivalent circuit composed by a capacitance C, that stands for the capacitance of the cable insulating material between the cable conductor and the external shield, and a resistance R connected in parallel, that stands for the resistive current flowing through the cable insulation. The same reasoning can be done for the cable joints and the same equivalent circuit can be used to represent the resistive losses through the insulation body. Indeed, the overall geometry of the joint is quite similar to the one of a shielded cable since they can both be roughly approximated with coaxial capacitors. It must be noticed that also the few studies about tan delta measurement in cable joints use the same equivalent circuit in their work [46, 47]. Then, recalling what presented in section 2.4, the joint insulation equivalent circuit is shown in figure 3.4, where:

- $\vec{V}_J$: phasor of the voltage applied between the conductor and the external grounded metallic shield of the joint;
- $\vec{I}_J = \vec{I}_C + \vec{I}_R$: phasor of the current flowing through the joint insulating material. It is equal to the vectorial sum between the capacitive current component $\vec{I}_C$, displaced by 90 degrees from $\vec{V}_J$, and the resistive current component $\vec{I}_R$, in phase with $\vec{V}_J$.

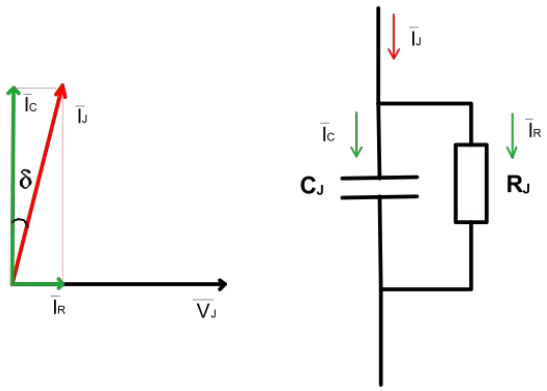

Fig. 3.4: *Equivalent circuit of the cable joint insulation and its phasor diagram.*

From what explained until now, it follows that the angle between the phasor of the current flowing through the joint insulation and phasor of the voltage applied to the joint is not 90 degree anymore (as in an ideal situation) but it is smaller than this value, due to the resistive current contribution in phase with the voltage applied. The δ angle, also referred as loss angle, indicates the amount of radiants to which the phase shift between $\vec{I}_J$ and $\vec{V}_J$ is less than $\pi/2$. Hence it is defined by:

$$\delta = \frac{\pi}{2} - \theta \tag{4}$$

In the latter equation, θ is simply the displacement angle between $\vec{I}_J$ and $\vec{V}_J$, also referred as power angle. From the phasor diagram in figure 3.4 and referring to section 2.4, it is easy to see that the tangent of the loss angle of a joint (but also of a generic insulating system) is be defined as the ratio between the magnitude of the

resistive component of the joint current and the magnitude of the capacitive one:

$$\tan\delta = \frac{|\vec{I}_R|}{|\vec{I}_C|} \tag{5}$$

From that equation is easy to understand that an increasing value in the magnitude of the resistive component of the current, caused by a deterioration of the insulating capability of the dielectric system analyzed, leads to an increasing value of tan delta. However, in practical applications, the equation (5) is difficult to be directly applied since the resistive current flowing through the joint capacitance presents a very low magnitude and then it is not easy to be measured. So, the idea behind the design of the measurement circuit comes out from the possibility to calculate the loss factor thanks to the knowledge of $\vec{V}_J$ and $\vec{I}_J$ in magnitude and phase. In particular, the loss angle δ is determined as the phase shift between the latter phasors. Consequently also the tan delta can be easily calculated. Hence, a voltage divider is used to measure the joint voltage $\vec{V}_J$ while a shunt resistor is used to measure the joint current $\vec{I}_J$, as shown in figure 3.5. For what concerns the subsequent calculations, it is assumed that the following quantities are known and fixed in time:

- $\vec{V}_{PS}$: supply voltage, known in amplitude and phase;
- R_{SH} : shunt resistor;
- R_L and R_H : voltage divider resistors.

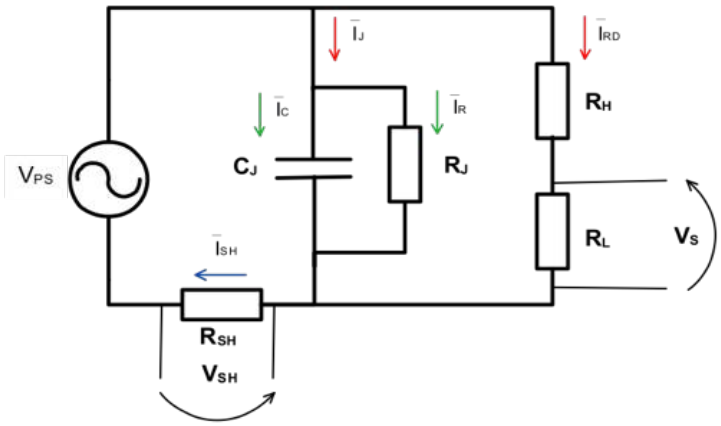

Fig. 3.5: *Basic setup of the tan delta measurement circuit.*

Furthermore, it is assumed that the voltage drops $\vec{V}_{SH}$ and $\vec{V}_{S}$ are acquired and measured: hence they are quantities known in amplitude and phase. From these assumptions, the joint current phasor $\vec{I}_{J}$ can be simply calculated as:

$$\vec{I}_{J} = \vec{I}_{SH} - \vec{I}_{RD} \tag{6}$$

The phasor of the current flowing through the shunt resistor and through the resistive voltage divider are calculated respectively as:

$$\vec{I}_{SH} = \frac{\vec{V}_{SH}}{R_{SH}} \tag{7}$$

$$\vec{I}_{RD} = \frac{\vec{V}_{S}}{R_{L}} \tag{8}$$

The joint voltage phasor $\vec{V}_{J}$ is determined using the voltage division law and it is expressed by the following equation:

$$\vec{V}_{J} = \left(\frac{R_{H} + R_{L}}{R_{L}} \right) \vec{V}_{S} \tag{9}$$

The loss angle δ is calculated in radiants and, from equation (4), it results as:

$$\delta = \frac{\pi}{2} - \theta_{IV} \tag{10}$$

In the latter equation, θ_{IV} is the displacement angle between current and voltage of the joint under test. From the knowledge of the phasors $\vec{I}_{J}$ and $\vec{V}_{J}$ thanks to equations (6) and (9), the displacement angle between them is calculated by:

$$\theta_{IV} = \widehat{I}_{J} - \widehat{V}_{J} \tag{11}$$

where, as said:

- $\widehat{I}_{J}$: phase angle of the joint current phasor, in radiants;
- $\widehat{V}_{J}$: phase angle of the joint voltage phasor, in radiants.

In conclusion, the loss factor can be simply calculated as the tangent of the loss angle δ.

In figure 3.6 the phasor diagram is shown. It is related to the measurement circuit represented in figure 3.5.

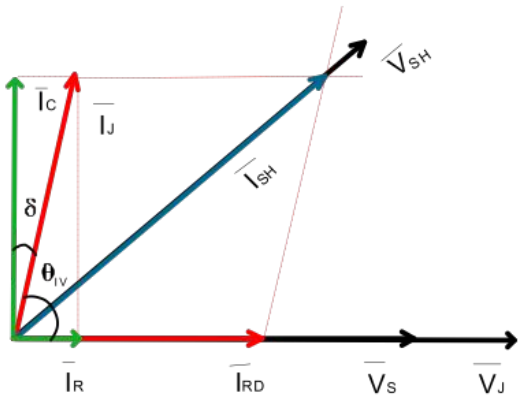

Fig. 3.6: *Phasor diagram referring to the measurement circuit. The magnitudes of the vectors do not reflect the real ones.*

Considering equations (7), (8) and (9) it is clear that even small drifts between the designed values of circuit resistances and their real values could cause non negligible errors in the calculation of $\overrightarrow{V_J}$, $\overrightarrow{I_{RD}}$ and $\overrightarrow{I_{SH}}$. Since the joint current phasor results from the difference between the shunt current phasor and the divider current phasor, from the diagram is clear that, if $\overrightarrow{I_{RD}}$ and $\overrightarrow{I_{SH}}$ are calculated using wrong resistance values, the calculated joint current phasor $\overrightarrow{I_J}$ will be consequently affected by errors, both in magnitude and phase. In particular, a possible error in the calculation of $\widehat{I_J}$ is expected to cause a drift between the measured and actual loss angle δ . Now, since the magnitude of the resistive current flowing through the joint insulation is usually very low due to the dielectric properties of the insulation itself, the loss angle is very small. So, errors in the assumption of circuit resistance values could result in large errors on the calculated dissipation factor. The measurement circuit of figure 3.5 is surely based on simple properties, cheap and easy to be constructed but their components need to be carefully designed and characterized in order to have not big errors on the measured tan delta. This is the purpose of the next subsections.

3.2.2 Design of circuit parameters

In the previous section the basic setup proposed for tan delta measurements on cable joints has been explained. Now, the actual arrangement of circuital elements and the design of every component used are going to be fully presented. In particular, the whole measurement circuit schematic is shown in figure 3.7. The circuit is characterized by the following components:

- A programmable power source Agilent 6813B;
- an isolation transformer;
- a step-up voltage transformer 100V/15000V;
- the resistive voltage divider;
- the shunt resistor;
- a National Instruments Data Acquisition Board (DAQ) NI 9239;
- the cable joint under test.

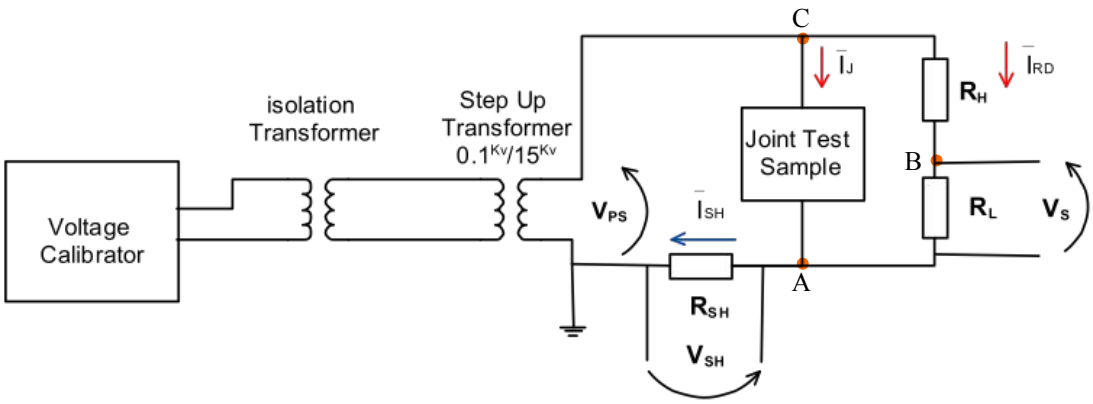

Fig. 3.7: *Schematic of the actual measurement circuit setup.*

As shown in the latter subsection, in order to calculate the loss factor of the joint sample, it is enough to know the value of the resistances composing the voltage divider and the shunt, thanks to the acquisition of the two voltages V_S and V_{SH} . In particular, these two voltages must not exceed a maximum amplitude limit imposed by the NI Data Acquisition Board. Hence, the value of circuit resistances have to be set in order to fulfill this requirements. Furthermore, the magnitude of the input voltage

$\overrightarrow{V_{PS}}$ has to be set satisfying some conditions too. The next two subsections are going widely treat these two points.

3.2.2.1 Design of the input voltage

In order to correctly set the measurement circuit input voltage, a trade-off between the need to recreate the actual cable joint working condition and the need to minimize the risk of sample breakdown must be found.

First at all, it is not convenient to directly feed the step-up voltage transformer using the plug voltage. Indeed, in order to avoid incorrect estimations of the dissipation factor, it is needed an highly stable voltage source, free from voltage distortions or frequency fluctuations. In particular, variations in the phase of the measurement circuit supply voltage phasor $\overrightarrow{V_{PS}}$ would cause modifications in the phase of both $\overrightarrow{V_S}$ and $\overrightarrow{V_{SH}}$ and, as it can be inferred by the phasor diagram in figure 3.6, errors in the calculation of $\widehat{I_J}$ would arise. Consequently, errors would be propagated on the loss angle and on the final measured value of the dissipation factor through the calculations made in subsection 3.2.1. For these reasons, instead of using the plug voltage, a stable AC power source, shown in figure 3.8, is adopted to supply the step up transformer. The output voltage of the power source is then applied to an isolation transformer that keeps electrically separated the low voltage grid of the laboratory from the test set up. This has been done for security reasons in case of breakdown of the test object. Lastly, the voltage is raised through the step-up transformer to feed the whole measurement circuit.

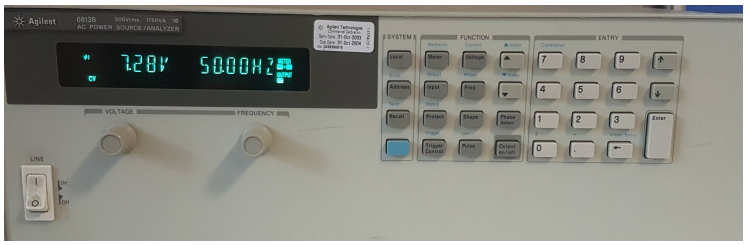

Fig. 3.8: *Agilent 6813B programmable power source.*

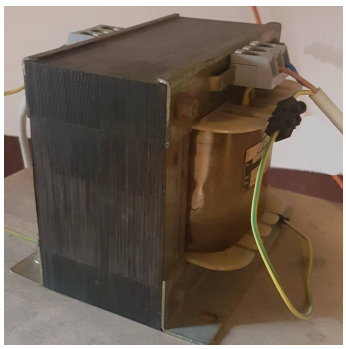

Fig. 3.9 *The isolation transformer.*

The magnitude of the voltage V_{PS} that feeds the circuit must be chosen in order to minimize the risk of surface discharges between the cable conductor and the grounded cable screen of the joint under test. Surface discharges must not be present on the joint under tests both for safety reasons and for measurement reasons. Indeed, they can lead to voltage breakdowns and they could affect measurement results, varying the magnitude of resistive component of the joint current I_R . Now, the more V_{PS} is low, the less is the risk to have big surface discharges. However, at the same time, it is also needed a test condition that almost tries to reproduce a working condition for the cable joint. A value for the voltage magnitude that could satisfy both the explained requirements is $V_{PS} = 1\text{kV}_{rms}$. This supply voltage magnitude corresponds to a working condition for the joint of ~0.2 p.u. and, as it is going to be seen in the next subsection, it leads to feasible values of the voltages in input to the Data Acquisition Board by using commercially available resistors. In order to demonstrate that, by using such a supply voltage magnitude, there is not any influence of surface discharges on the loss factor measured value, a simple test has been performed. When the measurement circuit was already been designed and constructed, the dissipation factor of one joint, not used as test sample, has been measured in two different conditions: when the distance between the conductor and the cable outer semiconductor was very long (picture 1 of figure 3.10) and when it was the shortest possible (picture 2 and 3 of figure 3.10). The result of both test were identical, hence the surface discharge effect is negligible using 1kV_{rms} as measurement circuit supply voltage. Furthermore, since the cable ends in sample joints are as in picture 1 of figure 3.10, the effect of surface discharges is not considered anymore in the following results.

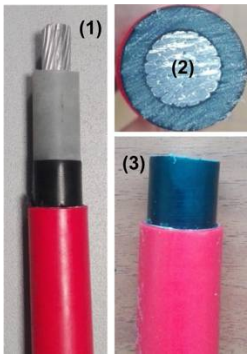

Fig 3.10: *Picture (1): cable end when the distance between conductor and outer semicon is maximum. Picture (2) and (3): the same cable end when the distance is at its minimum.*

In order to obtain the chosen value of the V_{PS} voltage at secondary of the step-up voltage transformer, the voltage value generated by the power supply that feeds the primary side must be carefully set. Now, the voltage ratio of the transformer, according to its nameplate (figure 3.12), is:

$$Voltage\ ratio_{Nameplate} = \frac{100\text{V}}{15000\text{V}} = \frac{1\text{V}}{150\text{V}} \tag{12}$$

However, due to the fact that the transformer used for this experiment is quite old, the voltage ratio indicated in the nameplate is not trustable anymore. Thus, the actual value of the transformer ratio has been measured by applying 1V to the primary of the step-up and measuring the secondary voltage using a multimeter. As expected, due to ageing, the real transformer ratio is different from the one shown on the nameplate and it is resulted to be:

$$Voltage\ ratio_{Real} = \frac{1\text{V}}{138\text{V}} \tag{13}$$

Therefore, in order to obtain $V_{PS} = 1\text{kV}_{rms}$ as measurement circuit supply voltage, the Agilent 6813B power supply has to be set in order to generate ~7.25V_{rms}, as it can be seen from the screen in figure 3.8.

Fig 3.11: *The step-up voltage transformer. At left there is the low voltage primary side while on the top there is the secondary high voltage bar.*

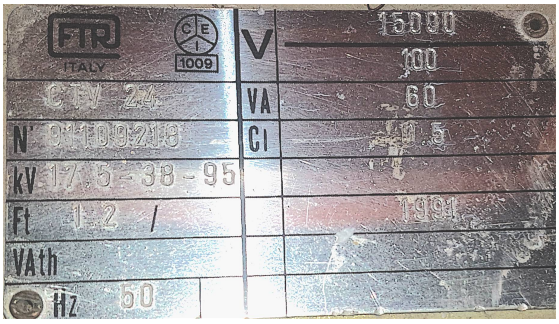

Fig. 3.12: *Nameplate of the step-up voltage transformer.*

3.2.2.2 Design of resistance values

According to what was explained in 3.2.1, thanks to the acquisition of the voltages V_S and V_{SH} **,** the loss angle can be easily calculated. As introduced previously, the two acquired voltages, namely the voltage drops over R_L and R_{SH} , must not exceed a maximum amplitude limit imposed by the NI Data Acquisition Board. Hence, the resistance values must be designed to fulfil this fundamental requirement. From the datasheet of the NI DAQ 9239 [48], it is shown that the used DAQ provides a $\pm 10\,\mathrm{V}$ measurement range: it means that the amplitude of the voltages V_S and V_{SH} , placed in input to the NI 9239, must not exceed $\pm 10\,\mathrm{V}$. Then, it has been decided to tailor the circuit resistances in order to obtain the following ideal DAQ input voltages:

$$V_S = V_{SH} = 5\mathrm{V}_{rms} \approx 7.07\mathrm{V}_{peak} < 10\mathrm{V}_{peak} \tag{14}$$

The resistances of the voltage divider are firstly considered. Assuming no load conditions, namely the DAQ not connected, the current I_{RD} flowing on both divider resistances is the same. Thus, it holds:

$$\frac{V_H}{V_S} = \frac{R_H}{R_L} \tag{15}$$

As hypothesis, the objective is to obtain $V_S = V_{SH} = 5\mathrm{V}_{rms}$. If that is achieved, the potential on the point A of the measurement circuit in figure 3.7 would be equal to $5\mathrm{V}_{rms}$ while the potential of the point B to $10\mathrm{V}_{rms}$. Furthermore, since $V_{PS} = 1\mathrm{kV}_{rms}$, the potential of point C would be kept at $1000\mathrm{V}_{rms}$ thanks to the supply voltage. It simply follows that the rms value of the voltage across the joint test sample would be $V_J = 995\mathrm{V}_{rms}$. The rms value of the voltage drop over the resistance R_H on the voltage divider would be then $V_H = 990\mathrm{V}_{rms}$. Hence, from equation (15), it results that, in order to obtain the desired DAQ input voltage $V_S = 5\mathrm{V}_{rms}$, the resistance ratio of the voltage divider must be set to:

$$\frac{R_H}{R_L} = \frac{V_H}{V_s} = \frac{990\text{V}_{rms}}{5\text{V}_{rms}} = 198 \approx 200 \tag{16}$$

So, in order to not exceed with V_S the DAQ imposed voltage limit, any values for R_H and R_L can be chosen, provided that the ratio between them is equal to 200. As first approach, the following choice is considered:

- $R_H = 200\,\Omega$
- $R_L = 1\,\Omega$

Now, this choice would surely lead to a voltage drop V_S over R_L feasible for the DAQ but the current flowing through the voltage divider branch would be:

$$I_{RD} = \frac{V_J}{R_L + R_H} = \frac{995\text{V}_{rms}}{220\,\Omega + 1\,\Omega} \approx 5\text{A}_{rms} \tag{17}$$

Hence, the power dissipated by each resistor would be in that case:

$$P_H = V_H \cdot I_{RD} = 990\text{V}_{rms} \cdot 5\text{A}_{rms} = 4950\text{W} \tag{18}$$

and

$$P_L = V_S \cdot I_{RD} = 5\text{V}_{rms} \cdot 5\text{A}_{rms} = 25\text{W} \tag{19}$$

Obviously, these power losses would be are too high to be sustained by commercially available high precision and high stability resistors. The current that flows on the divider must be decreased by increasing the value of the resistances. However the ratio between them must be kept equal to the design value of 200. The proposed solution is to use resistors having the following values:

- $R_H = 2\text{M}\,\Omega$
- $R_L = 10\text{k}\,\Omega$

The resistance ratio is respected so, from the voltage point of view, that choice fulfills the requirements. The power dissipated can be checked by determining firstly the

divider current, as previously done in equation (17):

$$I_{RD} = \frac{V_J}{R_L + R_H} = \frac{995\text{V}_{rms}}{2\text{M}\Omega + 10\text{k}\Omega} \approx 0.5\text{mA}_{rms} \approx 0.71\text{mA}_{peak} \tag{20}$$

Thus, the powers dissipated by the designed resistors are:

$$P_H = V_H \cdot I_{RD} = 990\text{V}_{rms} \cdot 0.5\text{mA}_{rms} = 0.5\text{W} \tag{21}$$

and

$$P_L = V_S \cdot I_{RD} = 5\text{V}_{rms} \cdot 0.5\text{mA}_{rms} = 0.0025\text{W} \tag{22}$$

These values are completely feasible for commercially available resistors characterized by high precision and stability, as it is going to be seen in the next subsection.

Now, the shunt resistor R_{SH} is considered. As explained in 3.2.1, the joint current can be calculated by the acquisition of the voltage-drop V_{SH} across it and, then, by the application of equations (6), (7) and (8). In order to choose a value for R_{SH} that leads to a voltage V_{SH} feasible for the DAQ, as a first approach, the joint sample is considered to be not connected into the measurement circuit. This assumption leads to the following consequences: $I_J = 0\text{A}_{rms}$ and $I_{SH} = I_{RD} = 0.0005\text{A}_{rms}$. Hence, in order to obtain the desired $V_{SH} = 5\text{V}_{rms}$, the shunt resistor value should be, in absence of the tested sample:

$$R_{SH} = \frac{V_{SH}}{I_{SH}} = \frac{5\text{V}_{rms}}{0.0005\text{A}_{rms}} = 10\text{k}\Omega \tag{23}$$

Obviously, in this case, the power dissipated by the shunt resistor is equal to the one of R_L. It is important to remember that the aim of the resistance tailoring is to obtain that the output voltages of the measurement circuit never exceed $\pm 10\text{V}$ in magnitude during its working. In other words, once the circuit parameters have been designed, it is not required that the output voltages must be strictly $V_S = V_{SH} = 5\text{V}_{rms} \approx 7.07\text{V}_{peak}$. This equality is important only for design purposes, namely to set the resistances that

have to be placed in the circuit. The only constraints about DAQ input voltages that must be satisfied during the actual working condition of the measurement circuit are:

- $V_S < 10\text{V}_{peak}$
- $V_{SH} < 10\text{V}_{peak}$

It is now important to notice that a critical assumption has been made during the shunt resistance tailoring, namely $I_J = 0\text{A}_{rms}$. In particular, it is important demonstrate that, with $R_{SH} = 10\text{k}\Omega$, the voltage drop over the shunt resistor does not exceed the DAQ imposed limit also when the cable joint sample is connected, i.e if $I_J \neq 0\text{A}_{rms}$. It is fundamental to perform this check in order to avoid a possible breakdown of the Data Acquisition Board during the loss factor measuring process. However, the capacitance of the sample must be a known quantity. To this purpose, the capacitance of the four cable joint samples have been initially roughly measured with a multimeter. Then, when it has been checked that there is no electrical problem for the DAQ, it has been better measured using the loss factor measurement circuit, as it will be seen in 3.3.2. Anyway, taking into the account the REPL joint samples, it resulted that their typical capacitance value is $C \approx 330\text{pF}$. Being the detected capacitance of the in-field samples lower than 330pF, in the following calculations only the REPL samples are taken into the account since they present higher joint capacitive currents. Now, considering the system frequency stably equal to 50 Hz, thanks to the calibrator used as power source, and considering that the voltage across the cable joint, imposed by the supply, should be $V_J = 995\text{V}_{rms}$, then the amplitude of the current flowing across the joint insulation is calculated as:

$$I_J = \omega C V_J = 2\pi f C V_J = 2\pi \cdot 50 \cdot 330 \cdot 10^{-12} \cdot 995 \approx 0.1\text{mA}_{rms} \approx 0.141\text{mA}_{peak} \quad (24)$$

It must be underlined that the joint current is now considered as purely capacitive. While the resistive component of $\vec{I}_J$ is a fundamental parameter for the definition of the loss factor, its amplitude, as said also in 2.4, is much lower that the capacitive component one. This is due to the very high resistivity of the dielectric insulating

material when it is on an healthy and not aged condition. Thus, for the purpose of this calculation, the resistive component of the joint current is neglected. In other words, since the objective is just to determine the amplitude of the shunt voltage-drop in real operating conditions, the impact of the resistive component of the joint current on that phenomenon is considered to be negligible due to its low magnitude comparing to the capacitive component. From this reasoning, the joint current phasor $\vec{I}_J$ is shifted by approximatively 90 degrees from the resistive divider current phasor $\vec{I}_{RD}$. So, the actual amplitude of the current flowing on the shunt resistor can be calculated thanks to the Pythagorean theorem:

$$I_{SH} = \sqrt{I_J^2 + I_{RD}^2} = \sqrt{(0.141\text{mA}_{peak})^2 + (0.71\text{mA}_{peak})^2} \approx 0.72\text{mA}_{peak} \approx 0.51\text{mA}_{rms} \quad (25)$$

Hence, the voltage drop over the shunt resistor is:

$$V_{SH} = R_{SH}\, I_{SH} = 10\text{k}\Omega \cdot 0.51\text{mA}_{rms} = 5.1\text{V}_{rms} \approx 7.2\text{V}_{peak} < 10\text{V}_{peak} \quad (26)$$

From these two equation it can be seen how the joint current does not particularly affect the magnitude of the current flowing on the shunt resistor, which is practically equal to the current that flows on the resistive divider. Hence, it has been checked that the voltage drop across the 10kΩ shunt resistor, in the actual case of the REPL joint sample connected in the circuit, is approximately equal to the hypothesized value of $V_{SH} = 5\text{V}_{rms}$ that holds under the assumption of having $I_J = 0\text{A}_{rms}$.

From all the calculations made in this subsection, thanks to the set values of input voltage and resistances, it has been demonstrated that the measurement circuit is able to produce output voltages feasible for the Data Acquisition Board.

3.2.3 Resistor characterization

As introduced at the end of 3.2.1, dissipation factor measurements are highly dependent on the value of the resistances present in the circuit. In fact, considering equations (7), (8) and (9), it is clear that even small drifts between the designed value of

the circuit resistances and the real value of them could cause non negligible errors in the determination of phasors $\vec{I}_J$ and $\vec{V}_J$. This error propagates to the delta angle and, consequently, on the measurement of the joint loss factor. Therefore, once the circuit is designed and constructed, the resistance value of the resistors must be as stable as possible in order to avoid errors in the estimation of tan delta. It follows that resistors with very high precision and very high stability over time must be used in the actual measurement circuit. The following two commercially available resistors are then selected:

- Ultra-Stable Low TC Ultra-Precision Film Resistor USF370 for the $2\,\mathrm{M}\Omega$ resistor from the company Caddock Electronics, Inc., shown in figure 3.13;
- Ultra High Precision Z Foil Though-Hole Resistor Z201 for the $10\,\mathrm{k}\Omega$ resistors from the company Vishay Precision Group, Inc., shown in figure 3.14.

The resistor specifications are summarized on the table 3.1. All the data are reported from the resistor datasheets [49] and [50]. It must be also underlined that both resistor types have a non-inductive and non-capacitive design in order to reduce at maximum the stray non linearities that could affect measurements.

Resistor	Resistance	Standard Tolerance	Power	Thermal Drift
R_H	$2\,\mathrm{M}\Omega$	$\pm 0.01\,\%$	$0.75\,\mathrm{W}$	$5\,\mathrm{ppm/°C}$
R_L , R_{SH}	$10\,\mathrm{k}\Omega$	$\pm 0.005\,\%$	$0.6\,\mathrm{W}$	$0.2\,\mathrm{ppm/°C}$

Table 3.1: *Resistors specifications* [49; 50].

Fig. 3.13: *Ultra-Stable Low TC Ultra-Precision Film Resistor, 2MΩ.*

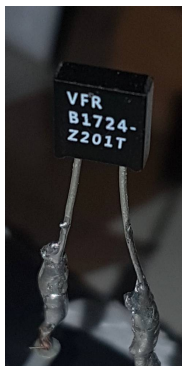

Fig. 3.14: *Ultra High Precision Z Foil Though-Hole Resistor, 10kΩ.*

The power dissipated by R_L and R_{SH} is significantly lower than their rated one. In fact, as it was previously obtained in equation (22), $P_L = P_{SH} = 0.0025\,W$. So, since there is not an high power dissipation, the resistance drift problem caused by a temperature increase is not present. On the other hand, the power dissipated by R_H , that is, from equation (21), $P_H \approx 0.5\,W$, is comparable to its rated one. However, thanks to the very low thermal drift of the USF370 resistor, the resistance value does not change in an appreciable way to affect the accuracy of the tan delta measurement, as it is going to be further underlined. From resistor datasheets [49] and [50] is also possible to check the long term stability of the resistors:

- The permanent resistance drift of the $10\,k\Omega$ resistors is less than 60 ppm (0.006%) after 10 years running at 0.1 W at 70°C;
- The resistance drift of the $2\,M\Omega$ resistor is ±0.030% at maximum after 10,000 hours at +85°C at rated voltage, not to exceeding the rated power.

From these data, it can be concluded that the used resistors are very stable over time thanks to their very low resistance drift. The stability in resistance value is also enhanced thanks to the fact that resistors are always used at ambient temperature (70°C or 85°C are never reached) and, as seen, the rated power is never exceeded.

Until now it has been shown that the chosen resistors are completely stable over time and over temperature variations. However, as said before, due to the importance of the resistance values in the calculation of tan delta, the actual resistance must be measured and known with low uncertainty. In this way, on the measurement LabVIEW program (that is going to be explained in section 3.3) the measured value of the resistances will be inserted, instead of the one communicated by the manufacturer. That fact, linked to the high stability properties of the used resistances, leads to a complete calibration of the measurement circuit and to the minimization of the error introduced by the resistances on the calculation of the loss factor. Therefore, 1000 resistances measurements have been performed for all the resistors using a Keysight 3458A

Multimeter. According to the multimeter datasheet [51], the following accuracy specifications are considered:

- 10 ppm of reading error and 0.5 ppm of range error for the $10\,\mathrm{k}\Omega$ full scale;
- 50 ppm of reading error and 10 ppm of range error for the $10\,\mathrm{M}\Omega$ full scale.

Now, table 3.2 lists the mean values m and the standard deviations σ of the 1000 measurement performed for each resistor:

Resistors	**Mean values** [Ω]	**Standard deviation** [Ω]
R_H	$2.0000 \cdot 10^6$	30
R_L	$9.9999 \cdot 10^3$	0.005
R_{SH}	$9.9994 \cdot 10^3$	0.003

Table 3.2: *Resistors mean values and standard deviations of the 1000 resistance measurements.*

The standard uncertainty due to random sources, as thermal noise or electromagnetic disturbances, is indicated with u_A and corresponds to the standard deviations of the resistance measurement performed:

$$u_A = \sigma \tag{27}$$

The systematic contribution to uncertainty coming from the digital multimeter is indicated with u_B . The following notation holds for the subsequent calculations:

- $\%L$: reading or gain error, provided by the multimeter manufacturer;
- $\%FS$: full scale or non linear error, provided by the multimeter manufacturer;
- G_{FS} : full scale value;
- m : mean value of the considered measurements.

The systematic contribution to uncertainty is calculated as:

$$u_B = \frac{\%L \cdot \frac{m}{100} + \%FS \cdot \frac{G_{FS}}{100}}{\sqrt{3}} \tag{28}$$

Notice that, since %L and %FS are provided by the multimeter manufacturer in ppm, the following conversion is needed in order to apply the latter equation:

$$1\text{ppm} = 0.0001\,\% = 1 \cdot 10^{-6} \tag{29}$$

After all, for every resistance value, the relative combined uncertainty is indicated with u_C and calculated as:

$$u_C = \frac{\sqrt{u_A^2 + u_B^2}}{m} \tag{30}$$

The table 3.3 lists the uncertainties calculated with the latter formulas using the data in table 3.2 and the data provided by the multimeter manufacturer [51]:

Resistors	u_A **[Ω]**	u_B **[Ω]**	u_C **[-]**
R_H	30	115	$5.9 \cdot 10^{-5}$
R_L	0.005	0.06	$6.0 \cdot 10^{-6}$
R_{SH}	0.003	0.06	$6.0 \cdot 10^{-6}$

Table 3.3: *Results of the resistors characterization.*

It is useful to represent the relative combined uncertainty values by means of percentages in order to compare them with the standard tolerances provided by the manufacturer, listed in table 3.1:

Resistors	u_C **[-]**	**Manufacturer Standard Tolerance**
R_H	$\pm 0.0059\,\%$	$\pm 0.01\,\%$
R_L	$\pm 0.0006\,\%$	$\pm 0.005\,\%$
R_{SH}	$\pm 0.0006\,\%$	$\pm 0.005\,\%$

Table 3.4: *Comparison between relative combined uncertainties and manufacturer standard tolerances*

It can be noticed that all the combined uncertainties of the measured resistance values are lower than the rated accuracy provided by the manufacturers.

Now, on table 3.5 are listed the definitive resistance measurement results considering the confidence intervals. They are obtained from the following equation:

$$R = m \pm k \cdot u_R \tag{31}$$

where:

- $u_R = m \cdot u_C$: resistance combined uncertainty;
- k : coverage factor of the confidence interval. In the calculations a coverage factor equal to 2 is considered.

Resistors	Measured Resistance
R_H	$[2\,000\,000 \pm 236]\ \Omega$
R_L	$[9999.9 \pm 0.12]\ \Omega$
R_{SH}	$[9999.4 \pm 0.12]\ \Omega$

Table 3.5: *Results of the resistance measurements with the confidence intervals.*

It must be underlined that the uncertainties in the knowledge of the resistance value are propagated to the quantities that are calculated using the resistance quantities themselves. In particular, one critical element required to the loss factor measurement setup is the resistive voltage divider that allows the measure of the voltage applied to the cable joint. Hence, it needs to be characterized. The voltage across the cable joint under test is calculated, from equation (9), as:

$$\vec{V}_J = K \cdot \vec{V}_S \tag{32}$$

where:

$$K = \left(\frac{R_H + R_L}{R_L} \right) \tag{33}$$

From the design of the circuit it is known that, in order that the output voltages respect the DAQ constraint, the ratio between R_H and R_L must be equal to 200. Now, by inserting in equation (33) instead of the value of the resistances their measured mean values of table 3.2, indicated with m_{RH} and m_{RL}, it follows that:

$$m_K = \left(\frac{m_{RH} + m_{RL}}{m_{RL}} \right) = \left(\frac{m_{RH}}{m_{RL}} + \frac{m_{RL}}{m_{RL}} \right) = \left(\frac{m_{RH}}{m_{RL}} + 1 \right) = (200.002 + 1) = 201.002 \tag{34}$$

Now, the uncertainty that propagates through the resistive divider formula to the cable joint voltage $\vec{V_J}$ must be determined. In particular, the relative combined uncertainty referred to *K* and indicated with u_{CK} is obtained by:

$$u_{CK} = \sqrt{\left(\frac{\sqrt{u_{RH}^2 + u_{RL}^2}}{m_{RL} + m_{RH}} \right)^2 + \left(\frac{u_{RL}}{m_{RL}} \right)^2} = 5.9 \cdot 10^{-5} \tag{35}$$

where:

- u_{RH} : combined uncertainty of the resistance R_H ;
- u_{RL} : combined uncertainty of the resistance R_L .

The latter two must not be confused with the relative combined uncertainties. In fact, as seen before, the combined uncertainties are calculated as $u_R = m \cdot u_C$, where u_c is the standard combined uncertainty. In view of this, once calculated the relative combined uncertainty of *K*, it can be determined its combined uncertainty simply as:

$$u_K = m_K \cdot u_{CK} = 0.0119 \tag{36}$$

Hence, the *K* value is calculated as follows, considering the confidence interval due to the uncertainties introduced by the resistances and using a coverage factor of 2.

$$K = m_K \pm k \cdot u_K = 201 \pm 0.0238 \tag{37}$$

In this subsection a complete characterization of the resistances used in the measurement circuits has been performed and the uncertainty propagation from resistance values to the joint voltage value through the voltage divider has been shown. The results of the calculations show that, thanks to the very high stability and precision of the chosen resistors, the uncertainties on the resistances knowledge are minimized. Hence, also the propagated uncertainties to fundamental parameters as joint voltage and

shunt current are minimized, being negligible with in comparison to other sources of uncertainty, as will be analyzed in 4.1.

3.2.4 Thermostatic chamber and temperature cycles

The principle aim of the present study is to investigate the trend of the joint tan delta with in relation temperature variations. Therefore, a thermal chamber inside which the cable joints can be easily heated up or cooled down is required. To this purpose, a big thermostatic chamber, constructed for a previous study conducted on voltage transformers [52] and already present in the DEI measurement laboratory, is used. The thermal chamber, shown in picture 3.15, is characterized by thick plexiglass slabs and it is internally insulated using big layers of polystyrene.

Fig. 3.15: *The thermostatic chamber used for the tests.*

In order to increase the joints temperature, inside the chamber an electric oven and a small fan to let the air move are present. The four joint samples are placed all together inside the chamber, as seen in figure 3.16. Then, the oven and the fan are turned on and the doors of the chamber are closed. Furthermore, they are carefully blocked and sealed with layers of adhesive tape. The joint are then left inside the chamber for about two hours. In this period of time, the difference between the chamber environmental temperature and the temperature of the joint insulation is minimized. In particular, the temperature is checked using two thermocouples: one inserted inside the outer layer of the joint insulation and one left outside, as it can be seen by figure 3.18. The maximum

stable temperature reached inside the chamber is 65 °C.

The joint temperature is cooled down using a portable air conditioner connected to the thermostatic chamber, as visible in figure 3.17. Also in this case the joints are left inside the chamber for two hours in order that the environmental temperature reaches the minimum stable value of 10 °C, as well as the joint internal temperature.

It must be noticed that, in the present study, temperature measurements have not been performed in a strictly precise way. In fact, the purpose is to investigate which is the trend of the the loss factor in case of temperature oscillations around the ambient one and not to correlate a specific value of the tan delta to a specific temperature. Furthermore, a precise correlation would be quite useless since the loss factor of a joint does not show a stable and unique value at one same temperature, as it will be discussed in the chapter 5. So, from what said, to achieve the purpose of this study, a precise and fixed thermal cycle is not strictly needed: it is enough a roughly measured hot-cold oscillation around the ambient temperature. This is also one of the reasons why it has not been used an expensive and bulky commercially available thermal chamber.

Fig. 3.16: *Disposition of joints, oven and fan inside the thermostatic chamber just before the heating up.*

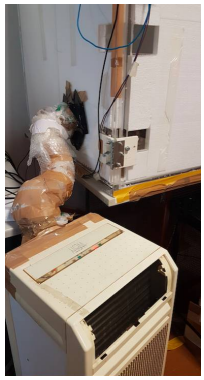

Fig. 3.17: *The portable air conditioner connected to the thermostatic chamber.*

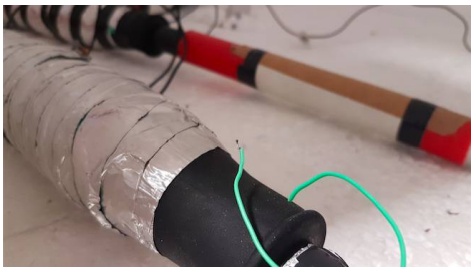

Fig 3.18: *The two thermocouples used for checking the temperature inside and outside the joint insulation.*

The thermostatic chamber is also used as protective chamber for the high voltage parts of the circuit. In fact, from figure 3.16, one can recognize the high voltage bar of the step up transformer to which it is connected the cable joint under test, as it will be explained on section 3.4.

3.3 Measurement LabVIEW program

Until now it has been explained how the tan delta measurement circuit works and how its components have been designed to achieve stability over time and amplitudes of output voltages feasible for the Data Acquisition Board. Now, the purpose is to implement a software able to perform the calculation of the tangent delta, presented in 3.2.1, starting by the knowledge of the waveforms of the voltages V_S and V_{SH}, referring to the circuit in figure 3.5 or 3.7. The main idea for the measurement algorithm is summarized in the flowchart in figure 3.19 and reflects, as said, the working principles of the measurement circuit.

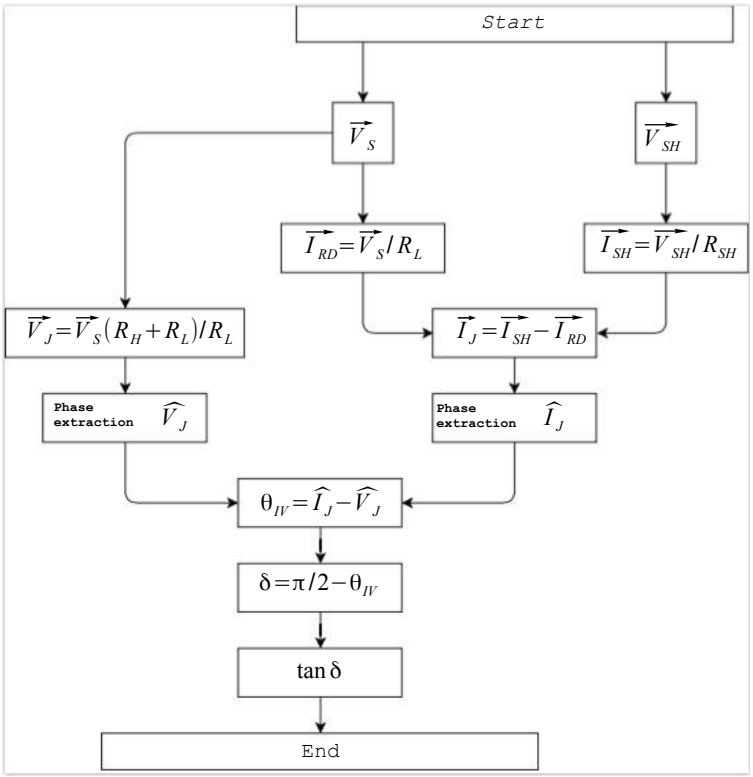

Fig. 3.19*: Measurement algorithm flowchart. The way in which tan delta is determined is the same as explained in section 3.2.1.*

An important aspect is that, from the acquisition of only two voltages and from the knowledge of the design parameters, namely the input voltage and the resistance values of the shunt and divider resistors, all the other calculations necessary to achieve the measurement result are made in digital form by the software. The measurement algorithm in figure 3.19 is implemented by developing a LabVIEW program. In the following it is going to be fully explained how the voltages V_S and V_{SH} are acquired and converted in digital information and how the program code works.

3.3.1 Data acquisition

The analogical voltages V_S and V_{SH} are the input quantities of the already introduced Data Acquisition Board (or DAQ) NI 9239. The task of this board is basically to perform a precise analog-to-digital conversion of the voltages in order to make available the information on their waveforms to the measuring program. The input circuit of one of the four channels of the DAQ is shown in figure 3.20. The analogical signal in input is basically conditioned, buffered and then sampled by an analog-to-digital converter (ADC). Furthermore, since each channel provides an independent signal path and an independent ADC, all channels can sample different voltages simultaneously [48]. From the DAQ datasheet [48], it is known that the ADC resolution is 24 bits, the maximum possible sampling rate is 50 kS/s/ch and, as said before, all channels can sample simultaneously.

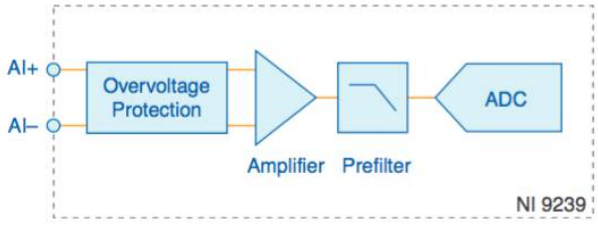

Fig 3.20: *DAQ input circuit of one channel* [48].

The Data Acquisition Board is connected through an USB cable to the computer where the LabVIEW program is running. The measuring program itself sets the

effective sampling rate and the samples per channel of the DAQ. In particular, from figure 3.21 the solution proposed on the developed LabVIEW code can be seen. Firstly, in order to create the violet analog input channel for the measured voltage data, the information on the physical channels used (in this case they are two, for the acquisition of V_S and V_{SH}), the input terminal configuration and the maximum and minimum value of the input signal are placed in input to the *DAQ Create Channel* block.

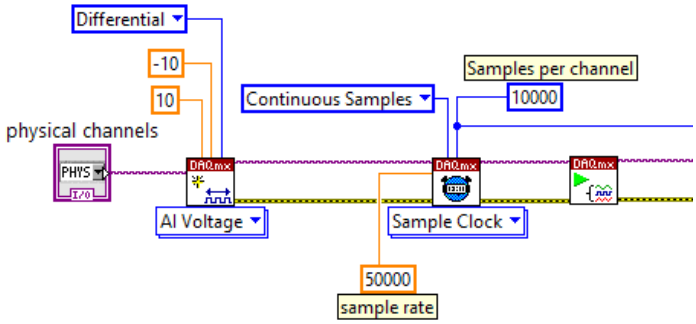

Fig. 3.21: *Part of the LabVIEW program that controls the acquisition of data.*

Then, the *DAQ Sample Clock* has to be set: this block is fundamental since it is the one that commands the sampling rate of the ADC on the physical DAQ. From figure 3.21, it can be seen that the sample rate is set to 50 kS/s, the maximum possible for the NI 9239. The number of samples per channel are instead set to 10 kS/ch and the sample mode to continuous samples. At last, after the sample clock, the *Start Task* block is placed. Its purpose is basically to create a transition between the task creation and the running state, ensuring in this way the beginning of measurements.

Now, it is required a better explanation about the sample rate and sample per channel used in the program. It is well known that the two voltage signals in input to the DAQ are sinusoids with frequency 50 Hz. Hence, the period of the signals is equal to 20 ms. Since the sampling frequency is set to 50 kS/s, every signal waveform is sampled 1000 times per period. Now, the setting of 10 kS/ch means that only 10 000 samples per time are processed by the program. In particular, considering a sampling rate of 50 kS/s, 10 000 samples are acquired by the DAQ in 200 ms. Then, considering a signal

frequency equal to 50 Hz, they correspond to 10 periods of the input signal. In other words, the input signals are sampled at 50 kS/s and, meanwhile, the sampled data are stored in two different arrays, one per channel, as it will be shown in the next subsection. Then, after 200 ms (1/5 of a second), the two arrays, containing each one 10 000 samples of the voltage waveforms (so 10 periods of the sinusoids), are processed by the program, basically by applying the algorithm in figure 3.19. The process then starts again. From what is explained, it is clear that the loss factor of the cable joint under test is measured five times every second and that each tan delta measure is performed on 10 000 samples of the input voltages. Hence, in order to collect almost 1000 tan delta data, almost 200 seconds are required for any joint under test.

3.3.2 Data processing

As it can be seen by figure 3.22, after the setting of the data acquisition stage, in order to make these digital data available for the program, the samples coming from the used channels must be read using the *DAQ Read* block. However, firstly a *while loop* is opened, containing all the code that permits the loss factor calculation. In that way, the tan delta measurements are continuously repeated until the operator decides to stop the program from the front panel. This code is going to be explained in the following.

3.3.2.1 Joint voltage and current calculation

As mentioned above, once entered in the *while loop*, firstly all the data of the voltage samples must be extracted from the already set task, containing the two used input channels. In particular, the *DAQ Read* LabVIEW block requires in input both the started task (violet wire) and the number of samples per channel (blue wire), already set before. In output, as it can be seen from figure 3.22, the block provides a two dimension array of data, since two DAQ channels are used in this application. This 2D array can be visualized as a matrix having 2 rows (distinguished by the indexes 0 and 1) and 10 000 columns. The first row corresponds to the data sampled by channel one and the second

corresponds to the data of the channel two. With the *Index Array* block is possible to separate the two rows from the 2D array in order to have in output two 1D arrays, each one constituted by 10 000 values. These are the input voltage samples that are going to be processed. Hence, the sampled data of 10 periods of the sinusoidal voltages V_S and V_{SH} are finally available. The waveforms of these voltages are visualized in the front panel through a multiplot waveform graph. Once the data of the waveforms of V_S and V_{SH} are available, the joint voltage V_J and the joint current I_J waveforms can be determined simply by applying the equations (6), (7), (8) and (9), presented in 3.2.1, as it can be seen also by the algorithm in figure 3.19. It must be underlined that these calculations are performed with 1D arrays of 10 000 elements representing time domain signals. The values of the resistances R_H , R_L and R_{SH} must be inserted from the front panel by the operator before starting measurements. This is why a complete characterization of the resistances has been performed in 3.2.3.

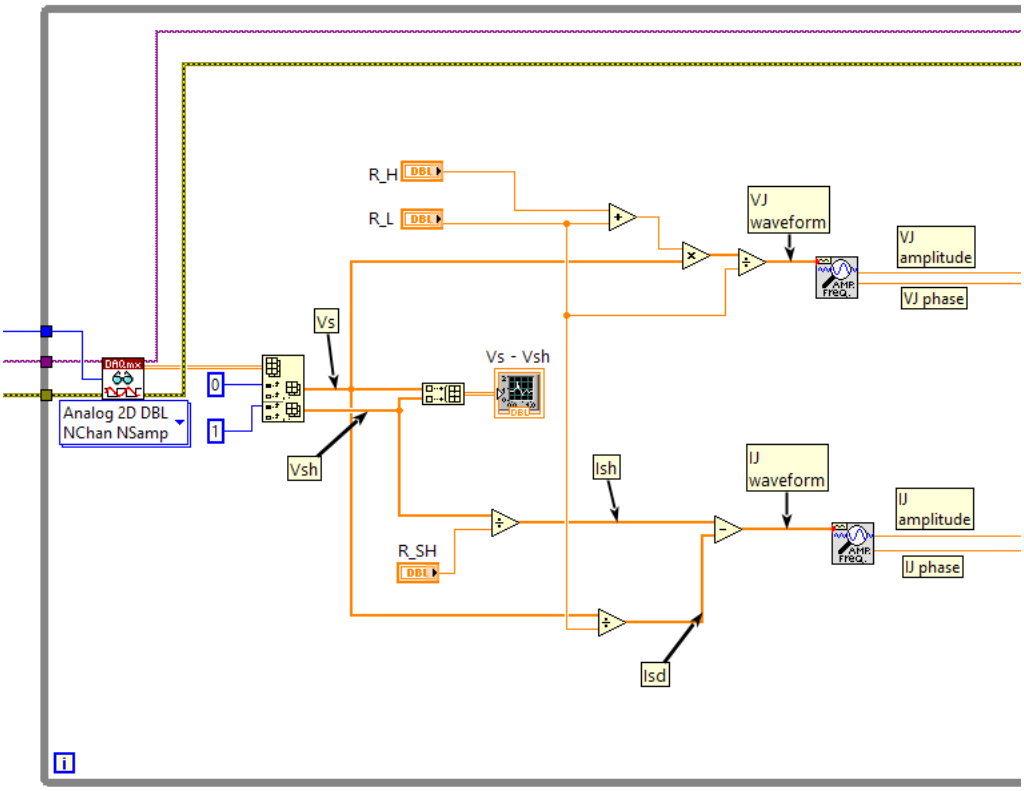

Fig. 3.22: *Part of the LabVIEW program responsible for the determination of the joint voltage and current in amplitude and phase.*

After all, the calculated V_J and I_J waveforms (each one characterized by a 1D array of 10 000 elements) come separately in input to the *Extract Single Tone* block. This block takes a time signal in, finds the single tone with the highest amplitude and returns the amplitude and the phase of this one. In this way, the amplitude and phase of the sinusoidal joint current and voltage are simply determined from the time domain signals, without performing the Fast Fourier Transform.

3.3.2.2 Joint capacitance, impedance and tan delta calculation

After the extraction of amplitude and phase of V_J and I_J, first at all, the rms values of the sinusoids, instead of their peak values, are shown in the front panel. Then, as it can be seen by figure 3.23, the amplitudes of the joint voltage and current are used to determine the joint impedance and capacitance by performing the following calculations:

$$Z_J = \frac{V_J}{I_J} \tag{38}$$

and

$$C_J = \frac{1}{\omega \cdot Z_J} = \frac{1}{2\pi f \cdot Z_J} = \frac{1}{2\pi \cdot 50 \cdot Z_J} \tag{39}$$

It must be underlined that the joint impedance is here considered as mainly capacitive. In fact, these calculations are useful only to have an indicative value of the sample capacitance in order to perform control calculations, as the one shown in subsection 3.2.2.2, or to check the presence of wrong connections or problems in the circuit setup while measurements are running. To this purpose, the value of the joint capacitance is shown in the front panel together with its waveform charts: if some capacitance peaks are visualized by the operator during measurement probably something in the circuit is wrong, as for example a bad connection of the sample to the measurement circuit.

The phases of the V_J and I_J sinusoids are used to calculate firstly the displacement angle θ_{IV} through equation (11). Then, the loss angle δ is determined,

in degrees, from equation (10), and converted subsequently into radiants. At last, the loss factor is calculated simply by performing the tangent of the loss angle. The result is shown to the user together with a waveform chart that plots also all the loss factor values calculated in the previous cycles. As it can be seen by figure 3.23, a moving mean calculation of 1000 tan delta values is also performed, together with a standard deviation calculation. Since, as previously explained, one value of tan delta is determined in 200ms, the measurement must go on for at least 200 seconds in order to collect 1000 dissipation factor values.

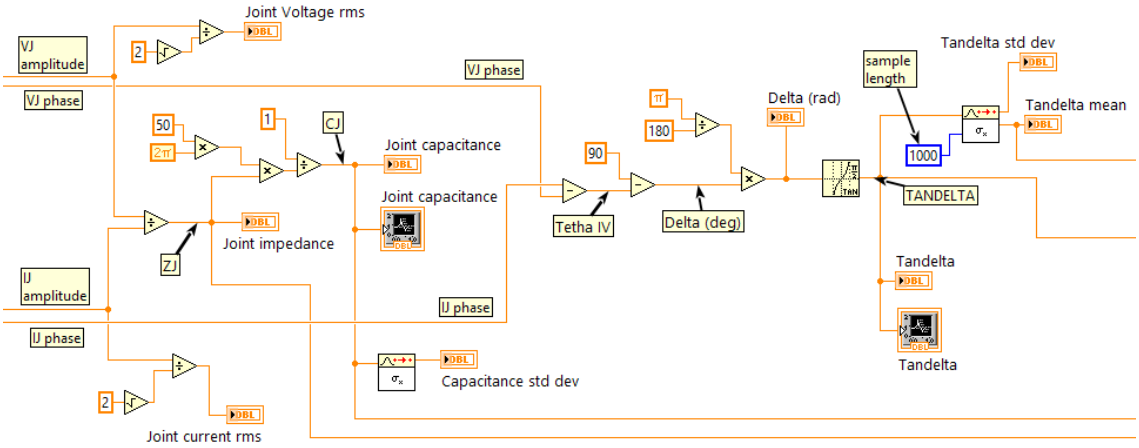

Fig. 3.23: *Part of the LabVIEW program responsible for the calculation of joint capacitance, impedance and tan delta.*

3.3.2.3 Saving of data

The final part of the LabVIEW program is responsible of the saving of the measured data on text files. In fact, as it can be seen by figure 3.24, three different *Write Delimited Spreadsheet* blocks are used in order to save the input values on the text files. These files are indicated by a file path that can be inserted from the front panel. The

input of the block is, in case of the tan delta mean file and tan delta file, a 1D array composed by one element at time or, in case of the C-Z file, by one 2D array composed by two rows with one element each at time. From the explanations made before, it is clear that, while the program is running, on each text file one measured value is written every 200ms, namely 5 values per second. Hence, basically the used block is able to convert the input array to a text string and to append it to an existing file. It is also possible to select the format and to transpose the element, in order to see the different measurement result on a column instead of in a row.

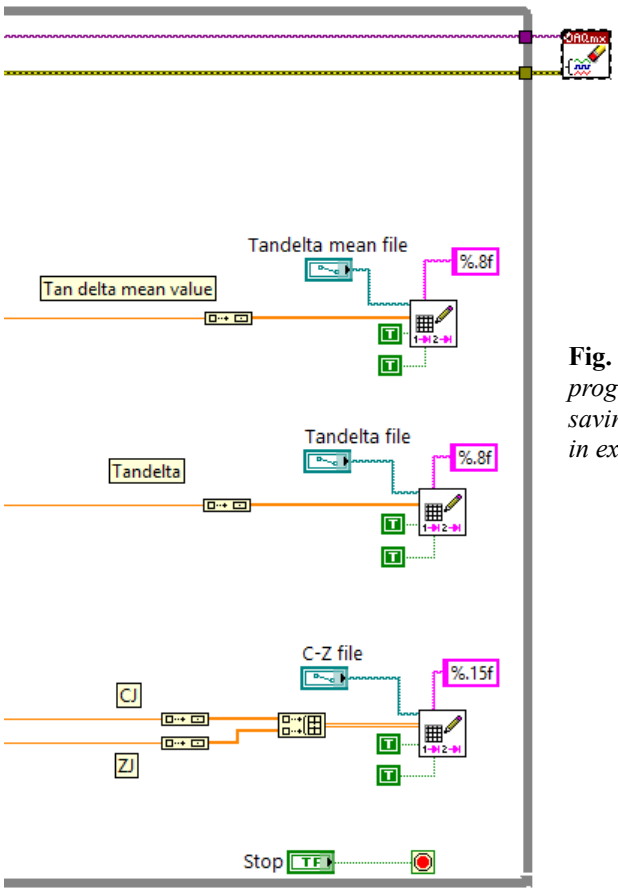

Fig. 3.24: *Part of the LabVIEW program responsible for the saving of all measurement data in existent text files.*

From figure 3.24 it is possible to see also the closing part of the *while cycle*. When the user presses the stop button on the front panel, the *while cycle* ends: all the calculations are stopped and no data are saved on the text files anymore. Furthermore,

thanks to the *DAQ Clear Task* block, when the *while loop* ends, also the acquisition of the voltage data from the Data Acquisition Board are stopped. When this happens, the measurements are over.

3.3.3 Front panel

The front panel is the only part of the program that, normally, is visible to the user. Thus, it must contain all the fundamental information needed for the correct continuation of the measurements. The front panel of the developed loss factor measurement program is shown in figure 3.25.

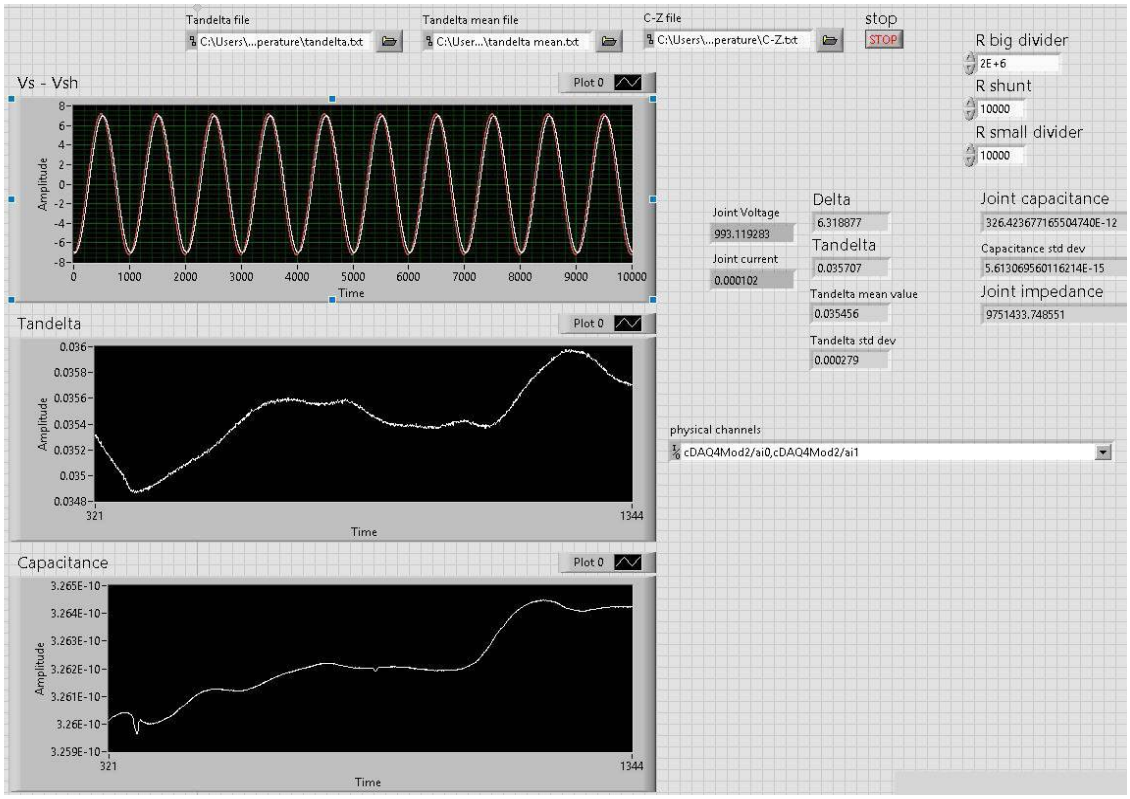

Fig. 3.25: *Front panel of the LabVIEW program at the end of a measurement session.*

First at all, the user must insert the value of the measurement circuit resistances, previously characterized. Furthermore, he must insert the file paths of the already existing text files where the measured values will be saved. Also the physical channel codes of the used channels of the Data Acquisition Board have to be expressed. The

figure 3.25 shows how the front panel looks after almost 200 second of working, so after more than 1000 tan delta measurements. Starting from the upper left part, the first graph presents the waveform of the input voltages V_S and V_{SH} and it is updated every 200ms: in practice it shows the 10 000 samples that are processed per time and that will lead to one measured value of the loss factor. It can be noticed that the amplitudes of these voltages reflect the designed ones of equation (14). Furthermore, it can be noticed that the V_{SH} (the red waveform) have effectively a slightly higher peak value due to the presence of the joint current, as predicted with equation (26) in 3.2.2.2. The other two charts show all the measured values of tan delta and of the sample capacitance in relation to the measurement time: in order to completely fill these graphs almost 200 seconds must be waited. The other information showed to the right of the waveform charts are the value of the loss angle, the tan delta value, the actual mean value of loss factor measurements, its standard deviation and, as last, the joint capacitance and impedance. Also these values are updated every 200ms. The measured rms values of the joint voltage V_J and current I_J are given too. From the values shown in picture 3.25 it can be checked that the actual measured joint voltage and currents reflect the rms values that were determined during the design stage of the measurement circuit, in subsection 3.2.2.2, in particular with equation (24). This is an important method for the user to check that, during the measurements, everything is proceeding in a good way, without issues as bad contacts, instabilities or overvoltages. Also these values are updated every 200ms.

3.4 Measurement procedure

In the following it is going to be explained how practically the dissipation factor measurements are performed, considering also the thermal cycles done on the joint samples. Now, as repeated many times, the objective of this research is to measure the loss factor of the cable joints in three conditions: at ambient temperature, high temperature and low temperature. In this way, night-day temperature cycle or an overload-non overload cable condition can be simulated. One cycle of tan delta

measurements performed on the joint samples consists on the following procedure:

- Loss factor measurement at ambient temperature;
- heating up of the four samples for 2 hours;
- loss factor measurement at high temperature;
- cooling down of the four samples for 2 hours;
- loss factor measurements at low temperature.

Then this cycle is repeated. As it will be better seen on chapter 4, in this study 8 measurement cycles have been performed on all the four joint samples. In particular, one full day of work is needed to complete one dissipation factor cycle of measurements. From what just said, in each measurement day, 12 loss factor measurements cable joints are then performed, since the tan delta of the four samples is measured at ambient temperature, at 60 degrees and at 10 degrees. Hence, the joint sample has to be changed in the measurement circuit exactly 12 times a day. Consequently, a fast procedure of sample replacement has to be developed. This procedure is needed mainly because after heating up or cooling down the joint samples, measurements must be performed as soon at possible in order to avoid that the joint temperature returns back to the ambient one.

In figures 3.26 and 3.27 the method adopted to speed up the sample change is shown, taking care also on the quality of the electrical connections. The bar of the secondary of the step up transformer is connected to the high voltage electrode of the joint (namely the cable conductor) using a cable tie. Then, the ground electrode of the sample (the external aluminum cage) is connected to the measurement circuit thanks to a screwed cable connector (a cable is already mounted on the external joint cage as seen on section 3.1). On this way, simply by using a screwdriver, the cable joint under test can be substituted with another one in about one minute, preserving the temperature of the samples. This requirement on the speed of sample change is due to the fact that the thermostatic chamber is used also as protection cage during loss factor measurements. In fact, since four joint samples are used, measurements cannot be performed directly

during their heating up or cooling down: the samples has to be changed in the measurement circuit with the procedure explained above. So, the chamber cannot be used as a thermostatic chamber anymore when measurement are ongoing. The only way to avoid a fast sample change could be to perform a thermal cycle leaving only one cable joint connected in the circuit at time and performing measurements without opening the chamber itself. However, this would not be feasible in term of the time needed to complete one cycle of tan delta measurements for each joint sample.

Fig. 3.26: *Before and after the sample joint installation. The two boxes let the sample ground to not touch the chamber.*

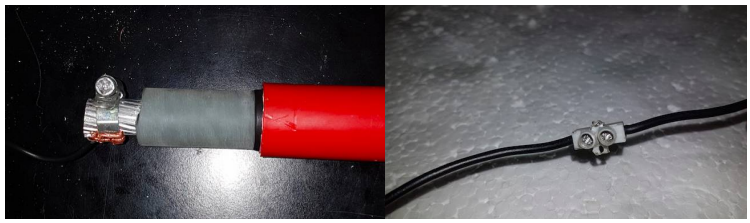

Fig. 3.27: *Focus on the connections of the sample to the measurement circuit: the high voltage cable tie on the left and the ground screwed cable connector.*

3.4.1 Safety precautions

Since the measurements are performed using a supply voltage of $1kV_{rms}$, some safety precautions have to be taken. First at all, the step up transformer, the resistor divider and the shunt resistor are placed inside a grounded cage located under the thermostatic chamber, as it can be seen by figure 3.28. In this way, the eventuality to

accidentally touch these high voltage parts of the measurement circuit is avoided.

The thermal chamber, as previously mentioned, is used also as protection chamber, containing the cable joints under test while measurements are running. Now, the main safety issue consists in the fact that samples have to be changed a lot of times: if supply voltage has not been correctly disabled, there is the danger of being shocked by the step up transformer secondary bar, located inside the thermal chamber, visible in figure 3.26. In order to absolutely avoid that occurrence, the chamber doors are equipped with a sliding contact that, when the doors are opened, sends a signal to a switch to open the circuit supply. However, obviously, before changing the sample, the supply voltage is manually disabled directly from the Agilent 6813B programmable power source.

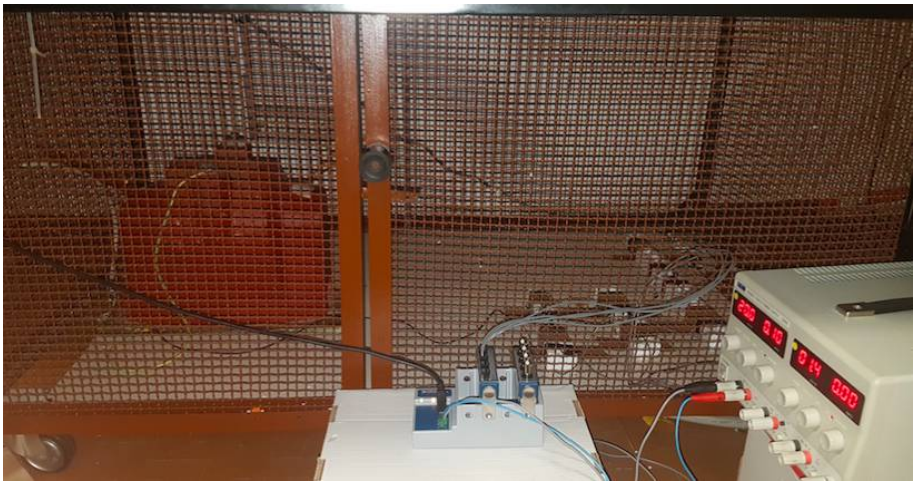

Fig. 3.28: *The working step up transformer and the circuit resistors inside the shielding cage. It can be also noticed the Data Acquisition Board connected to its supply generator.*

Fig. 3.29: *Particular of the thermostatic chamber in figure 3.15 showing the door sliding contact protection.*

4 Results

4.1 Statistical analysis of measurement data

In the latter chapter the methodology and the procedures used to perform loss factor measurements on medium voltage cable joints have been widely explained. Summarizing, a joint sample is mounted in the measurement circuit, the supply voltage is activated and then the LabVIEW program is started. The dissipation factor is measured once every 200ms and the measured values are saved on a text file. The user ends the measurement procedures after almost two minutes, when more that 1000 tan delta values have been obtained. For sake of brevity, this procedure is indicated in the following treatments as “measurement session”. The purpose of this section is to determine the procedure to be applied in order to calculate the loss factor result together with its uncertainty for any measurement session, regardless of the sample type and of the temperature condition. In other words, it is going to be analyzed how the hundreds of data obtained after one measurement session are statistically analyzed in order to obtain the final dissipation factor result for the considered session.

Errors in measurements are defined as deviations between the instrument reading and the true value of the measured quantity. In particular, they are distinguished in systematic and random errors. The uncertainty affecting the measurement result, instead, is the effect of errors on the measurement itself and it is defined as the lack of knowledge on the true value of the measurand [54]. In particular, the uncertainty of a measurement provides the range of values within the true value of the measurand can fall with a given probability. It is important to underline that the true value of a measured quantity cannot be never known exactly and that any measurement result is only its approximation. Hence, every measurement result must be necessarily accompanied by its related uncertainty, namely the range of value, constructed around the measurement result itself, in which the true value of the measurand can fall, as said, with a given probability.

4.1.1 Systematic error analysis

Systematic errors, considering a fixed measurement setup, have the characteristic to never change in time and to have precise and knowable sources. If these sources are identified, they can be compensated leading to a strong reduction on systematic errors affecting the measurements. In particular, in the measurement circuit of the present study, the main source of systematic error is the possible drift between the value of resistances inserted in the measurement LabVIEW program and the real one. This systematic error can be minimized through the calibration of the used resistors, as seen in section 3.2.3. In fact, after the measurement of resistance values, accomplished with very high accuracy, and thanks to the high stability characteristic of the resistors used, it is known that the value of resistance inserted in the measuring LabVIEW program reflects in a very accurate way the real one. So, the drift between the value of resistance inserted in the measurement program and the real one is minimized and, also thanks to observations in error propagation made in 3.2.3, the consequent error can be neglected.

Systematic errors can derive not only from circuital components but also from measurement instruments. In particular, in the actual measurement setup, systematic errors are introduced by the Data Acquisition Board during the sampling of the two voltage signals. However, by reading the NI DAQ datasheet [48], it can be noticed that, since in the present study $5V_{rms}$ sinusoidal signals at 50 Hz are acquired using the maximum sampling capability, the accuracy with which the sampling of the input voltage is performed is expected to be very high. Indeed, the following specifications can be extracted from the datasheet [48]:

- ±0.03% of gain error;
- ±0.008% of range error where the range equals 10.52 V;
- 0.075°/kHz maximum of phase mismatch channel-to-channel.

So, being the input signals sinusoids with $5V_{rms}$ and 50 Hz, the uncertainty due to the Data Acquisition board in the acquired voltage is in the range of mV for the amplitude

and of millidegrees for the phase mismatch between the two channels. Thus, the uncertainty in the determination of the input voltages is in the range of some hundredth of percent and it can be assumed negligible for the calculation of tan delta. This affirmation holds because, as it is going to be seen in the next section, the uncertainty in the calculation of the loss factor result introduced by random errors is more than one order of magnitude bigger than the one introduced by systematic ones. In other words, the contribution in the uncertainty of the measured tan delta value due to systematic errors introduced by the DAQ is neglected since it is much less significant in comparison to the contribution due to random sources of errors. Moreover, even the uncertainty introduced by random errors will never overcomes the tens of percent of the final result and, as it will be seen later, the variation of tan delta related to temperature oscillations is much larger than the uncertainty in the measured value. Hence, it is never met situation in which the loss factor behavior versus temperature is not clear because of uncertainties in the measured tan delta value. As a consequence, the decision of not consider the systematic contributions never affects the conclusions derived by analysis of the tan delta trend versus temperature: the uncertainty due to systematic error it is not significant in size relatively to the required measurement accuracy. From the latter considerations, it follows that the uncertainty on the tan delta measurement result is evaluated exclusively using the Type A methodology, thus through the statistical analysis of series of observations, as it is going to be explained.

4.1.2 Random error analysis

Random errors are always present in measurements and arise from unpredictable or stochastic temporal and spatial variation of influence quantities due, for example, to thermal noise [54]. The sources of this kind of error cannot be identified and compensated, thus random errors affecting measurements cannot be eliminated. In general, the effects of random variations in unknown influence quantities of the system cause variations in repeated observations of the measurand [54]. Indeed, in this particular case of study, when repeated tan delta observations are done during one

measurement session on a same joint, the dissipation factor reading continuously varies on the last decimal digits. Then, since random errors cannot be compensated, in order to manage their effects on measurements and reduce the uncertainty on the results, the only way is to increase the number of observations, as it is going to be demonstrated.

First at all, some assumptions have to be made. For electrical measurements, the samples are assumed to be intrinsically random. Therefore, all the tan delta observations are supposed to be independent and obtained in the same measurement conditions. Furthermore, it is assumed that, during a single measurement session, the true value of the loss factor of the joint under test is not varying but it remains stable. In other words, the measurand is an ideally constant quantity but actually the noise is superimposed to it. After these assumptions, it can be stated that the tan delta reading on the LabVIEW program is a random variable having unknown probabilistic distribution and unknown variance and that its true value is the constant tan delta that would be measured in a noiseless ideal world. The purpose is then to infer the tan delta true value with an estimation having the highest possible accuracy. Now, referring to documents [53] and [54], it can be also stated that, under the previous assumptions, the expected value of this kind of random variable is considered to be equal to its true value. So, if infinite loss factor observations would be done, the expected value of the probabilistic distribution of loss factor values would be exactly known but, in the real situation, the expected value can be only estimated.

According to [54], the best estimate of the expected value μ_q of a certain quantity q, that varies randomly and for which n independent observations q_k have been obtained under the same measurement conditions, is the arithmetic mean of the n observations, calculated as:

$$\overline{q} = \frac{1}{n} \sum_{k=1}^{n} q_k \tag{40}$$

In the present study, q_k corresponds to one single value of tan delta of the joint under test observed in 200 ms on the LabVIEW program while n corresponds to the total

number of tan delta measurements made on that joint on one measurement session. As repeated many times, for every measurement session, $n > 1000$ and, as said before, the individual observations q_k differ in value between each other because of the influence of random sources of error that affects the measured values. Since it has just been explained which is the best estimation of the dissipation factor true value, obtained through the observation of *n* loss factor values, what is now of primary interest is the quantification of how well $\overline{q}$ estimates the expected value μ_q .

In probability theory, thanks to the Central Limit Theorem, it can be demonstrated that, considering *n* values of a random variable q with any probabilistic distribution, the arithmetic mean is a new random variable with a distribution that tends to be Normal for $n \to \infty$. In particular, considering $n > 1000$, as in the present case of study, the probability distribution of the mean values can be surely assumed to be Normal. From this theorem, it can be also stated that the expected value of the probabilistic distribution of the mean values is μ_q , that is the same expected value of the original random variable q . Moreover, it can be demonstrated that the variance of the Normal distribution of the means is $\sigma_m^2 = \sigma_q^2 / n$, where σ_q^2 is the variance of the probabilistic distribution of q . Hence, it is clear that the probability distribution of the arithmetic means of *n* values of q is certainly less disperse around μ_q than the distribution of q itself and, furthermore, it has a Normal shape. The problem is that, considering a finite number of observations *n,* σ_q is unknown,. Now, by knowing only the estimated value $\overline{q}$ of the expected value of the population, an unbiased estimator of the unknown variance σ_q^2 of the probability distribution of q can be obtained by:

$$s^2(q_k) = \frac{1}{n-1} \sum_{k=1}^{n} (q_k - \overline{q})^2 \tag{41}$$

Hence, since from the Central Limit Theorem it can be written that $\sigma_m^2 = \sigma_q^2 / n$, thanks to the knowledge of the estimator of the variance $s^2(q_k)$ of the distribution of the observations, it is possible to estimate the variance of the Normal probability

distribution of the means as:

$$s_m^2(\overline{q}) = \frac{s^2(q_k)}{n} = \frac{1}{n(n-1)} \sum_{k=1}^{n} (q_k - \overline{q})^2 \tag{42}$$

In the following, instead of the variance, the standard deviation of the mean is used, $s_m(\overline{q}) = \sqrt{s_m^2(\overline{q})}$, since it has the advantage of having the same dimension of q .

Summarizing, until now it has been explained that, starting from a random variable q with any probabilistic distribution (green line in figure 4.1) and considering a fixed number n of observations of it, the mean value $\overline{q}$ of the n observations is the best estimator of the expected value μ_q . In particular, $\overline{q}$ is a random variable as well having a Normal distribution centered in μ_q (red line in figure 4.1) and with variance estimated from equation (42).

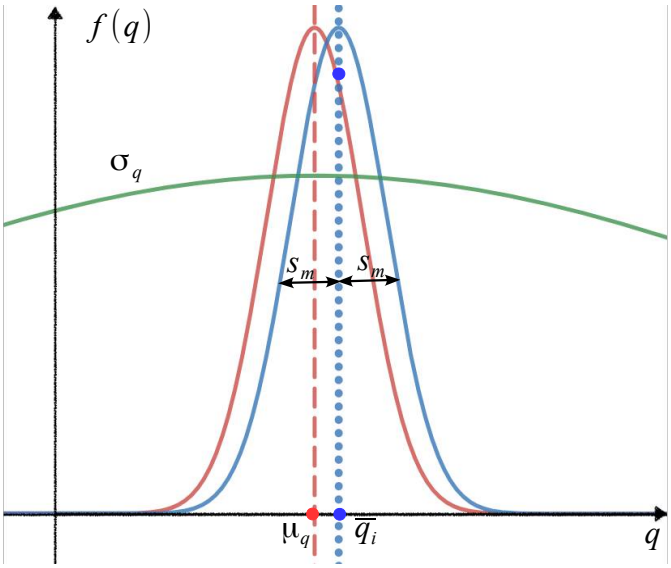

Fig 4.1: *Qualitative plot of the probabilistic distributions of the random variable q (green line) and $\overline{q}$ (in red). In blue is represented the fictitious distribution around one calculated mean value of n observations of q .*

Now, when n observations of q are practically performed and their mean value is determined, basically this calculated mean value is just one point (namely one sample)

of the $\overline{q}$ probabilistic distribution. However, this calculated mean value, indicated as $\overline{q_i}$, can be also considered as the expected value of a fictitious Normal distribution of means (blue line in figure 4.1) having the same standard deviation $s_m(\overline{q})$ of the real distribution of mean values of q. Therefore, every time n observations of q are done and their mean value is calculated, there is the 63% of probability that the expected value of the distribution of the mean values μ_q, namely the true value of the measured quantity, falls inside the interval $\pm s_m(\overline{q})$. Hence, a range can be built around $\overline{q_i}$, called confidence interval, in which the true value of the measured quantity can fall with a known probability. This interval quantifies of how well $\overline{q_i}$ estimates the expected value μ_q.

From equation (42) it is clear that, for a larger number of observations n, the confidence interval $\pm s_m(\overline{q})$ is expected to be smaller: it means that the arithmetic mean value will estimate, in this case, with less uncertainty the true value of the measured quantity. In particular, the number of observations n should be large enough to ensure that the probability distribution of the means is reliably approximated to a Normal function. Now, the interval $\pm k\, s_m(\overline{q})$ is defined as generic confidence interval where k is the coverage factor:

- if $k = 1$ then the true value μ_q in included in $[-s_m(\overline{q}), +s_m(\overline{q})]$ with 68% of probability;
- if $k = 2$, μ_q is included in the interval $[-2\, s_m(\overline{q}), +2\, s_m(\overline{q})]$ with 95% of probability;
- if $k = 3$, μ_q is included in the interval $[-3\, s_m(\overline{q}), +3\, s_m(\overline{q})]$ with 99.73% of probability.

It must be remembered that, in all the calculation performed in the present study, a coverage factor equal to 2 is always considered.

From the latter treatment it can be concluded that, even if the analyzed phenomenon

is quite variable or there are significant measurement errors, it is still possible to reduce uncertainty in the estimate of the mean by performing many measurements. The confidence interval represents the value of the measurement uncertainty due to random sources of errors and $s_m(\overline{q})$ is usually referred as standard uncertainty u . The tan delta result of one measurement session on any cable joint is then provided in the following form:

$$\tan\delta = \overline{\tan\delta} \pm k\ s_m(\overline{\tan\delta}) \tag{43}$$

From equations (40) and (42), the explicit calculations of the measurement result are, using a coverage factor of 2:

$$\overline{\tan\delta} = \frac{1}{n}\sum_{j=1}^{n}\tan\delta_j \tag{44}$$

$$\tan\delta = \overline{\tan\delta} \pm 2\sqrt{\frac{1}{n(n-1)}\sum_{j=1}^{n}(\tan\delta_j - \overline{\tan\delta})^2} \tag{45}$$

where n is the total number of tan delta observations done by the LabVIEW program and $\tan\delta_j$ is the jth result of one tan delta observation, performed in 200ms.

4.2 Tan delta measurement results

4.2.1 MATLAB functions for measurement result calculation and plot

Considering one tan delta measurement session, the LabVIEW program that rules all the measurement procedure gives in output a text file containing in column hundreds of loss factor observations made on the sample joint during the two minutes of test. In order to apply the equations (44) and (45) to obtain the measurement result together with its uncertainty, a very simple MATLAB function, showed in figure 4.2, is used.

In the MATLAB command window, the loss factor measurements contained in the text file are saved in one vector `a`. The length of this vector obviously corresponds to

the number of tan delta observations made by the LabVIEW program. The function `Result(a)` is subsequently called. It takes in input the `a` vector and it simply gives in output the tan delta mean value and the standard uncertainty of the measurement performed. These values are then copied and saved on an Excel file that collects all the loss factor measurement results referred to the joint sample considered in the session.

```
1   function [m,u] = Result( a )
2   num = 0;
3   n = length(a); %number of tan delta measurements
4   m = mean(a); %mean value of tan delta measurements
5   for i=1:length(a)
6   num = num + (a(i) - m)^2; %numerator of the the arithmetic mean variance
7                             % equation
8   end
9   sm = sqrt(num/(n*(n-1))); %Standard deviation of the mean
10  u = 2*sm; %Standard uncertainty
11
12  end
```

Fig 4.2: *The simple MATLAB function used to obtain the tan delta measurement result* `m` *together with its standard uncertainty* `u`.

After eight days, when all the thermal cycles have been performed and all the tan delta measurement data have been obtained for each joint, all the results have been collected in their own Excel tables. Then, these results must be plotted. To this purpose, the MATLAB function `barwitherr(errors,varargin)` is used. This function allows to obtain grouped bar plots together with the measurement uncertainty on every bar: it is a simple extension of the MATLAB bar function made in order to include error bars. The function is available for free in the file exchange section of the MATLAB web community [58]. The two parameters in input are firstly the errors to be plotted and then the parameters passed as in a conventional bar plot. Now, during every measurement day, three tan delta measurement sessions, each one at a different temperature, are performed on each joint. So, it is convenient to show the results in the bar plot in groups of three: each group corresponds to one thermal cycle done on the joint considered. By organizing the loss factor result plots in this way, the trend of the dissipation factor in relation to the joint temperature, during each cycle, should be more clear. Now, in order

to correctly apply the function `barwitherr` and create group plots, for each joint sample two 8x3 matrices have to be created. One matrix contains all the tan delta mean value data while the other one contains all the confidence interval data referring to the measurements performed on the joint sample considered. In each matrix row are present the information related to one single thermal cycle, always in the subsequent order: room temperature, high temperature, low temperature. Once the matrices have been created, the plot function is called in the command window, as it can be seen in figure 4.3, and consequently the graph will be showed to the user.

```
>> figure
h = barwitherr(err100, a100);% Bar plot with errorbars

set(gca,'XTickLabel',{'1st cycle','2nd cycle','3rd cycle','4th cycle',
     '5th cycle','6th cycle', ' 7th cycle','8th cycle'}) %The eight groups are named
legend('Room temperature','60 degrees','10 degrees') %The legend is set
ylabel('Tan delta')
title('Tg 100 REPL Cable Joint sample')
grid
   set(h(1),'FaceColor','y');
   set(h(2),'FaceColor','r');  %the bar colors are set
   set(h(3),'FaceColor','b');
```

Fig 4.3: *The MATLAB command window for the bar plot of Tg 100 REPL Cable Joint sample. Notice that* `err100` *and* `a100` *are simply the two 8x3 matrices previously constructed.*

4.2.2 Measurement results

In this subsection, the results of all the loss factor measurements performed on cable joints, associated to the different temperature conditions, are going to be presented. As explained in section 3.1, in the present study four joint samples are used, named for sake of clarity Tg 100 REPL, Tg 150 REPL, In-field Joint n°1 and In-field Joint n°2. The results are shown, at first, on a table collecting all the calculated data and then on the bar plot. In both cases the results are given together with their own uncertainties and they are always associated to the joint temperature. It must be noticed that, in the case of bar plots, uncertainties are showed using a line on the top of the bar that represents the confidence interval of the result. However, usually that interval is two order of magnitude lower than the tan delta mean value and so it is barely visible on

the bar plots while it is explicitly expressed on the tables. As explained for the bar plots in 4.2.1, also in the tables the results are grouped according to the temperature cycles.

Eight different thermal cycles have been performed. Thus, a consistent number of results is available to infer if some repetitive trend of dissipation factor in relation to temperature exists. Here below the measurement results are just presented with a short description of them. Their discussion will be the main topic of the next chapter.

4.2.2.1 Tg 100 REPL Cable Joint sample

As it can be seen from table 4.1 and figure 4.4, the loss factor of the Tg 100 REPL cable joint oscillates between, indicatively, 0.0018 and 0.12: the absolute range of variation seems then quite large.

Temperature	Tan Delta Mean Value	Confidence interval
Room temperature	0.018267	1.28E-05
60 degrees	0.006361	1.15E-04
10 degrees	0.068748	4.45E-04
Room temperature	0.041756	1.84E-05
60 degrees	0.003192	3.15E-05
10 degrees	0.044957	1.86E-05
Room temperature	0.035312	1.91E-05
60 degrees	0.004272	9.88E-06
10 degrees	0.119921	4.97E-04
Room temperature	0.042769	1.56E-05
60 degrees	0.002995	1.48E-05
10 degrees	0.055869	1.85E-04
Room temperature	0.035343	1.80E-05
60 degrees	0.001962	1.07E-05
10 degrees	0.053946	2.22E-04
Room temperature	0.046489	2.24E-05
60 degrees	0.002459	1.62E-05
10 degrees	0.042232	7.55E-05
Room temperature	0.041769	5.76E-05
60 degrees	0.002675	2.04E-05
10 degrees	0.038632	9.38E-05
Room temperature	0.040861	1.41E-05
60 degrees	0.003204	2.86E-05
10 degrees	0.053747	1.03E-04

Table 4.1: *Tan delta measurement results of the Tg 100 REPL cable joint sample.*

This tan delta variation seems to be not random but correlated with the temperature cycle performed on the sample joints. Indeed, from figure 4.4 a pattern can be recognized: by performing at 25 degrees the first tan delta measurement, when the temperature increases, the loss factor of the joint noticeably decreases while, when the joint is cooled down, the dissipation factor clearly increases in value. So, the loss factor seems to have a relation of inverse proportionality with the temperature. It must be also noticed that the confidence interval of tan delta results, at each temperature condition, is very small and it could be barely seen on the bar diagram.

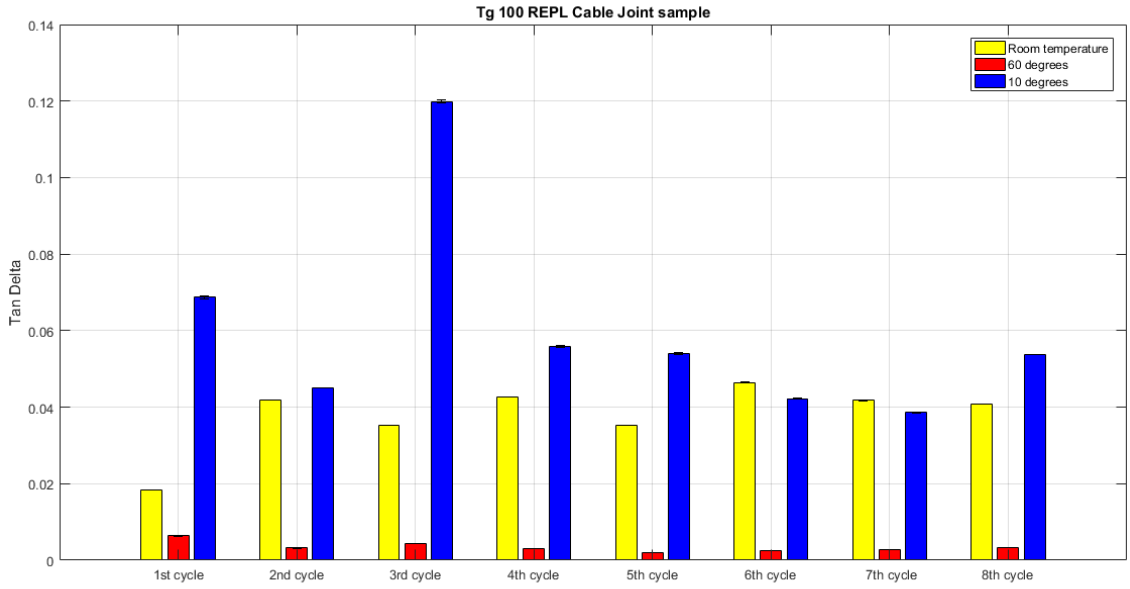

Fig 4.4: *REPL Tg 100 Tan delta bar diagram with results grouped in cycles.*

In contrast to the found results, considering studies that investigated the properties of silicon rubber insulating material taken alone (so without considering a whole complex system, as in the present work), the dissipation factor is expected to increase when the temperature of the material rises [55; 56; 57]. This tan delta behavior is widely explained in [57]: summarizing, the dissipation factor is expected to rise with the temperature growth due to the increase of particle collisions caused by the enhancement of the thermal energy. The proposed explanation on why the investigated tan delta behavior versus temperature is different in the present study will be widely analyzed in

the next chapter. The purpose of this section is mainly to check that the correlation between loss factor and temperature cycles seen in the Tg 100 REPL Cable Joint sample is confirmed also by measurements performed in the other three sample joints. In the following subsections the other results are going to be presented.

4.2.2.2 Tg 150 REPL Cable Joint sample

Temperature	Tan Delta Mean Value	Confidence interval
Room temperature	0.010825	1.14E-005
60 degrees	0.010676	1.04E-004
10 degrees	0.019169	5.51E-005
Room temperature	0.013438	3.49E-005
60 degrees	0.005149	2.76E-005
10 degrees	0.039632	2.25E-004
Room temperature	0.017096	6.45E-005
60 degrees	0.004453	1.38E-005
10 degrees	0.060845	3.41E-004
Room temperature	0.020078	2.87E-005
60 degrees	0.005037	2.34E-005
10 degrees	0.048588	1.24E-004
Room temperature	0.016701	1.73E-005
60 degrees	0.00539	1.40E-005
10 degrees	0.044536	4.35E-005
Room temperature	0.027264	4.98E-005
60 degrees	0.006318	1.70E-005
10 degrees	0.069076	2.27E-004
Room temperature	0.026077	6.42E-005
60 degrees	0.005241	1.80E-005
10 degrees	0.048452	9.45E-005
Room temperature	0.023348	2.89E-005
60 degrees	0.006137	2.23E-005
10 degrees	0.062968	1.33E-004

Table 4.2: *Tan delta measurement results of the Tg 150 REPL cable joint sample.*

As table 4.2 shows, for the REPL Tg 150 Cable Joint sample, in general, the tan delta measurement results seems to have a slightly lower value comparing to the REPL Tg 100 joint. Also for this sample, the absolute range of variation of the loss factor

depending on joint temperature is quite large. However, the most important aspect is that, from the bar diagram analysis, it can be concluded that the loss factor trend related to temperature oscillations is the same of the previous sample: increasing the temperature, the loss factor value drops (compared to its value measured at room temperature) and, vice-versa, it visibly increases when the joint is cooled down. The only difference can be appreciated during the very first temperature cycle where there is not a visible change in the value of tan delta between room temperature and high temperature condition. However, this phenomenon is never repeated in the subsequent seven temperature cycles.

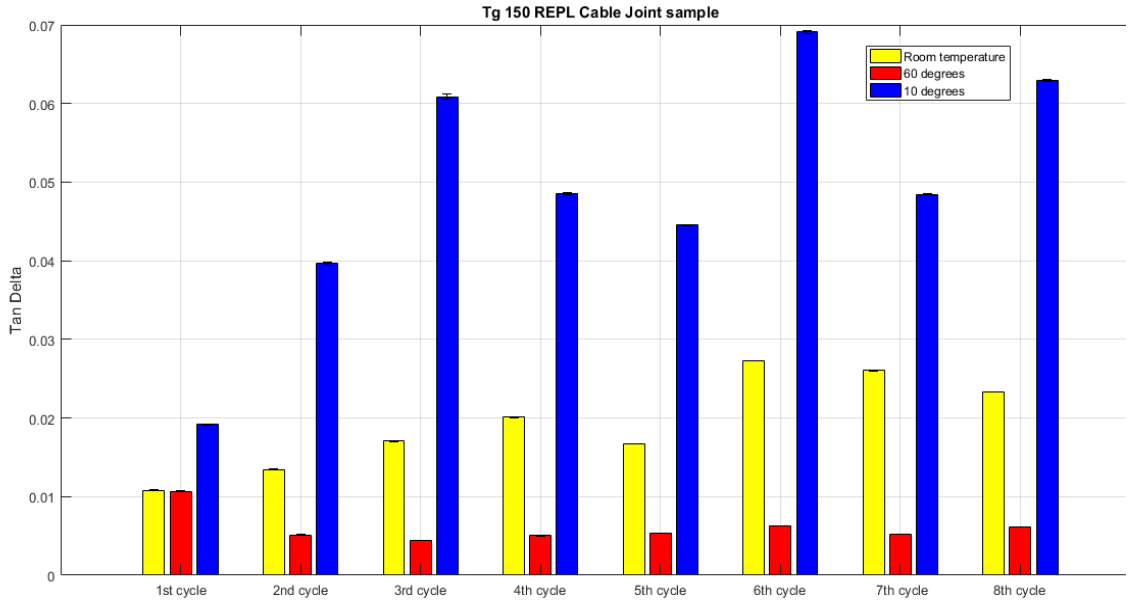

Fig 4.5: *REPL Tg 150 tan delta bar diagram with results grouped in cycles.*

4.2.2.3 In-field Cable Joint sample n°1

From the results shown in table 4.3 and from figure 4.6, it is possible to see that the absolute range of variation of the loss factor is in this case smaller than in the previous samples. This fact could be due to the differences in construction between the REPL and In-field samples and it will be analyzed more in detail in the next chapter. However, the most important aspect is that, even if the variation gap is smaller, also on this sample the

behavior of tan delta versus temperature is the same to the one seen in REPL joints.

Temperature	Tan Delta Mean Value	Confidence interval
Room temperature	0.017689	1.98E-005
60 degrees	0.011433	2.06E-004
10 degrees	0.014469	2.17E-005
Room temperature	0.022067	3.55E-005
60 degrees	0.012117	3.73E-005
10 degrees	0.012792	1.76E-005
Room temperature	0.017453	3.78E-005
60 degrees	0.014085	1.60E-005
10 degrees	0.013224	3.73E-005
Room temperature	0.020037	2.49E-005
60 degrees	0.013574	2.78E-005
10 degrees	0.015351	2.30E-005
Room temperature	0.020108	1.88E-005
60 degrees	0.013640	2.38E-005
10 degrees	0.016348	4.99E-005
Room temperature	0.017882	2.01E-005
60 degrees	0.013476	2.16E-005
10 degrees	0.016586	2.39E-005
Room temperature	0.021341	2.97E-005
60 degrees	0.013789	2.26E-005
10 degrees	0.021766	6.73E-005
Room temperature	0.024787	2.50E-005
60 degrees	0.013465	3.75E-005
10 degrees	0.023520	7.65E-005

Table 4.3: *Tan delta measurement results of the In-field Cable Joint sample n°1.*

From the diagram in figure 4.6 it can be noticed that, during the third temperature cycle, the loss factor decreases instead of increasing when the sample joint has been cooled down. That contrasting result is assumed to be due to an issue occurred during the measurement session: when the cable joint sample was mounted in the measurement circuit, the screw of the high voltage cable tie broke up. The measurement was attempted anyway, even if the cable tie could not be tightened as much as possible around the high voltage electrode of the sample. Luckily, this session was the last one of the third day of measurements and, the day after, the broken cable tie was substituted with a new one. In the subsequent five days of measurements, this conflicting behavior

of tan delta during the joint cooling was never found again. So, the tan delta measure of the last session of the third cycle of this sample has been defined as not trustable because of the explained cable tie issue and it is not taken into the account anymore.

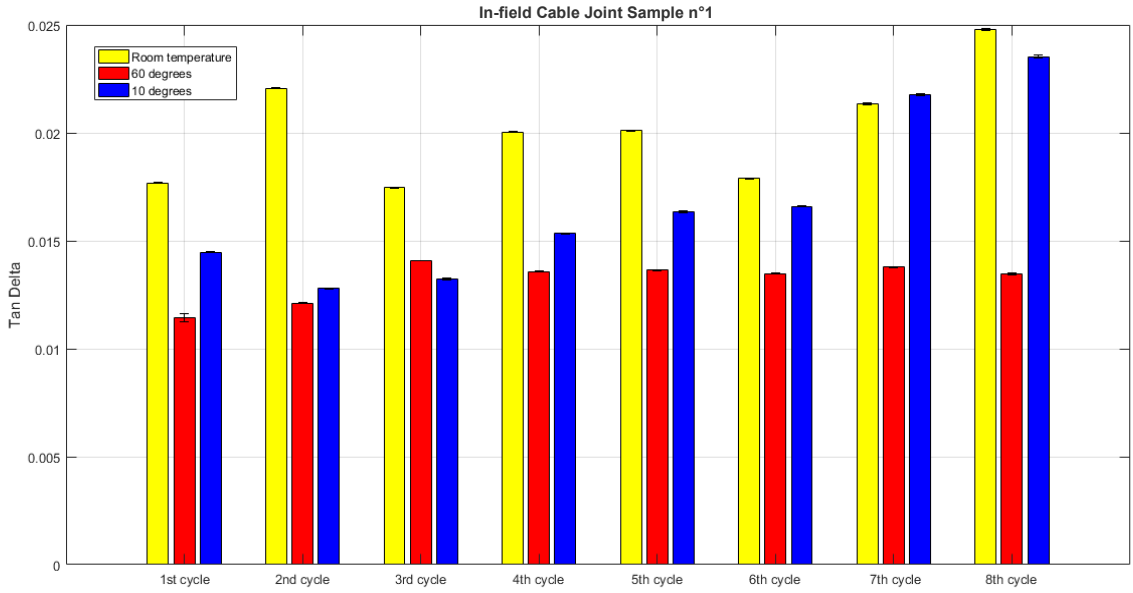

Fig 4.6: *In-field Joint n°1 tan delta bar diagram with results grouped in cycles.*

4.2.2.4 In-field Cable Joint sample n°2

Similarly to In-field Joint n°1, also on this sample the absolute range of variation of the dissipation factor is smaller than in the REPL joints. This behavior can be clearly seen by table 4.4. It is also clearly visible from the bar diagram in figure 4.7 that the tren of the loss factor in relation to temperature variation is the same of the other three joint samples: the tan delta tends to decrease as temperature increases relatively to the room one and tends to increase when temperature decreases.

In conclusion, this particular behavior of loss factor variations in relation to temperature oscillation seems to be a common trend among the different tested samples. This could indicate a possible correlation between the two phenomena. The discussion of this statement will be the main subject of the following chapter.

Temperature	Tan Delta Mean Value	Confidence interval
Room temperature	0.019661	1.51E-05
60 degrees	0.010795	1.40E-04
10 degrees	0.029822	6.66E-05
Room temperature	0.018977	3.44E-05
60 degrees	0.011207	4.50E-05
10 degrees	0.019502	7.43E-05
Room temperature	0.015931	1.76E-05
60 degrees	0.012170	1.41E-05
10 degrees	0.030786	3.21E-05
Room temperature	0.018669	2.25E-05
60 degrees	0.013552	2.14E-05
10 degrees	0.035146	8.13E-05
Room temperature	0.016599	1.76E-05
60 degrees	0.010895	1.79E-05
10 degrees	0.026844	1.43E-04
Room temperature	0.018879	2.48E-05
60 degrees	0.011360	2.25E-05
10 degrees	0.032067	6.88E-05
Room temperature	0.016994	2.95E-05
60 degrees	0.013737	3.69E-05
10 degrees	0.037572	9.78E-05
Room temperature	0.017723	2.09E-05
60 degrees	0.011372	4.16E-05
10 degrees	0.029115	5.50E-05

Table 4.4: *Tan delta measurement results of the In-field Cable Joint sample n°2.*

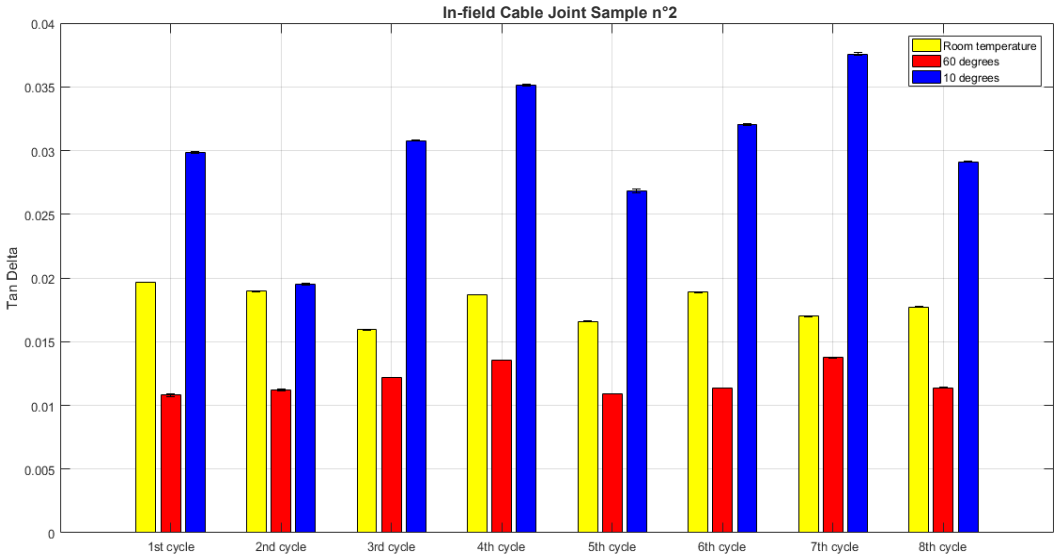

Fig 4.7: *In-field Joint n°2 tan delta bar diagram with results grouped in cycles.*

This page intentionally left blank

5 Discussion

In the latter chapter, where measurement results have been shown, a correlation between temperature cycles and dissipation factor trend has been detected: when the temperature rises, the loss factor of the joint decreases and vice-versa. In the present chapter, thanks to the analysis of some studies about thermal cycles performed on cable junctions, inferences on why loss factor in joints depends by the temperature in the detected way are proposed.

As said in 2.4, an increase in the loss factor value is associated to a rise of resistive losses in the dielectric material. Usually, when the tangent delta is measured in homogeneous insulating systems using a planar or cylindrical capacitor configuration, it results that the loss factor tends to increase when temperature rises: indeed, the conduction current through the insulating material is expected to increase due to the increment of particle collisions caused by the enhancement of thermal energy in the system [55; 56; 57]. However, the exact opposite relation between loss factor and temperature has been detected during the tests performed on cable joints. To explain this phenomenon, first at all, it should be considered that a cable joint is characterized by a much different and much more complex configuration, for what concerns the insulation system, comparing to a planar or cylindrical capacitor. Indeed, as explained in section 2.1, a complex dielectric constituted by several layers of different materials is arranged between the high voltage and the ground electrodes of a cable joint and not an homogeneous insulating system. In particular, the interface between cable dielectric and joint insulation is of crucial relevance: this interface is very important for what concerns the understanding of the loss factor behavior since it is the joint region in which the majority of losses are localized. In fact, as widely explained in section 2.3, the interfacial dielectric strength is always considerably lower than the joint main insulation body one. Now, a photo of a REPL cable joint with the shrinkable body cut in half is shown in figure 5.1 and the high voltage and low voltage electrodes are emphasized.

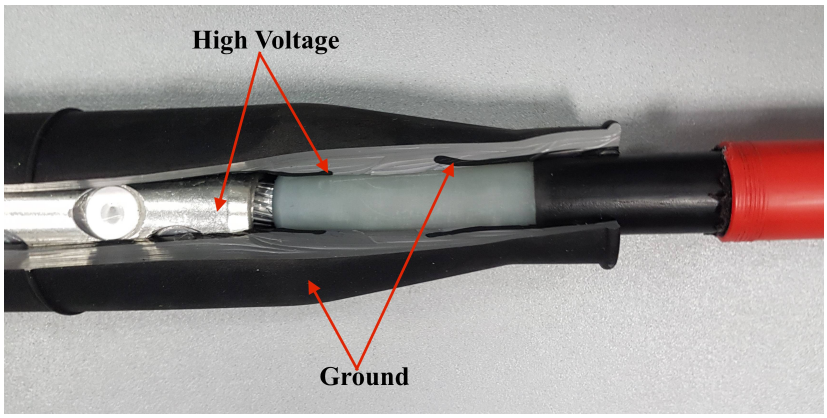

Fig. 5.1: *Cut REPL cable joint sample with high voltage and ground electrodes emphasized.*

It is clear that there are mainly two main possible paths for a charge that is crossing the joint dielectric from high voltage to ground, namely between the internal high voltage electrode and the outer armature, as in a normal power cable, or between the high voltage internal electrode protrusion and the grounded field grading deflector. In the first case, the charge is driven by the normal component of the electric field and this situation can be modeled using a simple planar capacitor having an homogeneous dielectric material through the armatures. Instead, the second case corresponds basically to the situation at the interfacial region and it can be effectively schematized by figure 5.2. In must be underlined that only the case of a cold shrink cable joint with geometrical grading is now considered but the same observation could be done for an heat shrink joint with refractive grading, for example.

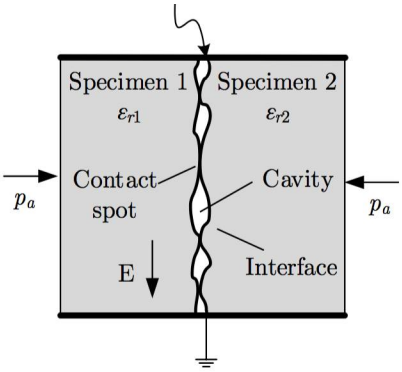

Fig 5.2: *Scheme of the situation at joint interface* [20].

In a cable joint, the majority of the resistive losses are expected to be concentrated in the dielectric interface since it is supposed to be the preferable way for the charges to pass from the high voltage electrode to the low voltage one: the microscopic voids present in the contact area of the two dielectrics should ease the conduction current to flow. In other words, the resistivity of the path between high voltage to low voltage electrodes is expected to be considerably lower along the interface rather than along the homogeneous dielectric material constituting the joint insulation body. Furthermore, reminding section 2.2, the dielectric interface present in cable joints is particularly critical also because an high value of the tangential component of the electric field, parallel to the interface itself, is present in that region. Hence, since the electric field has not a radial distribution anymore, it should force even more charges to flow between high voltage to ground through the interface. This situation is visualized using a simple model of the REPL joint sample done with the COMSOL Multiphysics software. This model has been developed to show that an high value of the tangential component of the electric field is necessarily present in the interfacial region because of the particular shape of the equipotential line in consequence of the cable joint geometry. In figure 5.4 the red lines represent the tangential component of the electric field and it can be easily seen that it is mainly located on the interface region, represented by a black line in the concerned figure.

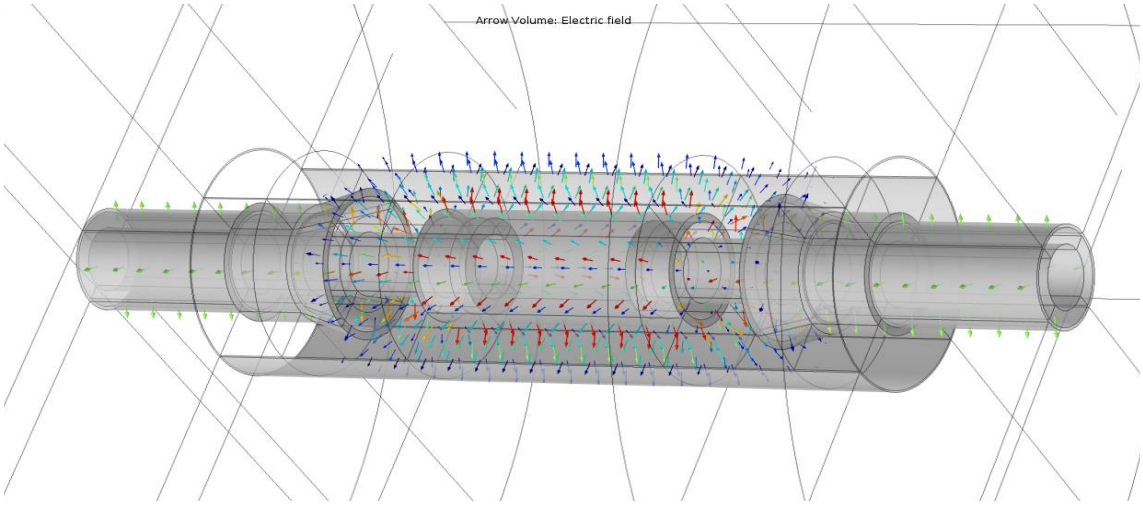

Fig 5.3: *Exploded view of the 3D REPL joint model where the distribution of the electric field in the insulation materials is represented.*

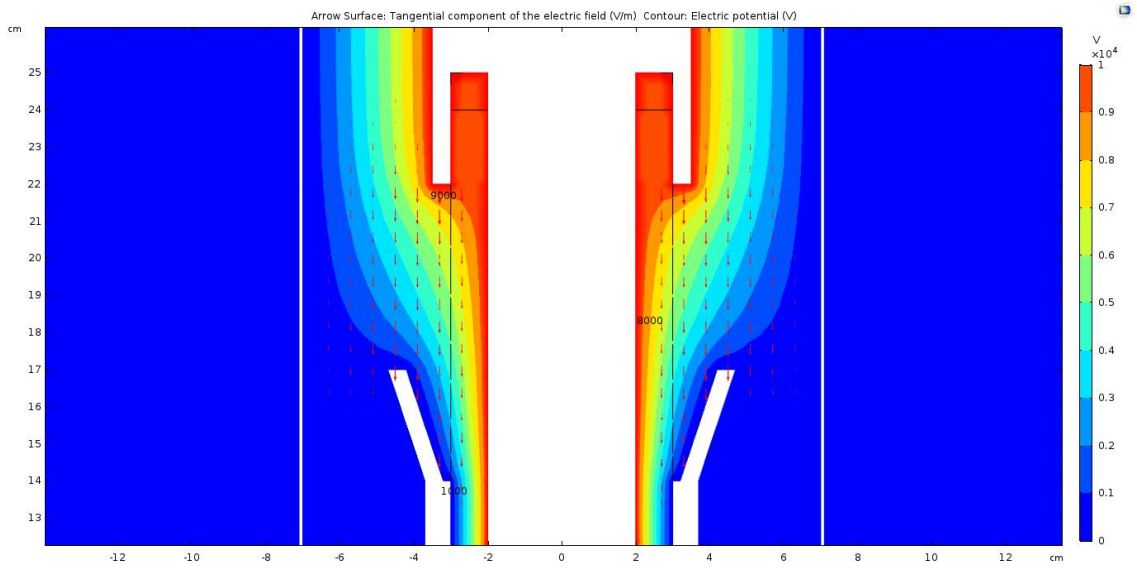

Fig 5.4: *Two dimension view of the XLPE-SiR interface region. With the rainbow colors the distribution of the electric potential is represented while the red arrows indicate the direction and magnitude of the tangential component of the electric field.*

Because of the fact that the majority of resistive losses in the joint dielectric system is supposed to be located at the interface and since the loss factor is defined as an indicator of the resistive power losses on a dielectric system, the tan delta value of a cable joint is expected to be strictly correlated on the conduction losses in the interfacial region. In other words, the joint loss factor should depend strongly by the amount of conduction current at the interface since the concerned current is expected to be always greater than the one flowing through the main joint insulation body. Then, if the resistive losses between high voltage to ground decrease in the bulk insulation while, in the same moment, they increase in the interfacial region, the tan delta is expected to increase since the magnitude of the conduction current flowing through the interface is supposed to be higher than the one present in the bulk insulation. Hence, it is hypothesized that the resistive losses located at the interfacial region drive the tan delta trend.

From what supposed, if some mechanical stresses are applied to the interface, leading for example to an increase or decrease of the interfacial pressure, the tan delta behavior is expected to be related to the condition of the interface. Being more clear, for

a same joint under test, the loss factor should increase if the pressure that tightens the interface decreases since, as explained in section 2.3, more and larger voids would create at the interface, decreasing the interfacial dielectric strength, facilitating the passage of charges between the high voltage electrode to the low voltage one and, at last, leading to an increase in conduction losses for the joint insulation.

It must be underlined that the two main hypotheses made in the latter treatment have to be demonstrated by tests, some of which are currently ongoing in the measurement laboratory of the University of Bologna. In particular, these tests have the objective to perform a measurement of the interfacial conduction current during a working condition of the joint. Then, the interfacial conduction current will be compared in magnitude with the resistive current flowing through the homogeneous joint insulation body, from the high voltage to ground electrode. The final aim is to demonstrate that the amount of dielectric resistive losses happening in the interfacial region are effectively higher than the ones in the main insulation body, constituted by an homogeneous dielectric. Furthermore, measurements of joint loss factor are going to be performed by increasing gradually the interfacial pressure, tightening more and more the cable joint body through the application of external forces. The aim is in this case to demonstrate that tan delta will be seen to decrease when the interfacial pressure increases.

The hypothesized link between the loss factor and the amount of conduction losses in the joint interfacial region has been just presented. However it should not be forgotten that the final objective is to find a possible explanation for the detected behavior of tan delta in relation to temperature. Therefore, it is important to focus now on the mechanical effects of temperature on cable joints. In [59], the variations of the interfacial pressure in a cable joint have been put in relation with temperature variations of the joint itself. The device under test was a 25 kV joint connecting two XLPE cables and insulated with an EPR shrinkable body. In particular, a tiny load cell was embedded at the interface together with a thermocouple, as it can be seen from figure 5.5. The graphs in figure 5.6 show that the interfacial pressure strictly follows the temperature

oscillations: it increases when temperature rises and it decreases with temperature reductions.

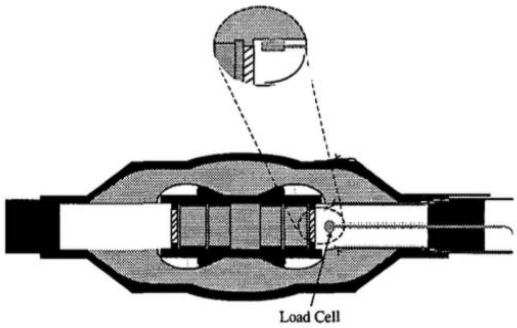

Fig 5.5: *Load cell location in the cable joint to detect the interfacial pressure* [59].

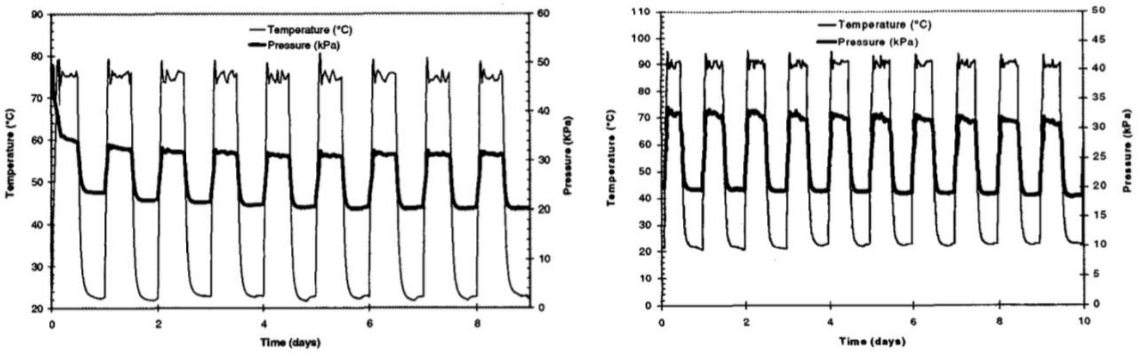

Fig 5.6: *Temperature profile and interfacial pressure: 75°C cycles at left and 90°C cycles at right* [59].

The same relation between interfacial pressure and joint temperature can be found in [60], where a test similar to the previous one has been performed during the development of a cold-shrinkable 66 kV SiR joint for XLPE cables. In particular, the temperature of the joint has been increased and the variation of the interfacial pressure has been measured. The test results are showed in figure 5.7. The causes of the increase of interfacial pressure with temperature rise has not been investigated in the latter studies. Now, in [23] is highlighted that physical properties, as the modulus of elasticity, of two insulating materials as XLPE and EPDM are quite different, especially when the temperature is involved as a parameter. The increase of interfacial pressure with temperature rise and vice-versa could be due to the different thermal expansions of the two dielectric materials constituting the interface: if the internal insulation, when

temperature rises, expands more than the external one, a pressure enhancement should be detectable in the interfacial region. However, the latter statement must be demonstrated by further tests on this field. Furthermore, better investigations have to be done on how cold and hot shrinkable materials behave under temperature variation conditions. Moreover, due to the very few studies about the linking between interfacial pressure variation and joint temperature, some tests having the objective to correctly correlate interfacial pressure and temperature on the joints samples are currently ongoing in the measurement laboratory of the University of Bologna.

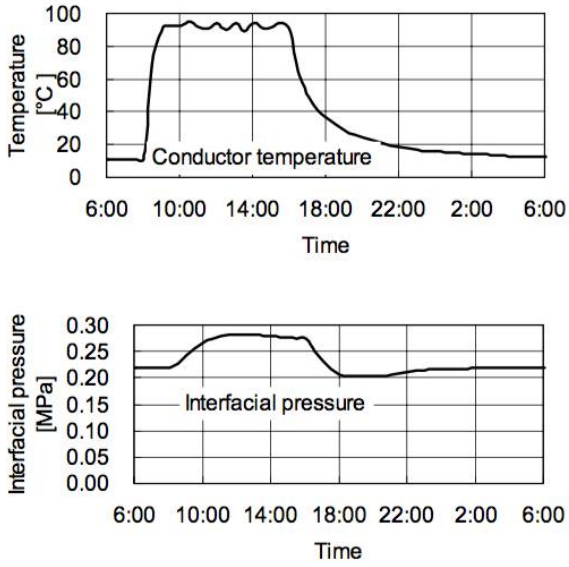

Fig 5.7: *Conductor temperature and corresponding interfacial pressure of 66 kV class cold shrink joint during heating cycle test* [60].

Thanks to what previously explained in section 2.3, it is known that a rising interfacial pressure leads to an increase in the breakdown strength of the joint dielectric interface while, when pressure loss occurs, the interfacial dielectric strength decreases as well. Now, partial discharge monitoring has been performed during the joint thermal cycling in [59]. As expected from what previously said, when the temperature decreases, namely when the interfacial pressure is at its lowest, a maximum in PD intensity has been detected.

Summarizing, until now two main hypotheses have been done, namely the tan delta value is supposed to be in relation to the joint interfacial pressure and the interfacial pressure is expected to increase when temperature increases and vice-versa. By linking these two, an explanation of the loss factor trend in relation to the temperature that has been detected in this study can be finally proposed. In particular, when the external temperature arises, the interfacial pressure is expected to increase and, consequently, the breakdown strength does the same. Hence, less interfacial discharges should happen and the interface is expected to behave more as an homogeneous insulation: the conduction current flowing from high voltage to ground should decrease in the interfacial region with a consequent decrease of the measured loss factor value. The inverse situation happen when the temperature falls down, relatively to the room one: now the interfacial pressure is expected to decrease and, consequently, more and larger voids should be present, leading to a reduction of the dielectric strength in the interface. Then, the high value of the tangential field is supposed to force more charges to pass from the high voltage to ground electrode, leading to an increase of the conduction current, namely to the losses in the dielectric. Consequently, the loss factor value is expected to rise.

It must be underlined again that the latter explanation of the detected loss factor trend in relation to temperature in cable joints is, until now, just an hypothesis. The proposed reasonings are supported by literature theory and laboratory experiments conducted by other researchers but, as previously said, some aspects have to be fully demonstrated yet by tests that are planned to be done in the measurement laboratory of the University of Bologna.

By supposing that the detected behavior of tangent delta is due to oscillations of the interfacial pressure induced by the temperature variations, some particular aspects of the results that have been presented in the latter chapter can be explained. In particular, it can be understood why the range of variation in the loss factor of the In-field Cable Joint samples is considerably lower than that in REPL ones. Now, as said in section 3.1, the In-field samples are completely finished joints having the external shrinkable outer sheath correctly installed while REPL ones present the lack of this external tightening

layer. Thus, the interfacial pressure on In-field Joint samples is expected to be greater since the main insulation body should be more tightened across the cable insulation and connection. Now, few days of temperature cycles are not expected to let the insulating materials lose so much fit in the interfacial region. Consequently, from the hypotheses made before, the loss factor should show less oscillations comparing to the ones detected in REPL joints, as it actually does. Another aspect that has to be commented about the loss factor results is that the tangent delta of a same joint measured at a same temperature but in different days is sometimes very different. This phenomenon could be explained by the fact that, after a temperature cycle, the topology of the interface will never be as it was before it. Indeed, variations in temperature are expected to cause mechanical stress modifying microscopically the interfacial topology with expansion and relaxation of the two dielectric materials. Hence, the position and the number of the contact spots and cavities will be necessarily different after a temperature cycle since the two dielectric materials will settle in a different way comparing to their arrangement after the previous thermal cycle. Thus, considering one sample at a same temperature before and after a thermal cycle, from what suggested the value of its loss factor will be consequently different, unlike what it could be found by measuring the dissipation factor on homogeneous insulating materials. It have always to be taken into the account that the tan delta is here evaluated on complex insulating systems that could variate their topology over time, depending on the mechanical stresses acting over them. Now, as underlined in [59], the interfacial pressure, and thus the interfacial dielectric strength, varies a lot between different joints due to different material composition and joint design. Hence, even if the detected loss factor behavior is the same in the different samples tested in the present study, better investigations have to be performed in order to fully demonstrate that the same tan delta trend in relation to temperature is verified also in joints having different designs and materials.

Concluding, from the discussion done in the present chapter it can be noticed that the hypotheses related to the causes of the detected loss factor trend are supported by some indirect studies found in technical literature. Now, if these speculations will be

demonstrated through to the mentioned laboratory tests, the dissipation factor could be used as an indicator of the cable joint interfacial pressure, thanks to the described relation between the two quantities. This means that the loss factor could behave also as an indicator of the interfacial breakdown strength, thanks to the strong correlation of the latter with the interfacial pressure. In particular, as presented in 2.2.1, the continuos day-night temperature variations coupled with the higher mean temperature typical of the summer period may cause pressure instabilities inside the joint structure due to the continuous expansion and contraction of the insulating materials. These phenomena could lead to a loss of fit between the two dielectrics and to the formation of more and bigger voids at the interface, causing a strong decrease in the interfacial breakdown strength. The final effect is expected to be the occurring of premature joint faults due to surface tracking affecting the most aged joints or the ones with more construction defects. Hence, from the hypotheses made, if on-site joints are monitored with *ad-hoc* tan delta measurement devices, the detection of a rise in loss factor oscillating peaks comparing to past values could indicate a critical joint operating condition because of gradual decreasing in interfacial pressure. Consequently, it could be decided to perform preventive maintenance on them in order to prevent the occurrence of a tracking failure caused by a too low interfacial dielectric strength.

At last, it has to be underlined that, in the actual electric distribution scenario, a commonly used method to monitor the health condition of the dielectric interfaces in cable joints is absent, despite the fact that they are univocally considered the most critical regions of the most critical apparatuses present in distribution cable networks. Hence, it can be understood the importance of a deeper analysis of the subject just only started with the works presented in this master thesis.

6 Conclusion and future works

In conclusion, the objectives set at the beginning of the present work has been completely achieved. Indeed, a simple and cheap laboratory setup to measure the loss factor of cable joints has been designed, constructed and completely characterized. Furthermore, the loss factor trend in relation to joint temperature variations has been investigated and widely discussed. Summarizing, in all the joint samples it has been detected that, when the temperature of the joint increases, the loss factor value tends to decrease and vice-versa. In chapter 5 these results have been discussed supposing that this particular trend of the loss factor could be originated by an increase and decrease of the joint interfacial pressure related to temperature variations. Indeed, it has been explained that the detected phenomenon seems to be a consequence of expansions and contractions of the two dielectric materials that are in contact. In particular, when the joint temperature increases, the interfacial pressure is expected to increase as well, leading to a better tightness of the two dielectrics at the interface and, then, to an higher interfacial dielectric strength. Hence, the resistive current should flow with more difficulty across the interface and, thus, the whole insulating joint system is expected to show less conduction losses. As a final consequence, the loss factor measured should decrease, as effectively does. The exact contrary is expected to happen when the temperature decreases.

As highlighted in the previous chapter, the latter hypotheses, even though they are supported by other theoretical and experimental studies, must be demonstrated by future tests that are going to be performed on the measurement laboratory of the University of Bologna. In particular, the conduction current must be measured in the interfacial region and it must be checked that the concerned current is always higher in magnitude than the one flowing across the joint homogeneous dielectric body, from the high voltage to ground electrode of the joint sample. In this way, it could be demonstrated that the loss factor is more sensitive to variation of interfacial resistive current than variations of the one that flows through the bulk insulating body. Moreover, it must be checked that, by

increasing mechanically the joint pressure, the measured loss factor effectively decreases and vice-versa. Subsequently, by constructing a cable joint with a very thin load cell placed at the interface, as in figure 5.5, it must be demonstrated that the interfacial pressure visibly increases with temperature rising and vice-versa. In this way, the tan delta trend can be correlated both with pressure and temperature variation. Another test could be also the measurement of the interfacial resistive current in order to demonstrate that it decreases with pressure rises and vice-versa.

If the future laboratory tests will confirm the proposed hypotheses about the causes of the detected joint loss factor trend, the dissipation factor could be effectively used as a good indicator of the interfacial pressure, as mentioned in the latter chapter. In fact, through the analysis of the historical loss factor values of a cable joint, it could be understood when the interfacial pressure is harmfully decreasing thanks to the fact that, in this case, a strong increase of tan delta comparing to past values is detected. As explained in section 2.3, a decrease in the dielectric interfacial pressure of a joint causes a strong decrease of its dielectric strength: this could lead to the complete flashover of the interface and the breakdown of the joint due to surface tracking. Hence, the loss factor could be used as diagnostic indicator useful to prevent the occurrence of this breakdown phenomenon, which has been recognized to be the most frequent failure event of cable joints, being themselves the component of the cable network with the highest failure rate. In other words, the loss factor measurement could be a diagnostic tool useful to know indirectly which is the pressure condition of the joint interface and so it could help to know in advance when the interfacial dielectric strength of the joint starts to decrease. Thanks to this knowledge, preventive maintenance could be scheduled and, consequently, cable line outages caused by surface tracking in joints would strongly decrease.

From what said, it is clear that this work is intended to be only the starting point for a deeper investigation on the reason why so many cable joint failures happen during summer period and on what is possible to do to avoid that occurrence. One of the main objectives of future tests conducted in the measurement laboratory of the University of Bologna is to built an accurate and cheap tan delta monitoring device for cable joints

that can be utilized on field and not only in laboratory. In this way, on site test and analysis could be performed on joints that are effectively working in distribution medium voltage cable networks. Hence, if also in this case it will be demonstrated that loss factor shows clearly the same correlation with interfacial pressure and temperature as in laboratory tests, it will be finally demonstrated that the tan delta is a good indicator of the internal dielectric strength condition of the cable joint under test. Then, the impact of surface tracking phenomena on cable outages and consequent disservices for the distribution utility would strongly decrease thanks to the possibility to perform preventive maintenance on cable joints that are detected to be on critical conditions.

In the end, it is worth saying that, from the present master thesis work, a conference paper [61] has been already published. The concerned paper basically explains how the developed tan delta measurement setup for cable joints has been designed and calibrated. It was presented and discussed during the 9th IEEE International Workshop on Applied Measurement for Power System (AMPS), held in Bologna on 26-28 September 2018. Moreover, also a journal paper [62] has been recently submitted and, currently, it is waiting to be published into IEEE Transactions on Instrumentation and Measurement. In particular, this paper treats the effects of temperature on cable joint loss factor measurements which are performed using the developed setup.

7 Acknowledgments

This master thesis is the result of months of work in the measurement laboratory of the Electrical, Electronic and Information Engineering Department of the University of Bologna. During this period, I was lucky enough to be inside a fervid research environment and to meet great people.

I would like to express my gratitude to my thesis supervisor, Prof. Lorenzo Peretto, for his kindness and availability despite his several commitments. I am grateful for the opportunity to attend this important and interesting project. My special thanks also to Abbas, without whom this work would not even exist.

I am really thankful to Albi, Miglio and Vale. By supporting each other during these two years of master degree, we have become a great team. Probably, without you I might still pass the exam of Applied Electromagnetic.

I wish to thank Martina, my great love, with whom I spent, and I will spend, the most beautiful days of my life. We shared our university years by encouraging each other during the difficulties and trying to silence our anxieties. Obviously, I would never be where I am today, without you. PS: did you see that I dedicated an entire paragraph to you, this time?

I would like to express my deepest gratitude to my parents and to my brother, Federico, for being always present and for always believing in me. A special word of thanks also to my grandparents, rocks without time, an to the big family whom I am lucky to have.

Last, but not least, I gratefully acknowledge all my friends with whom I can always relax and make laughs. You guys are great.

The university years go by in an instant, especially the two of master degree. Often there is not the time to stop even for a moment and to think how you are spending them. This period is now over. Looking back, I realize how many awesome people are around me and I cannot do anything but smile.

7 Acknowledgments

8 References

[1] IDC Technologies, “Overview,” in *Practical HV Cable Jointing and Terminations for Engineers and Technicians*, 3rd ed., Ed. West Perth: IDC Technologies, 2006, pp 1-9.

[2] BICC Cables, “Joints and Terminations for Distribution Cables,” in *Electric Cables Handbook*, 3rd ed., G. F. Moore, Ed. Oxford: Blackwell Science, 1997, pp 401-417.

[3] O. Kuusisto, “The Effects of Installation-Based Defects in Medium Voltage Cable Joints,” Bachelor Thesis, Helsinki Metropolia University of Applied Sciences, Helsinki, 2016.

[4] A. Eigner and S. Semino, "50 years of electrical-stress control in cable accessories," *IEEE Electrical Insulation Magazine*, vol. 29, no. 5, pp. 47-55, Sep-Oct 2013.

[5] P. N. Nelson and H. C. Hervig, "High Dielectric Constant Materials For Primary Voltage Cable Terminations," *IEEE Transactions on Power Apparatus and Systems*, vol. PAS-103, no. 11, pp. 3211-3216, Nov. 1984.

[6] G. Bas, “Electric Field Analysis in Stress Controlled High Voltage Cables”, Master Thesis, Middle East Technical University, Turkey, 2005.

[7] Europacable, “Best Practice for the installation of medium voltage cable accessories.” Internet: http://www.europacable.eu/energy/medium-voltage-accessories, 2016.

[8] S. Nopri, “Temperature Changes in Different Layers of Cable Joints and Insulation,” Master Thesis, Tallinn University of Technology, 2015.

[9] Tyco Electronics, “Power Cable Accessories Catalogue.” Internet: http://www.te.com/content/dam/te-com/documents/energy/global/productdocuments/Miscellaneous%20Locations/energy-epp0500-PowerCableAccessoriesSouthEastEurope.p

df, 2015.

[10] Europacable, “Cable Accessories in Underground Medium Voltage Distribution Networks.” Internet: http://www.europacable.eu/energy/medium-voltage-accessories, 2016.

[11] E. Csanyi. “Shielding of Power Cables.” Internet: http://www.csanyigroup.com/shielding-of-power-cables, Jul. 2010.

[12] REPL International Ltd. “Installation of a Heatshrink Straight Joint on Three-core MV Armoured Cable.” Internet: https://www.youtube.com/watch?v=Ss5AKxl_yIM&t=836s, Oct. 2017.

[13] REPL International Ltd., “REPL Cable Accessories Product Catalogue 2017.” Internet: https://www.repl.com/downloads/, 2017.

[14] R. P.Y. Mehairjan. “Application of Statistical Life Data Analysis for Cable Joints in MV Distribution Networks,” Master Thesis, Delft University of Technology, 2010.

[15] X. Wang, C. C. Wang, K. Wu, D. M. Tu, S. Liu and J. K. Peng, "An improved optimal design scheme for high voltage cable accessories,” *IEEE Transactions on Dielectrics and Electrical Insulation*, vol. 21, no. 1, pp. 5-15, Feb. 2014.

[16] H. A. Illias, Z. H. Lee, A. H. A. Bakar, H. Mokhlis and A. M. Ariffin. "Distribution of electric field in medium voltage cable joint geometry," in *2012 IEEE International Conference on Condition Monitoring and Diagnosis*, Bali, 2012, pp. 1051-1054.

[17] H. L. Halvorson. “Condition Assessment of Wind Farm Medium Voltage Cable Joints,” Master Thesis, Norwegian University of Science and Technology, 2012.

[18] B. X. Du and L. Gu, "Effects of interfacial pressure on tracking failure between XLPE and silicon rubber," *IEEE Transactions on Dielectrics and Electrical Insulation*, vol. 17, no. 6, pp. 1922-1930, Dec. 2010.

[19] B. X. Du, X. H. Zhu, L. Gu and H. J. Liu, "Effect of surface smoothness on tracking mechanism in XLPE-Si-rubber interfaces" *IEEE Transactions on Dielectrics and Electrical Insulation,* vol. 18, no. 1, pp. 176-181, Feb. 2011.

[20] E. Kantar, F. Mauseth, E. Ildstad and S. Hvidsten, "Tangential AC breakdown strength of solid-solid interfaces considering surface roughness," in 2*017 IEEE Conference on Electrical Insulation and Dielectric Phenomenon (CEIDP)*, Fort Worth, TX, 2017, pp. 580-583.

[21] M. Hasheminezhad and E. Ildstad, "Application of contact analysis on evaluation of breakdown strength and PD inception field strength of solid-solid interfaces," *IEEE Transactions on Dielectrics and Electrical Insulation*, vol. 19, no. 1, pp. 1-7, Feb. 2012.

[22] C. Dang and D. Fournier, "Dielectric performance of interfaces in premolded cable joints," *IEEE Transactions on Power Delivery*, vol. 12, no. 1, pp. 29-32, Jan. 1997.

[23] D. Fournier and L. Lamarre, "Effect of pressure and temperature on interfacial breakdown between two dielectric surfaces," in *992 Annual Report: Conference on Electrical Insulation and Dielectric Phenomena*, Victoria, BC, Canada, 1992, pp. 229-235.

[24] A. Mingotti *et al*., "Low-Cost Monitoring Unit for MV Cable Joints Diagnostics," in *2018 IEEE 9th International Workshop on Applied Measurements for Power Systems (AMPS)*, Bologna, 2018, pp. 1-5.

[25] R. Jongen, E. Gulski and J. Smit, "Failures of medium voltage cable joints in relation to the ambient temperature," in *CIRED 2009 - 20th International Conference and Exhibition on Electricity Distribution - Part 1*, Prague, Czech Republic, 2009, pp. 1-4.

[26] A. Sturchio, G. Fioriti, M. Pompili and B. Cauzillo, "Failure rates reduction in SmartGrid MV underground distribution cables: Influence of temperature," in *2014 AEIT Annual Conference - From Research to Industry: The Need for a*

More Effective Technology Transfer (AEIT), Trieste, 2014, pp. 1-6.

[27] S. M. Hasheminezhad, “Tangential Electric Breakdown Strength and PD Inception Voltage of Solid-Solid Interface,” PhD Thesis, Norwegian University of Science and Technology, 2016.

[28] E. Kantar, F. Mauseth, E. Ildstad and S. Hvidsten, "Longitudinal AC breakdown voltage of XLPE-XLPE interfaces considering surface roughness and pressure," *IEEE Transactions on Dielectrics and Electrical Insulation*, vol. 24, no. 5, pp. 3047-3054, Oct. 2017.

[29] D. Fournier, C. Dang and L. Paquin, "Interfacial breakdown in cable joints," in *Proceedings of 1994 IEEE International Symposium on Electrical Insulation*, Pittsburgh, PA, USA, 1994, pp. 450-452.

[30] C. Dang and D. Fournier, "A study of the interfacial breakdown in cable joints," in *Proceedings of IEEE Conference on Electrical Insulation and Dielectric Phenomena - (CEIDP'94)*, Arlington, TX, USA, 1994, pp. 518-523.

[31] Junhua Luo, Jikang Shi and Jian Yuan, "Study on surface discharge of composite dielectric in XLPE power cable joints," in *Proceedings: Electrical Insulation Conference and Electrical Manufacturing and Coil Winding Conference (Cat. No.01CH37264)*, Cincinnati, OH, USA, 2001, pp. 341-343.

[32] D. Fournier and L. Lamarre, "Effect of pressure and length on interfacial breakdown between two dielectric surfaces," in *Conference Record of the 1992 IEEE International Symposium on Electrical Insulation*, Baltimore, MD, USA, 1992, pp. 270-272.

[33] B. X. Du, L. Gu, X. Zhang and X. Zhu, "Fundamental research on dielectric breakdown between XLPE and silicon rubber interface in HV cable joint," in *2009 IEEE 9th International Conference on the Properties and Applications of Dielectric Materials*, Harbin, 2009, pp. 97-100.

[34] INERTIA-REPL Inc. “Low Voltage & Medium Voltage Cable Accessories.” Internet: http://www.inertia-repl.com, 2009.

[35] J. C. H. Mejía, “Characterization of Real Power Cable Defects by Diagnostic Measurements,” PhD Thesis, Georgia Institute of Technology, 2008.

[36] M. L. Sanden, “Condition Assessment of Medium Voltage Cable Joints - Dielectric Spectroscopy of Field Grading Materials”, Master Thesis, Norwegian University of Science and Technology, 2015.

[37] J. C. H. Mejia, “Dissipation factor (Tan δ),” in *Cable Diagnostic Focused Initiative (CDFI) Handbook Phase II*, Georgia Institute of Technology - The National Electric Energy Testing Research and Applications Center (NEETRAC), Feb. 2016, pp. 7-94.

[38] N. B. Raičević, “Electrical Field Modelling at the Cable Joints,” *Facta Universitatis, Series: Electronics and Energetics*, vol. 20, no. 1, pp. 9–20, Mar. 2007.

[39] N. Raicevic, S. Ilic, S. Aleksic and R. Dimitrijevic, "Improving safety of cable networks by modeling deflectors of cable accessories," *4th International Conference on Power Engineering, Energy and Electrical Drives*, Istanbul, 2013, pp. 70-75.

[40] A. Ponniran, N. A. M. Jamail and N. A. Jalaludin, “Tan Delta and Capacitance Characteristics of Underground XLPE Cables – 11 kV,” in *Proceedings of MUCEET2009 Malaysian Technical Universities Conference on Engineering and Technology,* Pahang, 2009, pp 42-46.

[41] A. Ponniran and M. S. Kamarudin, "Study on the performance of underground XLPE cables in service based on tan delta and capacitance measurements," in *2008 IEEE 2nd International Power and Energy Conference*, Johor Bahru, 2008, pp. 39-43.

[42] REPL International, “Cold Shrink MV Cable Joint Kits Datasheet.” Internet: https://www.repl.com/cold-shrink-mv-cable-joint-kits, 2017.

[43] J. J. Smit and E. Gulski, "Advanced condition assessment of high voltage power cables," in *Proceedings of 2005 International Symposium on Electrical Insulating Materials, 2005. (ISEIM 2005)*, Kitakyushu, 2005, pp. 869-872 Vol.3.

[44] Elcon Megarad s.p.a., “Assembly instruction ECOLD GLSM – 3490 RCR A joint kit.” Instruction paper (in Italian).

[45] “IEEE Guide for Field Testing and Evaluation of the Insulation of Shielded Power Cable Systems," in *IEEE Std 400-2001 (Revision of IEEE Std 400-1991)*, vol., no., pp.1-40, 29 Jan. 2002

[46] H. Shafi, T. M. Anthony, A. Basri, A. Raj and C. Chakrabarty, "Extraction of cable joints tangent delta from bulk tangent delta measurement using HFAC method," in *2016 IEEE International Conference on Power and Energy (PECon)*, Melaka, 2016, pp. 306-310.

[47] N. Permal, C. K. Chakrabarty, A. R. Avinash, T. Marie and H. Shafi Abd Halim, "Tangent delta extraction of cable joints for aged 11kV underground cable system," in *2016 International Conference on Advances in Electrical, Electronic and Systems Engineering (ICAEES)*, Putrajaya, 2016, pp. 265-270.

[48] National Instruments, “NI 9239 Datasheet.” Internet: http://www.ni.com /manuals/i/, Apr. 2016.

[49] Caddock Electronics Inc., “Type USF Ultra-Stable Low TC Film Resistors 200 Series and 300 Series Datasheet.” Internet: http://www.caddock.com /Online_ catalog/Mrktg _Lit/ TypeUSF.pdf, 2017.

[50] Vishay Precision Group Inc., “Ultra High Precision Z Foil Though-Hole Resistor with TCR of ±0.2 ppm/°C, Tolerance of ±0.005% (50 ppm), Load Life Stability of ±0.005% Datasheet.” Internet: http://www.vishaypg.com/docs/63143/vs a101.pdf, Jul 2014.

[51] Keysight Technologies, “Keysight 3458A Multimeter Datasheet.” Internet: http:// literature.cdn.keysight.com/litweb/pdf/5965-4971E.pdf

[52] A. Mingotti, L. Peretto, R. Tinarelli, F. Mauri and I. Gentilini, "Assessment of Metrological Characteristics of Calibration Systems for Accuracy vs. Temperature Verification of Voltage Transformer," in *2017 IEEE International Workshop on Applied Measurements for Power Systems (AMPS)*, Liverpool, 2017, pp. 1-6.

[53] C. A. Peters, “Statistics for Analysis of Experimental Data,” in *Environmental Engineering Processes Laboratory Manual,* Ed. Champaign: AEESP, 2001, pp.1-25.

[54] J. Committee Guides Metrology, *Evaluation of Measurement Data—Guide to the Expression of Uncertainty in Measurement*, Bureau International des Poids et Mesures, Sevres, France, 2008

[55] G. Gavrilovs and S. Vītoliņa, “Measuring Specificities of Dissipation Factor of Electrical Equipment in Substations,” *Electrical, Control and Communication Engineering*, vol. 27, no. 1, pp. 92–95, Jan. 2010.

[56] Y. M. Poplavko, Y. V. Didenko, and D. D. Tatarchuk, “Temperature Dependences of Losses in High Frequency Dielectrics,” *Electronics and Communications*, vol. 19, no. 4, pp. 28–35, Dec. 2014.

[57] A. Dognini, ‘Investigations on mechanical and electrical properties of silicone rubbers,’ Master Thesis, Politecnico di Milano, Italy, 2014.

[58] M. Callaghan, “barwitherr(errors,varargin)”, Internet:https://it.mathworks.com /matlabcentral/fileexchange/30639-barwitherr-errors-varargin , Jun. 03, 2018

[59] N. Amyot and D. Fournier, "Influence of thermal cycling on the cable-joint interfacial pressure," in *Proceedings of the 20001 IEEE 7th International Conference on Solid Dielectrics*, Eindhoven, Netherlands, 2001, pp. 35-38.

[60] S. Kobayashi, D. Muto, S. Tanaka, H. Izuka, H. Niinobe, M. Suetsugu, "Development of Factory Expanded Cold-Shrinkable Joint for EHV WLPE Cables," *Proc. of 6th International Conference on Insulated Power Cables (Jicable'03)*, no. A.5.1, 2003.

[61] A. Mingotti, A. Ghaderi, L. Peretto, R. Tinarelli and F. Lama, "Test Setup Design and Calibration for Tan Delta Measurements on MV Cable Joints," in *2018 IEEE 9th International Workshop on Applied Measurements for Power Systems (AMPS)*, Bologna, 2018, pp. 1-5.

[62] A. Ghaderi, A. Mingotti, F. Lama, L. Peretto and R. Tinarelli, “Effects of Temperature on MV Cable Joints Tan Delta Measurements,” *IEEE Transactions on Instrumentation and Measurement* (Submitted).